Master's thesis

Master of Engineering, Industrial Quality Management

2023

Mikko Kähäri

TACTILE COORDINATE MEASURING MACHINE MEASUREMENT PARAMETERS

TURKU AMK
TURKU UNIVERSITY OF APPLIED SCIENCES

Master’s Thesis | Abstract

Turku University of Applied Sciences

Masters of Engineering, Industrial Quality Management

2023 | 87

Mikko Kähäri

TACTILES CMM MEASUREMENT PARAMETERS

There are no clear "rules of measuring" for the coordinate measuring machine (CMM). When measuring the diameter or form of a hole or shaft, there are no clear instructions regarding the number of measurement points or setup of filters. In comparison measurements, this problem is not revealed, because a gauge ring is often used in comparison measurements and the gauge rings do not have a form error. When measuring the form error of an ideal hole with a small or large determination of the measuring point, the results yield differences of, at most, a micrometer. The need for measurement rules increases when switching to use product manufacturing information (PMI) data in computer aided design (CAD) models. This thesis focuses on examining parameters that are missing from PMI data: the PMI data missing measurement point quantities per element, scanning speed, and measurement force. In addition, the PMI data also missing parameter values for form filtering and outlier filtering. Based on the existing research literature and standards, there are no clear guidelines for these parameters. In this thesis, the measuring parameters of tactile CMMs were determined. To determine the parameters, varied sizes of the reference normal and one size the test part were measured using three different tactile sensors. As a result of this research, a table of measurement parameters was built. The challenge of the all-encompassing measurement parameter tablestyl was taking into account the differences in the measurement stylus.

Keywords:

PMI, MBD, CAD, CMM, MBD, Outlier

Opinnäytetyö (YAMK) Tiivistelmä

Turun ammattikorkeakoulu

Industrial Quality Management

2023 | 87

Mikko Kähäri

Koskettavan KMK:n mittausparametrit

Koordinaattimittauskoneelle (KMK) ei ole selkeitä "mittaussääntöjä". Mitattaessa reiän tai akselin halkaisijaa tai muotovirhettä, ei tiedetä kuinka monta mittauspistettä elementistä on otettava tai kuinka monta mittauspistettä on otettava muodon evaluoimiseksi luotettavasti. Tämä ongelma ei paljastu vertailumittauksissa, koska vertailumittauksissa käytetään muotovirheettömiä referenssinormaaleja. Ideaalisen reiän muotovirheen mittaamisessa vähäisillä tai suurilla mittauspistemäärillä saadaan tuloksiin ainoastaan mikrometrin tai sen osien eroavaisuuksia. Mittaussääntöjen tarve kasvaa siirryttäessä käyttämään PMI:tä (tekniset tuotemäärittelytiedot) CAD-malleissa.

Opinnäytetyössä keskitytään tarkastelemaan parametrejä, jotka puuttuvat PMI-tiedoista. PMI-tiedoista puuttuvat elementtikohtaiset mittauspistemäärät, skannausnopeus ja mittausvoima. Tämän lisäksi PMI-tiedoista puuttuvat myös parametriarvot muodon suodatukselle ja outlier-suodatukselle. Olemassa olevan tutkimuskirjallisuuden perusteella edellä mainittuihin parametreihin ei ole selkeitä ohjeita. Opinnäytetyössä määritettiin koskettavalla toimintaperiaatteella toimivien koordinaattimittauskoneiden mittausparametrit. Parametrien määrittämiseksi mitattiin eri kokoisia referenssinormaaleja ja testikappaletta kolmella erilaisella koskettavalla sensorilla. Tutkimuksen tuloksena saatiin rakennettua mittausparametritaulukko. Kaikenkattavan mittausparametritaulukon haasteeksi osoittautui mittauskärkien eroavaisuuksien huomioiminen.

Asiasanat:

KMK, CAD, MBD, PMI, UPR, Lc, Trigger, Outlier

Content

List of abbreviations (or) symbols **7**

1 Introduction **11**

2 Product and manufacturing information (PMI) **13**

2.1 What is MBD? 13

2.2 What is annotation? 13

2.3 What is PMI? 14

3 2 Sensor principles for CMMs **15**

3.1 Force coin 16

3.2 Passive sensor principles 16

3.2.1 The principle of a passive sensor 17

3.3 The principle of an active sensor 19

3.3.1 The principles of active measuring heads 20

3.4 The principle of the trigger sensor 21

3.4.1 Trigger form error 22

4 Uncertainty of measurement **24**

4.1 CMM uncertainty 27

4.2 Environmental uncertainty 29

4.3 Stylus uncertainty 30

4.4 Part uncertainty 31

4.5 Calculation of measure uncertainty 31

5 Filtering of Measurement Results **34**

5.1 Harmonic waves 36

5.2 Evaluation of the Gaussian filter 37

5.3 Undulations per revolution (UPR) 39

5.4 Wavelength (Lc) 41

5.5 ISO 16610 standard series 43

5.6 Mechanical filter 44

5.7 Outlier filter 45
5.7.1 Manual outlier filter 45
5.7.2 Automatic outlier filter 46

6 Measurement Parameters 50
6.1 The test part 50
6.1.1 Roundness—hole with a small form error 51
6.1.2 Roundness—hole with a big form error 52
6.1.3 Diameter—hole with a small form error 53
6.1.4 Diameter—hole with a big form error 54
6.1.5 Repeatability—hole with a small form error 54
6.1.6 Repeatability—hole with a big form error 55
6.2 Flatness 56
6.3 Gauge ring test 62
6.3.1 Scanning speed passive sensor 63
6.3.2 Scanning speed active sensor 68
6.4 Effect of stylus length 71

7 Recommended Values of Measurement Parameters 74
7.1 Free form element 75
7.2 Circle 75
7.3 Plane 76
7.4 Line 76
7.5 Cylinder 77
7.6 Cone 77

8 Thinking about what was discovered 78
8.1 Conclusions 80

References 83

Appendices

Appendix 1. Temperature stability

Appendix 2. Reproducibility and repeatability

List of abbreviations (or) symbols

1σ, 2σ, 3σ	Combined and expanded uncertainty confidence level of about 1 = 68.3%, 2 = 95.4% 3 = 99.7%
2D drawing	The abbreviation for two-dimensional drawing is 2D
3D model	The process of creating three-dimensional representations of an object or a surface
A	Repeatability of the measuring device
C	Chebyshev also called the "minimax"
d	Diameter
h	Wave height
K	Measuring length factor
k	Coverage factor
L	Length
U	Uncertainty
Active sensor	Tactile principle measure sensor
Annotation	Visible (human readable) mark attached to CAD model
Attribute	Additional information that is not geometry or annotation
CAD	Computer aided design
CMM	Coordinate measurement machine
Ds	Probe diameter
Band-pass	Waviness filter

E_n	Normalized error is a statistical evaluation used to compare proficiency testing results where the uncertainty in the measurement result is included
Fc	Measure force
Fs	Spring force
FFT	Fast Fourier transformation
GX	Maximum inscribed cylinder
Gauge ring	Cylindrical ring of a thermally stable material, often steel, whose inside diameter is finished to gauge tolerance and is used for checking
High-pass	Roughness filter
Lc	Wavelength
Low-pass	Form filter
MBD	Model-based definition
MPE	Maximum permissible linear measuring tolerance
mK	part correlation coefficient
NAS	National Aeronautical standard
Outlier	an observation that lies an abnormal distance from other values in a random sample from a population.
PFTM	Multiple-stylus probing error
PMI	Product and Manufacturing Information
Probe	Measuring tip that touches the surface of the part to be measured
Passive sensor	Tactile principle measure sensor

RMS	Root Mean Square is the square root of the mean of the data values.
RONt	The roundness form tolerance measures the deviation of a measured circle to a geometrically ideal circle, at the same centre point.
Repeatability	The closeness of the agreement between the results of successive measurements of the same measure, when carried out under the same conditions of measurement.
Span	Range between minimum- and maximum value
Sigma	Mathematical sum/standard deviation
TED	Theoretically exact dimensions
THP	Maximum permissible probing tolerance
Tactile	Measurement principle is based on touch
Trigger sensor	Measurement principle point to point
Type A	Measurement uncertainty is estimated using statistical methods
Type B	Measurement uncertainty is estimated using non-statistical methods
SQRT	A square root of a number is a value that, when multiplied by itself, gives the number.
Stylus	Stylus with have one probe
Stylus system	Stylus with have several probe in different directions
StDev	Standard deviation is average amount of variability dataset
UPR	Undulations per revolution
*U*ref	Reference uncertainty

*U*cal, *U*xi	Uncertainty components
*U*p, *U*b, *U*w	Uncertainty components
*W*c	Filter cut-off
λ	Wavelength
δα	length of workpiece
δavarage	Average temperature
δT	Uncertainty of correlation coefficient and part correlation coefficient
δtempe	Uncertainty in room temperature measurement and part correlation coefficient
δTsensor	Temperature range
$\delta\tau$	Uncertainty of temperature measurement
Δt	Uncertainty in room temperature measurement
π	ratio of the circumference of a circle to its diameter
Ø	Diameter

1 Introduction

The purpose of this thesis is to determine the measurement parameters of coordinate measuring machines (CMMs) that operate on the tactile principle. Currently, there is no standard available that defines the "measurement rules" for a CMM.

The lack of measurement rules become evident when analyzing the differences in the measurement results, when the same part has been measured by two different people and using two different coordinate measuring machines. The measurement uncertainties determined by the manufacturers of CMMs are the same. In a comparison measurement, the results of these CMMs differ from each other by a few micrometers.

When using product and manufacturing information (PMI) in the measurement, a measure parameter that is not included in the PMI information is encountered. The PMI data does not contain, for example, the number of measurement points per element, scanning speed, or filtering. Therefore, the programmer must define this parameter information. These abovementioned parameters are the largest single factors that influence the measurement result. If it is possible to determine the measurement parameters per measuring element, the result is consistent with the measurement results of different CMM brands, operators, software, and sensors.

The standard of Geometrical Product Specifications – Standard reference temperature for the specification of geometrical and dimensional properties (SFS-EN ISO 1:2022) determines a standard temperature of 20°C for geometrical and distance measurements. In extant studies, measurement uncertainty is determined according to the standard of Geometrical Product Specifications: CMMs Technique for Determining the Uncertainty of Measurement (SFS-EN ISO 15530-3: 2011). There are two types of formula uncertainties: type A and type B. Their distributions are determined according to the evaluation of measurement data in the Guide to the Expression of Uncertainty in Measurement (JCGM, 2008, p.100). Uncertainty factors are based on Evaluation of the Uncertainty of Measurement in calibration EA 4-02 definitions. Type A measurement uncertainty is estimated using statistical methods and type B measurement uncertainty is estimated using non-statistical methods. The current design software enables a model-based definition (MBD), where the basic idea is to add product definition information to a 3D model. As the 3D model contains product specification information,

traditional drawings can be dispensed with. The biggest advantage of MBD is saving time (Rapinoja et al., 2016). The standard Geometrical Product Specifications: Geometrical Tolerances of Form, Orientation, Location, and Run-out (SFS-EN ISO 1101, 2017) defines the notation of filtering values for 2D drawings, but has not yet defined this for the PMI information used in the 3D model. The standard series Geometrical Product Specifications–Filtration (ISO 16610) has also defined the operating principles of the filters, but the standard does not specify which filter should be used at any given time. In a previous study, Roithmeier (2006, 2009) considered how different filtering values are determined for measurement elements. On the other hand, Tikka (2007) defined the number of measurement points from the point of view of measurement economics only in point-to-point measurement. However, the reference measurement defined by the ISO standard does not take a stance on filtering or the number of measurement points. According to the standard, the measurement method should be the same (SFS-EN ISO 15530-3: 2011).

The aim of the thesis was to determine the measurement parameters for tactile CMMs. This thesis aims to provide the measurement parameters for the scanning speed of different tactile sensors and to determine the number of measurement points and filtering value. These parameters are tied to the size of the measured element. The goal of this research was to ascertain how these different measurement parameters affect the measurement result.

To determine the parameters, reference standards of assorted sizes (gauge ring) and the test part prepared for this study were measured with a CMM. Four CMMs were used in the study to prove the reliability of the results. The measurement results were obtained using an active or passive measuring head. The test part was measured using different numbers of measurement points and different scanning speeds. Reference standards were measured with different sensors using different scanning speeds.

In the next section, what PMI is and how the measuring heads work explained. Thereafter, how measurement uncertainty and filtering are defined is discussed. Finally, the recommended measurement parameters for CMMs are tabulated.

2 Product and manufacturing information (PMI)

Current design software enables an MBD specification, where the basic idea is to embed product specification information in a 3D model. In this case, traditional drawing is not needed at all. The benefits of MBD can be seen in, for example, more unambiguous product definition, time savings in steps using product information (e.g., production planning, production, measurement, etc.), data transfer automation capabilities, etc.

MBD is a relatively old invention, but it has taken a foothold in the world slowly. Currently, the method is mainly applied by the automotive and aircraft industries. MBD is expected to become more widespread in other industries as well (Rapinoja et al., 2016, p. 6.)

2.1 What is MBD?

MBD encompasses the complete definition of product data using a 3D model, without drawings. The product model can include all information related to the manufacture of the product in various forms. This information includes dimensions, tolerances, surface roughness, material, images, sections, and exploded views. External documents, such as text files, can also be attached to an MBD product model (Rapinoja et al., 2016, p. 6.).

2.2 What is annotation?

Annotation is a marking attached to the model through which information regarding the characteristics of the product is transmitted (e.g., dimensions, tolerances, surface treatment, and materials). In certain contexts, when referring to annotation, we discuss PMI data; PMI data also contains attribute information (metadata) (Rapinoja et al., 2022, p. 29.) According to the Technical Product Documentation: Digital Product Definition Data Practices (SFS-ISO 16792:2021:en), the annotations include length and angular dimensions, theoretically exact dimensions (TED), datums, and geometric tolerances.

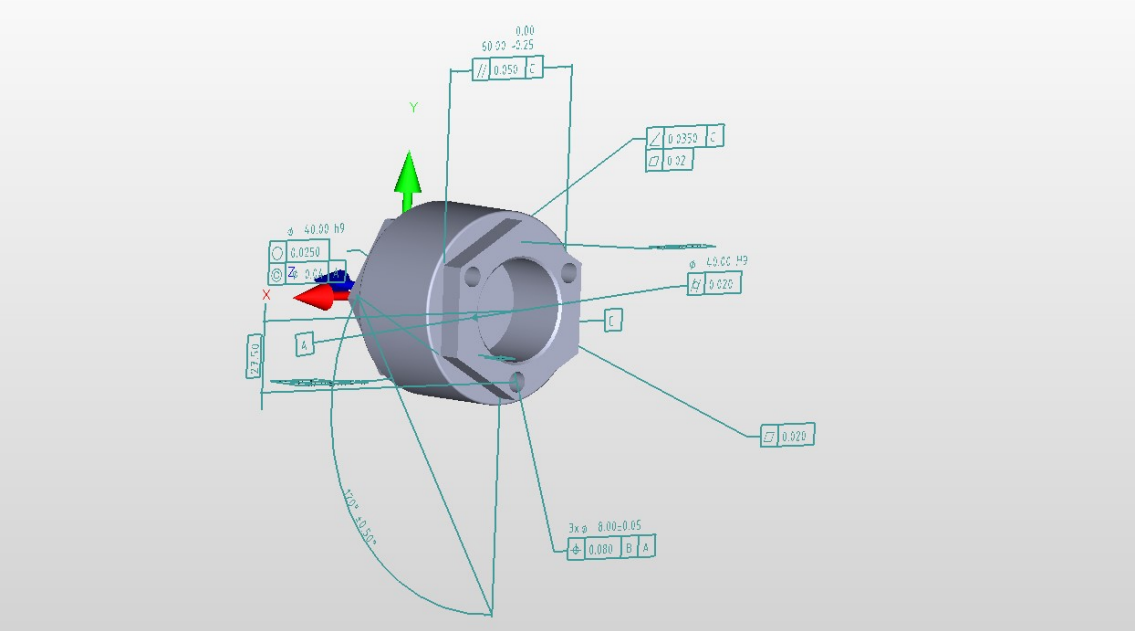

Figure 1. A model in which all the annotations are visible.

2.3 What is PMI?

PMI refers to the attributes that define a product, with the exception of geometry information. These attributes include dimensions, tolerances, and markings of surface properties. Thus, MBD is a broader concept than PMI (see Figure 3) (Rapinoja et al., 2016, p. 6.)

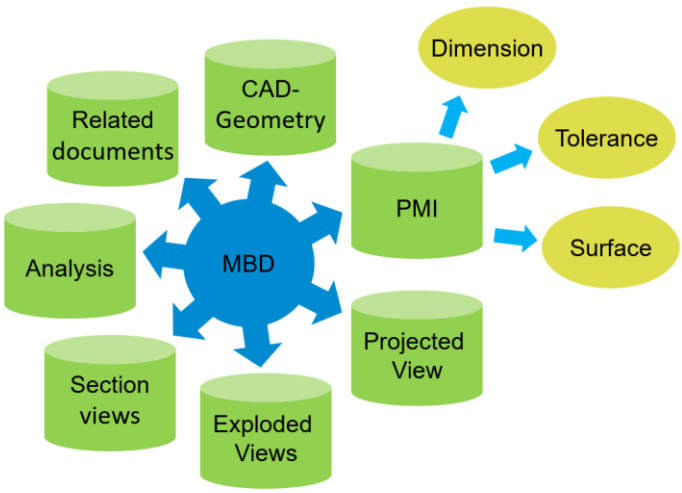

Figure 2. Relationship between MBD and PMI. (Original figure Malliperustaisen tuotemäärittelyn (MBD), Mahdollisuudet, 2016; modified by the author.)

3 2 Sensor principles for CMMs

This thesis deals only with sensors based on tactile measurement. The principles of operation of optical sensor videos, cameras, lasers, or white light sensors are not discussed in this thesis. The principles of mechanical sensors are presented in Figure 4. The principles of optical sensors are presented in Figure 5.

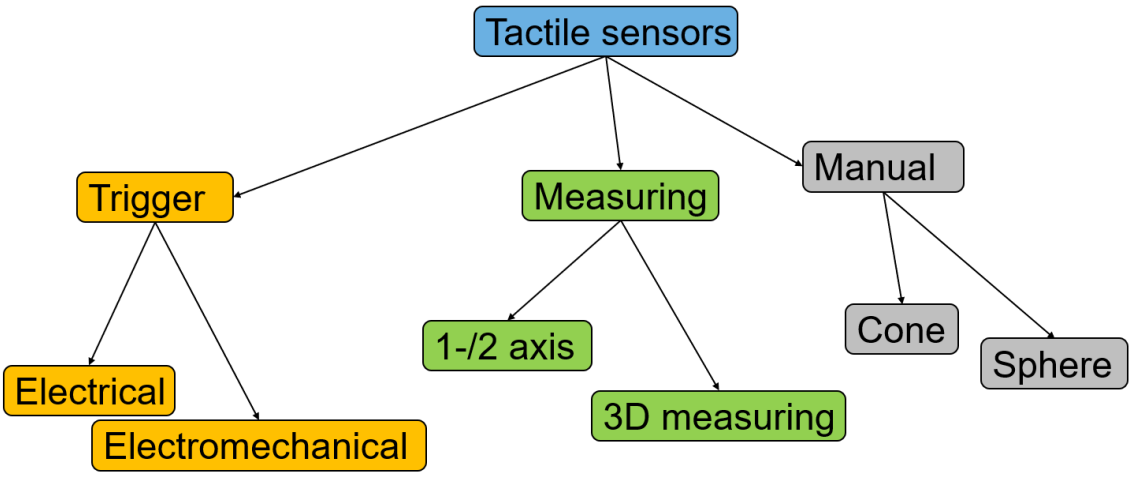

Figure 3. Principles of the tactile sensors.

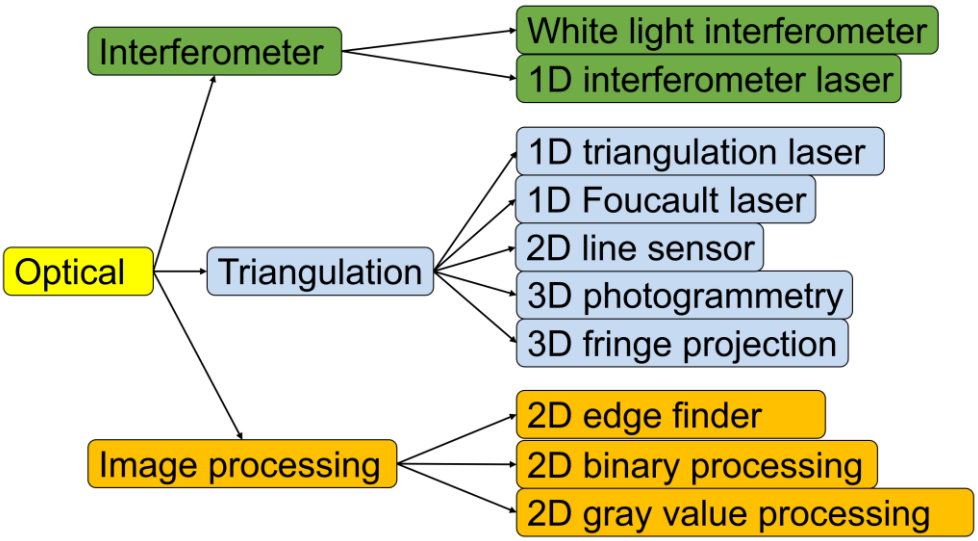

Figure 4. Principles of the optical sensors.

3.1 Force coin

There are two types of scanning sensors: 1) passive scanning sensor and 2) active scanning sensor. The principle of both sensors is based on the so-called force coin, in which action is based on induction (see Figure 6). The scanning sensor has three force coins. With three force coins, we can measure the displacement of the measuring probe in the directions of the X, Y, and Z axes (AUKOM, 2017b).

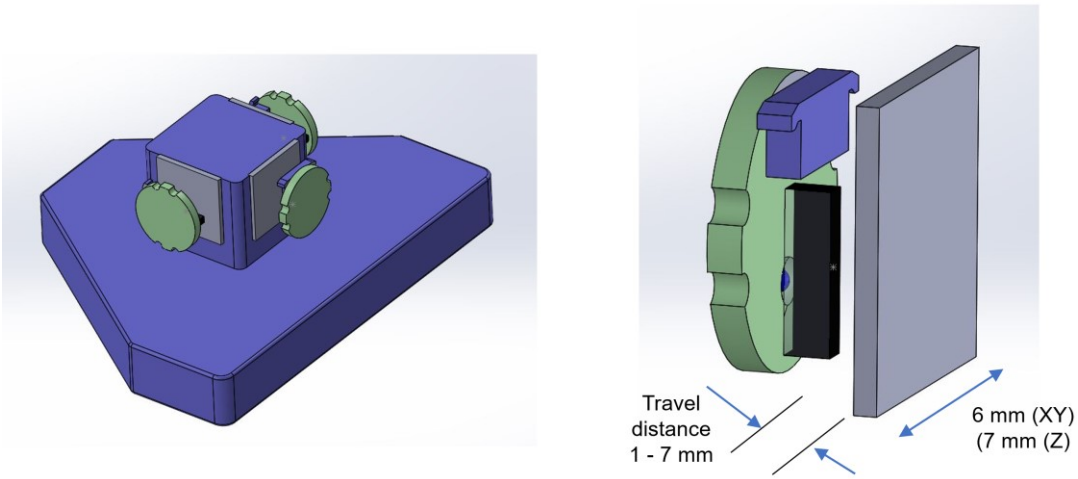

Figure 5. The principle of force coin.

3.2 Passive sensor principles

A factor that contributes to the difference between passive and active scanning sensor measurement accuracy is the control of measuring force during measurement. A passive sensor cannot control the measuring force; instead, the measuring force comes from the axis servos of the CMM. The measuring force increases as the scan progresses. As the measuring force increases, the deflection of the measuring probe also increases (see Figure 7). The decrease or increase in measuring force is caused by a form, orientation, or position error of the element being measured. The elements to be measured from manufacturing parts are plane, cylinder, circle, line, or point. The elements are never located in the same location as where they are located in the CAD model. The measured elements of the manufacturing part always have errors in position, orientation, and form compared to the ideal CAD model. These differences

between the manufactured part and the CAD model are due to inaccuracies in the manufacturing methods. The CMM's control accuracy also affects the measurement force. At a very high scanning speed, the CMM control is unable to follow the measuring path perfectly. Thus, the passive sensor will have to use lower scanning speeds compared to the active sensor. Figure 8 depicts the principle of the passive measuring head based on the force coin (AUKOM, 2017a, 2017b)

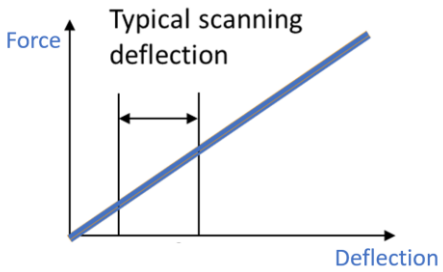

Figure 6. Passive sensor scanning deflection.

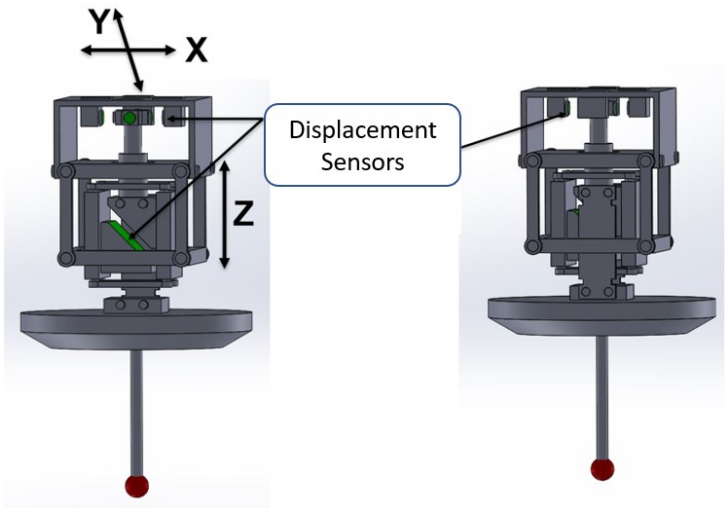

Figure 7. The principle of a passive sensor.

3.2.1 The principle of a passive sensor

Figure 10 depicts the principle of a passive sensor that is based on a laser. The scanning result according to the standard Geometrical Product Specifications: Acceptance and Reverification Tests for Coordinate Measuring Machines (ISO 10360-4, 2000) for the laser operating measurement head is always approximately 2 µm or

more, regardless of the module. Figure 9 presents a comparison of two passive sensors according to the ISO 10360-4:2000 standard scanning test result. The figure presents the effect of the probe length on the measurement result with two different sensors. The sensors are the laser principle and force coin principle passive sensors. When buying a CMM, the measuring head plays a big role in the overall accuracy of the CMM. Figure 9 depicts the measurement uncertainty of the CMM according to Geometrical Product Specifications: Acceptance and Reverification Tests for Coordinate Measuring Machines (ISO 10360-2:2009) standard $U^3 = 0.5+L/1000$. In the same figure, it is evident that the scanning ability of the sensor is approximately 2 µm. Then, according to which value should the measurement uncertainty of that coordinate measuring machine be determined? Chapter 4 presents a thorough explanation of the measurement uncertainty of the CMM.

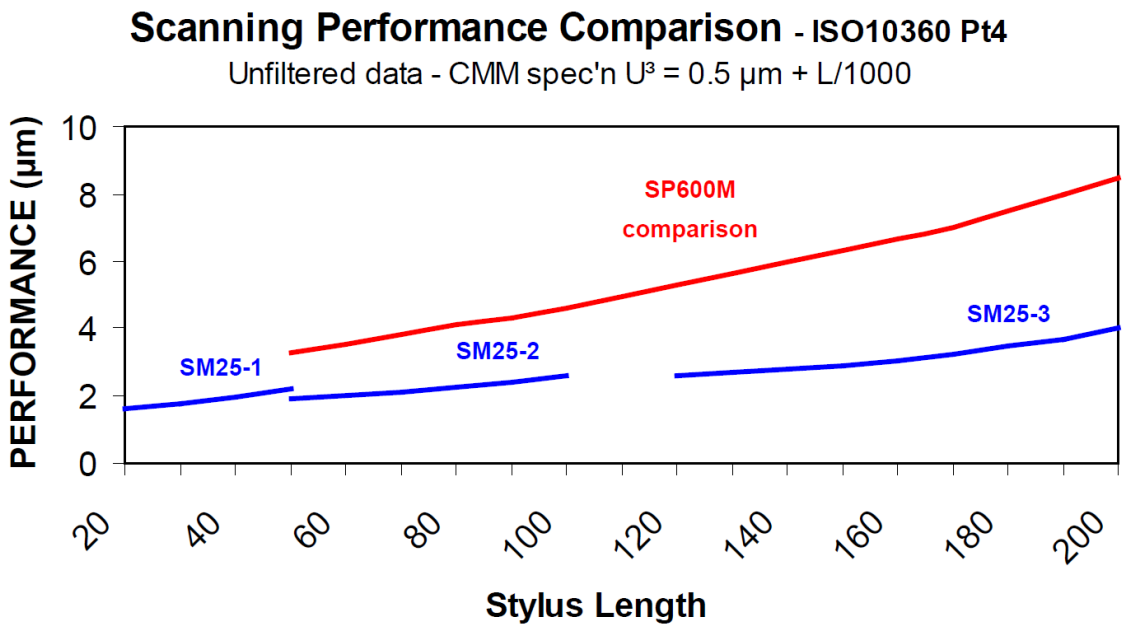

Figure 8. Laser and force coin sensor performance. (Renishaw, n.d.-b., p. 11).

The superscript 3 in Figure 9 has the same meaning as, for example, $k = 3$ in the calibration certificate of measuring devices and implies combined and extended uncertainty. Further, $k = 1$ indicates a confidence level of approximately 68.3%; $k = 2$ indicates a confidence interval of approximately 95.4%, and $k = 3$ indicates a confidence interval of approximately 99.7%.

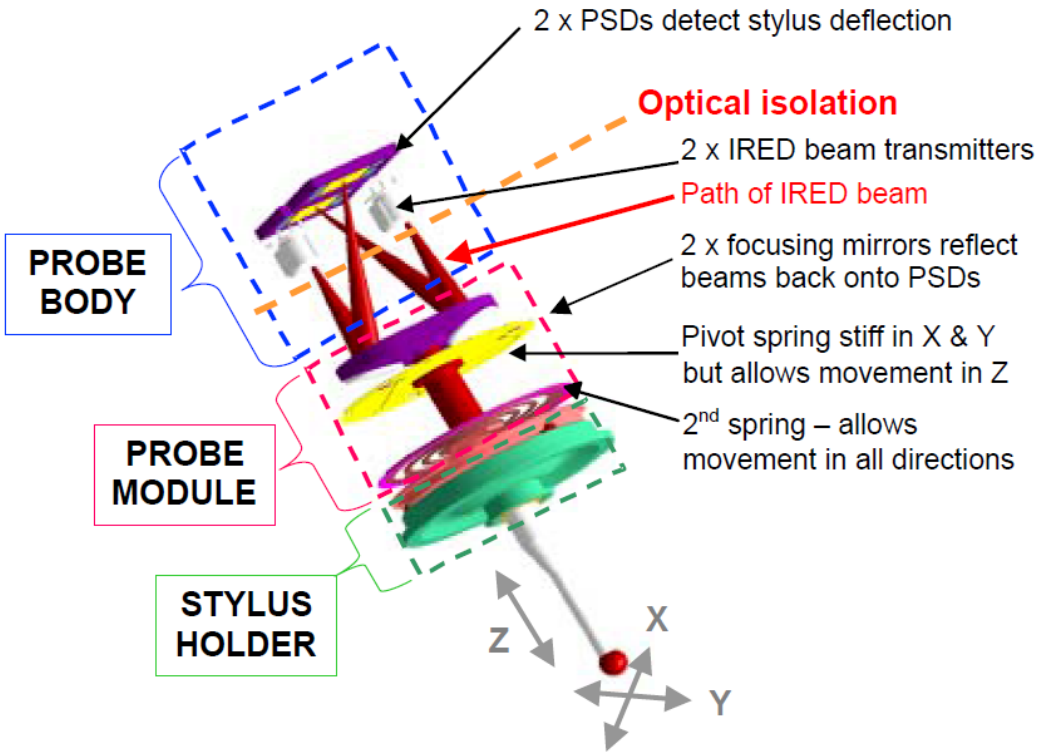

Figure 9. Principle of passive sensor Renishaw SP25. (Renishaw, n.d.-b., p. 8).

3.3 The principle of an active sensor

An active sensor is able to control the measuring force. The measuring force is regulated by servo motors inside the sensor. All three force coins have their own servo motor. A servo motor is used to create a counterforce to the weight of the stylus system and a force for the measurement direction. In scanning an active sensor, the measuring force does not increase or decrease as the scan progresses. Thus, the deflection problem of a probe is not unlike that with a passive sensor. The probe deflection problem is compensated by means of servo motors at the sensor (see Figure 11). Servo motors compensate the measuring force to remain the same throughout the measurement. The measuring force can be determined individually for each measuring probe (see Figure 12).

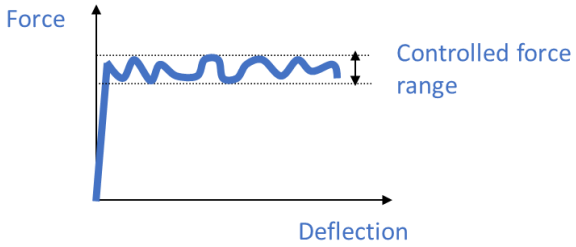

Figure 10. Active sensor scanning deflection.

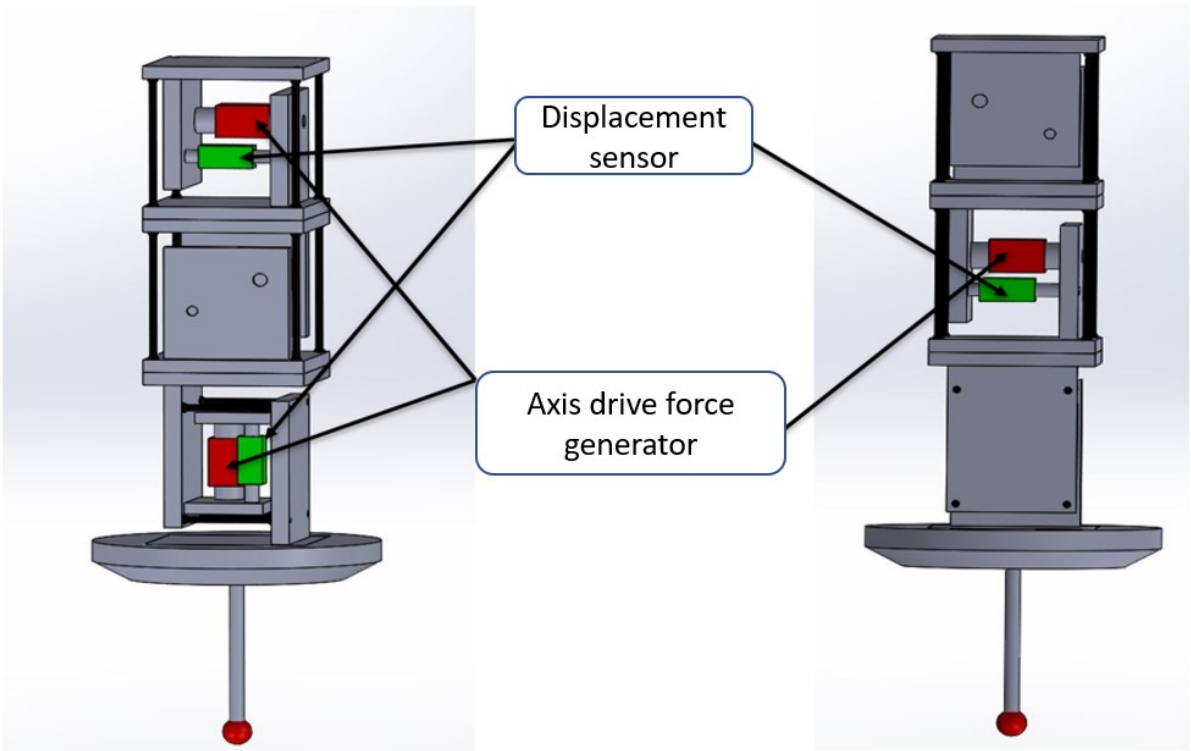

Figure 112. The principle of an active sensor.

3.3.1 The principles of active measuring heads

The active sensor compensates for the inaccuracy of the CMM's control with the help of servomotors and the form, orientation, or position errors of the element being measured. Servo motors move the probe from the surface of the element either forward or backward, depending on whether the measuring force increases or decreases. The active sensor moves the probe toward the surface to be measured before touching the surface. On contact, the probe moves to zero on the measurement scale and the point registers (see Figure 13). The same part can scan faster with an active sensor compared to a passive sensor. Different types of measurement point registration methods are presented in Figure 14 (AUKOM 2017a, 2017b).

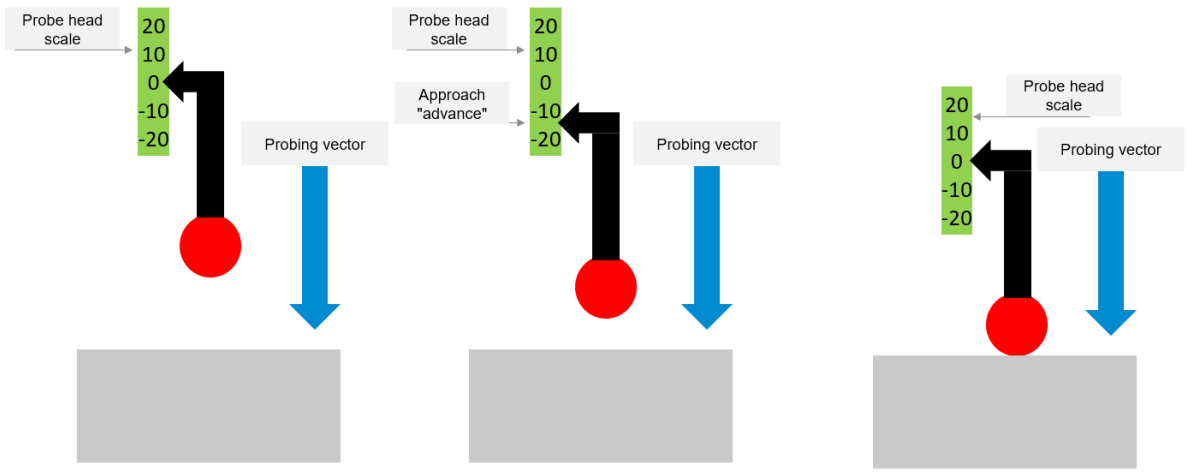

Figure 12. The principle of an active sensor in point registration.

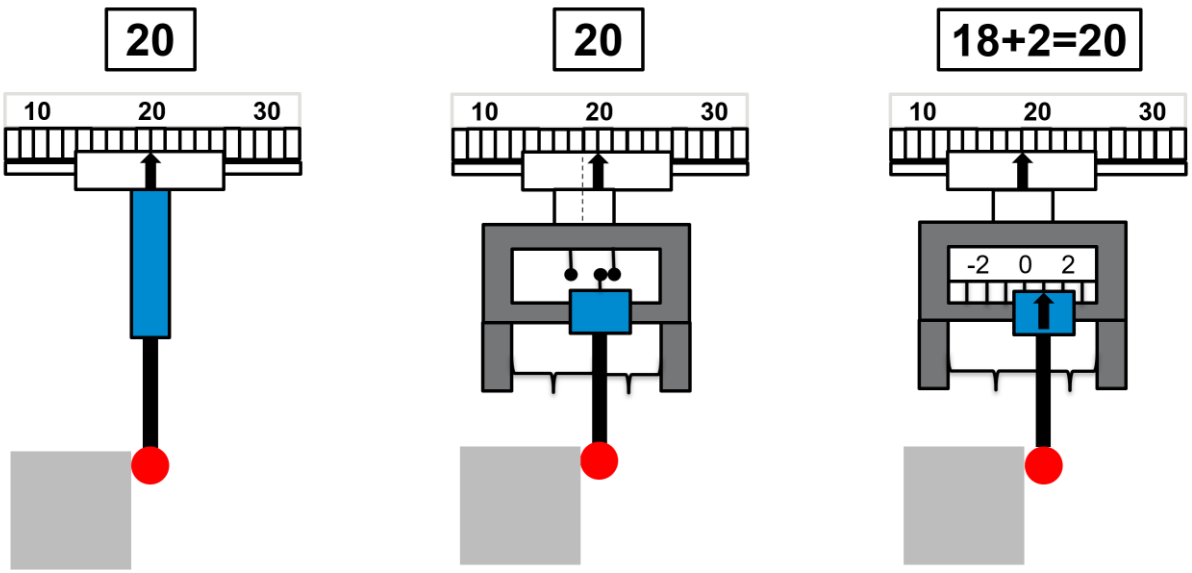

Figure 13. Three different principles of an active sensor.

3.4 The principle of the trigger sensor

The principle of the trigger sensors is a switch. When the measuring probe touches the part, the switch circuit breaks and the point is registered. The trigger sensor measures individual points, but the trigger sensor is unable to scan (see Figure 15) (AUKOM 2017a, 2017b).

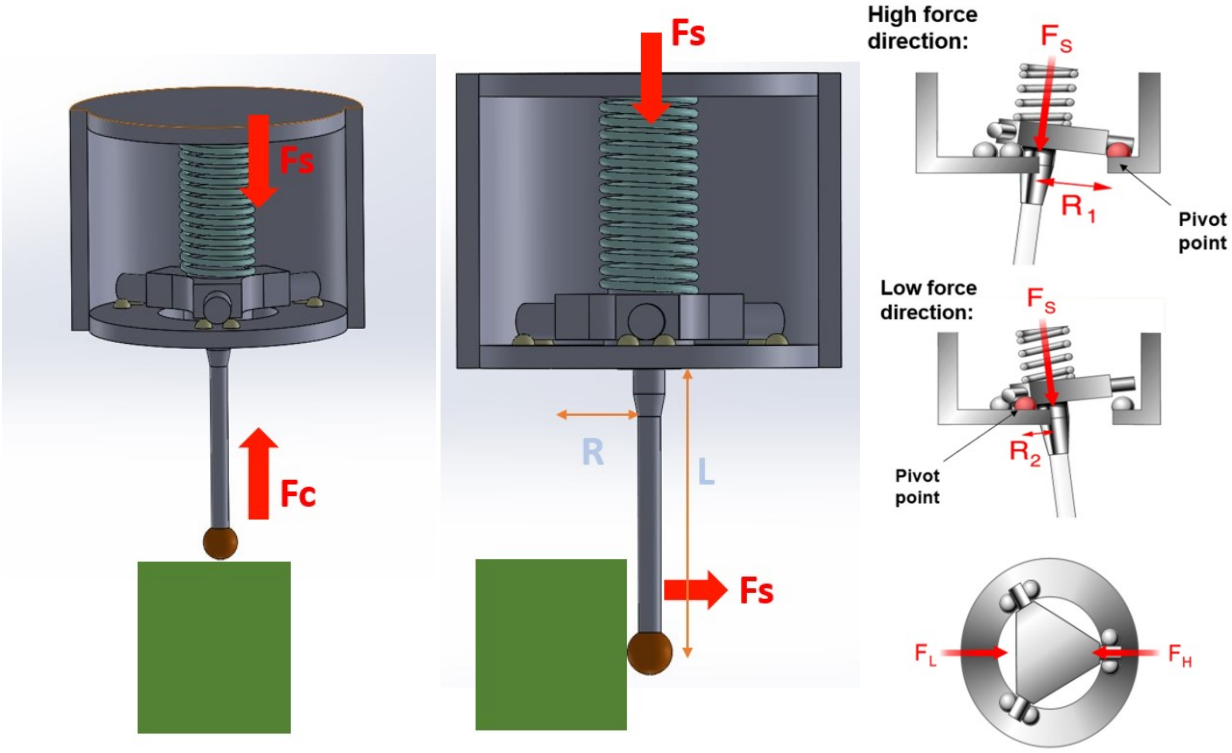

Figure 14. The principle of a trigger sensor.

3.4.1 Trigger form error

Due to the direction of the contact force and the triangular structure of the sensor, the deflection of the sensor varies in different contact directions. For example, when measuring a gauge ring, this error appears as a triangular form error. This error can be reduced by changing the measuring module to a low-force module, which is more sensitive than a normal force module. A more sensitive measurement module breaks the circuit with less force. The difference between normal and low-force modules is depicted in Figures 16 and 17 (Renishaw, n.d.-a., p. 16).

Typical pre-travel variation

Scale in µm

- XY plane

Probe:	TP6
Stylus:	50 mm
Pre-travel variation:	3.28 µm
Trigger force:	15 gram
Repeatability (2 Sigma):	0.5 µm

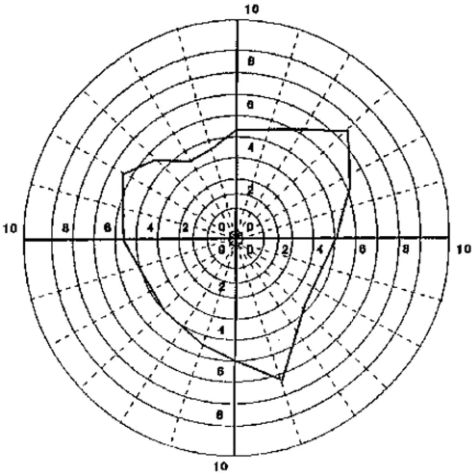

Figure 15. Trigger sensor form error with normal force (Renishaw, n.d.-a., p. 16).

Low lobing measurement

Scale in µm

- Trigger force is uniform in all directions
  - Very low pre-travel variation

Probe:	TP7M
Stylus:	50 mm M4
Maximum variation:	0.34 µm
Sensitivity:	HIGH

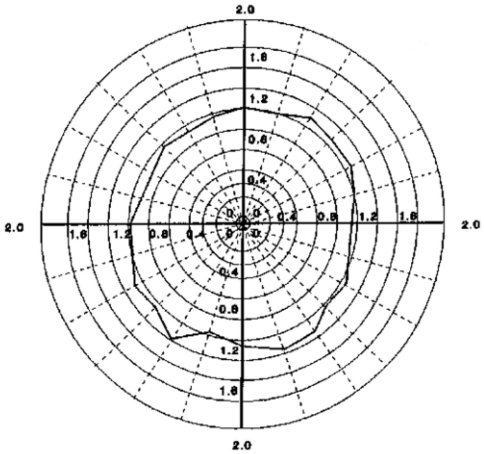

Figure 16. Trigger measuring head form error with low-force (Renishaw, n.d.-a., p. 28).

4 Uncertainty of measurement

The measuring capability of a coordinate measuring machine is understood as the suitability of a measuring machine for a task. When assessing suitability, the size, sensor, speed, measurement uncertainty, automation, and software is considered.

This chapter examines the measurement uncertainty of a CMM. The measurement uncertainty of a machine can be determined, for example, for a specific measurement task in accordance with ISO 15530-3:2011. This method of determining measurement uncertainty is an experimental method for measurements made using a CMM.

There are two types of uncertainty estimates. In the Type A procedure, measurement uncertainty *U (xi)* is assessed using statistical methods from multiple measurement results. For calibrations, this procedure applies if measurements have been made under the same conditions. In this case, the standard deviation of the mean of measurement results is used as an estimate of the standard uncertainty. If the number of repeated measurements is small, the uncertainty estimate is not reliable. In this case, if possible, the number of observations should be increased. If it is not possible to increase measurements, measurement uncertainty can be assessed on the basis of previous measurements made under the same measurement conditions. (JCGM 1000, 2008, p. 10.)

In the Type B procedure, measurement uncertainty *U (xi)* is assessed using non-statistical methods. In this case, the estimate should be based on other substantiated information. These include past measurement results, experience and general knowledge of the characteristics or device, manufacturer's specifications, calibration certificates, results obtained from other reliable documents, and table values obtained from manuals and their uncertainties. (JCGM 1000, 2008, p.11.)

In brief, the standard method is based on the measurement of calibrated workpieces or measuring norms. In turn, on the calibrated workpiece, at least 10 quantities should be measured. These quantities are, for example, distance, roundness, and parallelism. Measurements must be repeated at least 20 times and repeat standard deviation is calculated. Thus, the measurement uncertainty of the measurement is determined by the standard deviation of measurements and the results of calibration of the part.

The expanded measurement uncertainty, U, of the measured quantities is calculated from the uncertainties using a formula in which u_{cal} is the uncertainty component of the measuring device and u_p, u_b, and u_w are uncertainty components defined by the author of the measurement uncertainty. The calculation of measurement uncertainty in accordance with ISO 15530-3:2011 is presented in Table 1.

$$U = k \times \sqrt{u_{cal}^2 + u_p^2 + u_b^2 + u_w^2} \quad (1)$$

Contributor	Measurement of:			
	diameter mm	angularity mm	position mm	...
u_{cal}	0,001 0	0,002 0	0,001 5	...
u_p	0,000 8	0,001 6	0,000 7	...
u_w	0,000 2	0	0,000 5	...
u_b	0,000 2	0	0,000 5	...
$U\ (k = 2)$	0,003	0,006	0,004	...

Table 1. Calculation of measurement uncertainty (ISO 15530-3 2011, p. 19)

Another method to determine measurement uncertainty is to create a measurement uncertainty budget. An uncertainty calculation is traditionally prepared for a measurement by estimating uncertainties and their magnitudes. A few of the uncertainties are known and a few are estimated factors. The method is challenging and not very reliable. Table 2 provides an example of a measurement uncertainty budget (Tikka, 2007, p. 394).

KOORDINAATTIMITTAUSEPÄVARMUUDEN ARVIOINTI

Esimerkki!

EPÄVARMUUSBUDJETTI

Mittausepävarmuus esitetään muodossa U = A + KL, missä
pituudesta riippumaton osuus = A-termi, ja pituudesta L riippuva osa = K-termi
Kaikki epävarmuustekijät on seuraavassa käsitelty k = 2 -arvoina, eli 95 % luotettavuudella!

			Epävarmuustekijät µm:nä	
1. Satunnaisvirheet (saadaan toistuvuuskokeesta)			**A-termi**	**K-termi**
	2s	Toistuvuus (2 x keskihajonta (s) 20 mittauksesta)	2	(metriä kohti)
2. Epävarmuustekijät				
1)	u1	Lämpötilaerot ja lämpöpitenemiskertoimet		3
1)	u2	Kärkien kalibrointi (lika, taipumat, koneen dynamiikka)	1	
1)	u3	Kappaleen kiinnitys (muodonmuutokset, liikkuminen)	2	
1)	u4	Kappaleen suuntaus (asetus väärä)	1	5
1) 3)	u5	Kosketusmäärät, mittaustapa	2	
1)	u6	Peruselementti/toleroitu		
1)	u7	Kappalee pinnankarheus, pehmeys	2	
	u8			
2)	u11	Referenssi- eli kalibrointikuulan kalibroinnin epävarmuus	0.5	
2)	u12	Koneen 3D-paikoituksen epävarmuus	2.5	4
2)	u13	Koneen geometria (suoruus, tasomaisuus, kohtisuoruudet)		5
2) 3)	u14	Laskentarutiinit ja mittausohjelma	2	2
	u15			

1) Työkappalekohtaisia epävarmuustekijöitä
2) Erikseen kalibroitavia tekijöitä
3) Kappalegeometrian virheestä riippuva

KMK-epävarmuus saadaan summaamalla yllä olevat epävarmuustekijät neliöllisesti seuraavasti: SQRT($2s^2 + u1^2 + ... + un^2$)		**A**	**K**
		A ja K = µm,	**L = m**
	Kokonaisepävarmuus (k = 2 eli 95 %) U = ±	**5.3**	**+ 7.3**

Table 2. Example of the measurement uncertainty budget for coordinate measurement at *k*=2 (Tikka, 2007 p. 394).

The author's own method of determining the measurement uncertainty of a coordinate measuring machine in production conditions is based on ISO 15530-3:2011, the uncertainty budget calculation and guidance EA 04-2 for determining measurement uncertainty. Four uncertainties are required to determine uncertainty—the CMM, environment, stylus, and workpiece. Figure 18 presents the determination of the uncertainty of the coordinate measurement at coverage factor *k* = 2.

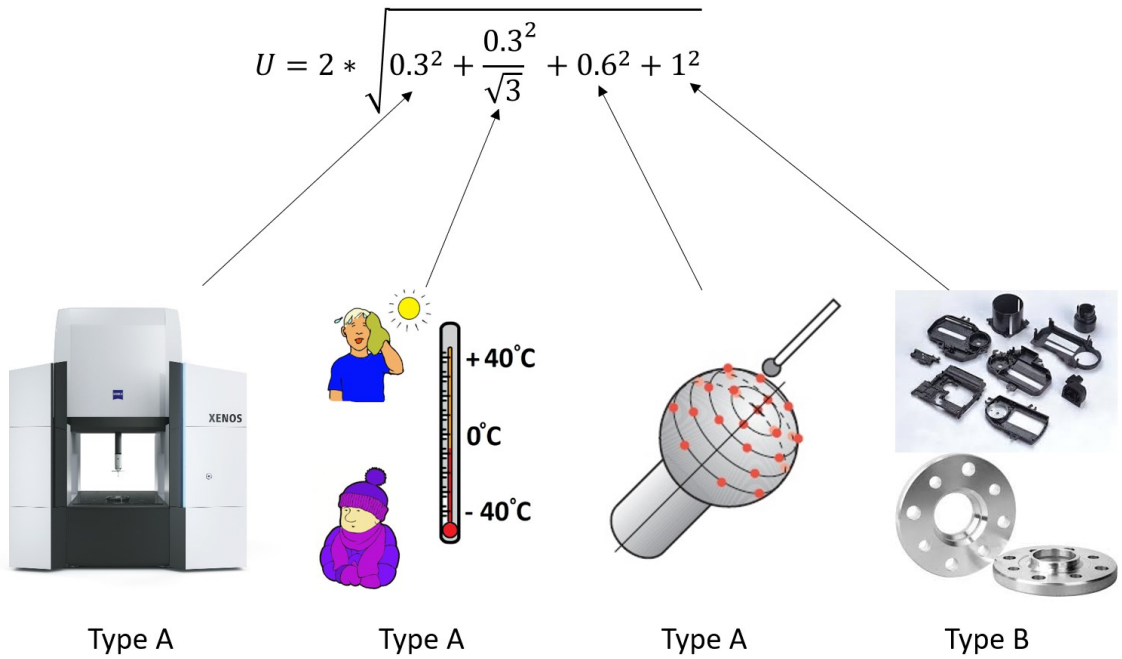

Figure 17. Determination of uncertainty for the coordinate measurement at *k*=2.

4.1 CMM uncertainty

In the opinion of the author, the MPE quantity according to ISO 10360-2:2009 is not sufficient to determine the uncertainty of the CMM. Verification of the measurement error in length measurement according to the ISO standard is suitable for reporting the measurement error of machines in technical sales brochures. For the determination of measurement uncertainty and periodic verification of the company, the roundness total (RONt) defined by Geometrical Product Specifications: Roundness Vocabulary and Parameters of Roundness (ISO 12181-1:2011) is a better quantity. The roundness dimension is measured by scanning from the gauge rings that are commonly known in periodic verification. This result is more representative of machine workshop measurements that are also done by scanning. The diameter of the gauge ring can be measured in individual points from the same gauge ring. It is also possible to determine the diameter of the ring from the scan data. This test is repeated three to five times with different sizes of gauge rings. Thus, the lengths measured at individual points on the gauge rings correspond to the standard MPE magnitude because the MPE is based on the distances of the individual points from each other. The MPE value does not represent the manner in which modern CMMs are used, because the method of

measurement used today is scanning. Individual point distances are rarely measured in the industry..

According to the author's perspective, there are two ways to determine the uncertainty of the CMM. 1) The measurement uncertainty is determined using the ISO 10360-4:2000 THP value. This measurement uncertainty covers one probe or one articulating position. The result represents a scanning measurement method. 2) Measurement uncertainty is determined using ISO 10360-4:2000 THP and Geometrical Product Specifications Acceptance and Reverification Tests for Coordinate Measuring Machines using single and multiple stylus contact probing systems using discrete point and/or scanning measuring mode (ISO 10360-5:2020) PFTM values. This measurement uncertainty covers multiple probes or multiple articulating positions. The result yields a scanning method of measurement.

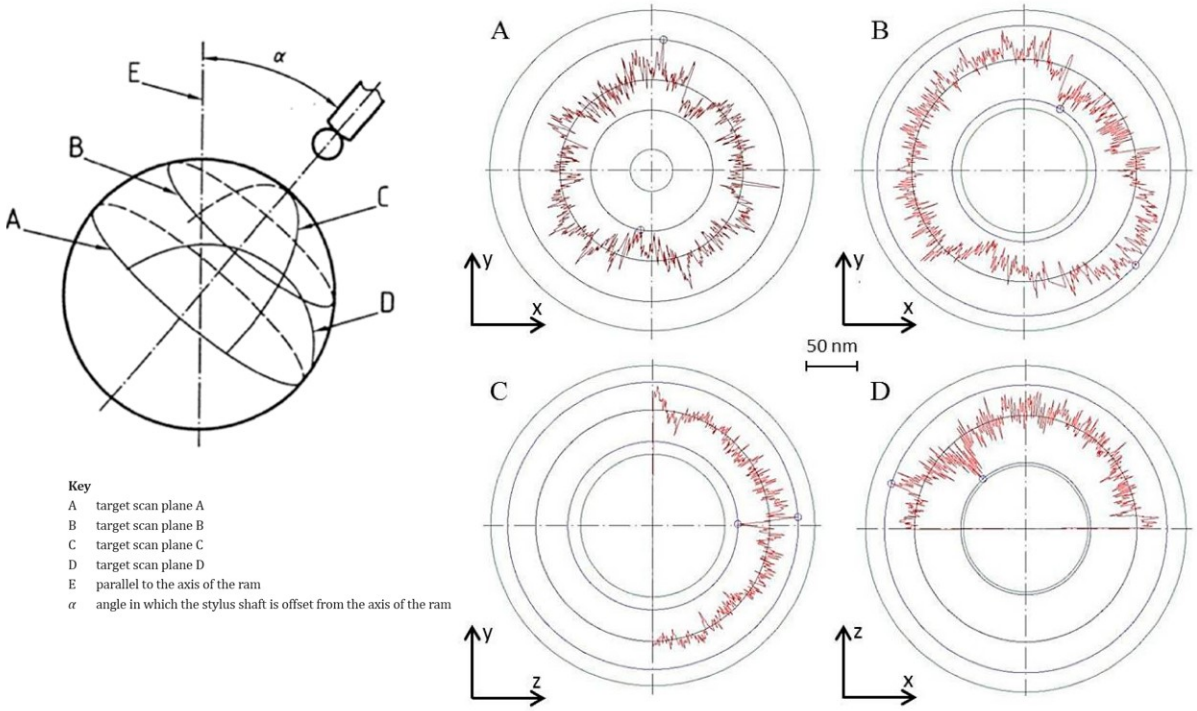

Figure 18. THP scan test (Thalmann et al., 2016 p. 6).

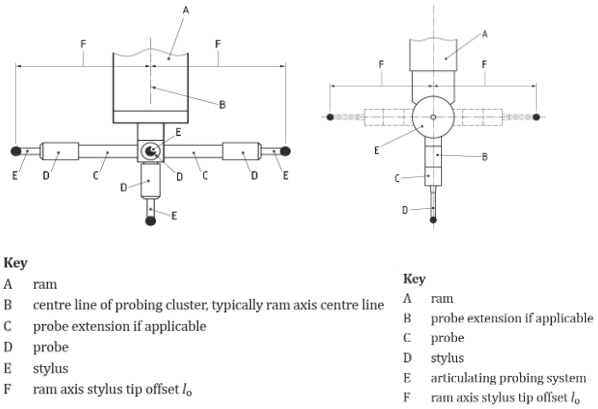

Figure 19. PFTM test (SFS-EN ISO 10360-5:2021, p. 25).

4.2 Environmental uncertainty

The determination of uncertainty in the measurement environment is based on two key accreditations—the Evaluation of the Uncertainty of Measurement in Calibration (EA 4-02) and Evaluation of Measurement Data-Guide to the Expression of Uncertainty in Measurement (GUM). The determination of environmental uncertainty estimates the temperature uncertainty of the room and the measurement object. Temperatures are rectangularly distributed. Uncertainty is also assessed for the thermal expansion coefficient. The uncertainty of the thermal expansion coefficient is a triangle distribution. The maximum length of the measurement object is required to determine the uncertainty. Moreover, environmental uncertainty should be calculated from these uncertainties (see Table 3).

Wp	Length of workpiece		110	mm						
δT	Uncertainty of temperature measurement	±	0.5	°C	0.289	°C		Rectangular		
ΔT	Uncertainty in room temperature measurement	±	0.5	°C	0.289	°C		Rectangular		
δλ	Part thermal expansion coefficient		0.000023	m/K	-2300	m/K				
δα	Uncertainty of correlation coefficient		0.000001	m/K						
	Correlation coefficient difference is assumed	±	2	m/K	0.816	m/K		Triangular		
δTxδλ					-663.953	nm	1	Normal	-663.953	
δTxδλxΔT			0	°C	0.289	°C	-1150	Rectangular	-331.976	
δT×δα×Wp			0		0.236	10^-6	110	Special	25.927	
								U=	1.49	µm

Table 3. Environmental measurement uncertainty.

The uncertainty determination according to EA4-02 may be too heavy for use in a small machinery shop. By measuring the temperature of the measuring object several times during the measurement and calculating the standard deviation of the temperature, the temperature uncertainty is simpler to determine. In determining uncertainty, the standard deviation is multiplied by the length of the part. Another factor of uncertainty is the estimated temperature measurement uncertainty multiplied by the thermal expansion coefficient of the measurement object. The reduced environmental uncertainty is presented in Table 4.

Collection time	Temperature sensor 1 [°C]	Temperature sensor2 [°C]
start	19.338	19.448
midle	19.478	19.428
end	19.478	19.458

Temperature avarage	Tave	19.438	°C	
Temperature min/max	Tminmax	0.14	°C	
Length of workpiece	Wp	110	mm	
Uncertainty of temperature measurement	δT	0.5	[°C]	
		0.289	[°C]	
Part thermal expansion coefficient	δα	-1150	m/K	
	δα×Tminmax	-161		Rectangular
	Wp×δT	31.754	10^-6	Special
	U=	0.33	µm	

Table 4. Environmental measurement uncertainty.

4.3 Stylus uncertainty

The sigma value of probe calibration is one of the factors of measurement uncertainty. Depending on the software used, there are different probe calibration routines. There are three types of probe calibration routines: 1) The calibration sphere is scanned at two different speeds; 2) 25 pieces of individual points are measured on the calibration sphere (see Figure 21); and 3) at its simplest calibration sphere, six points are measured.

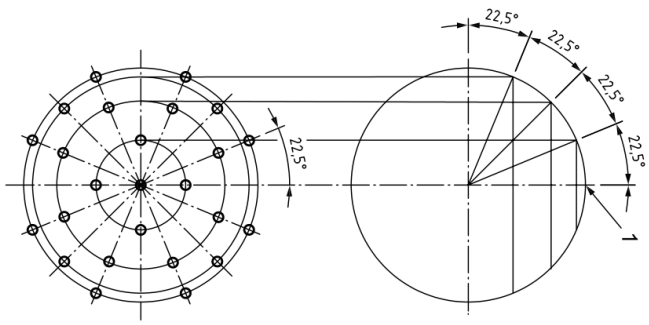

Figure 20. Probing 25 points (ISO 10360-5:2021, p. 12).

4.4 Part uncertainty

The uncertainty of the measurement object, the part being measured, is the uncertainty of type B. The uncertainty estimate is based on past measurement results, experience, part shape, material, wall strengths, and flexibility of the part.

4.5 Calculation of measure uncertainty

From the four abovementioned uncertainties, the measurement uncertainty of the measurement can be calculated. The first three uncertainties are type A uncertainties. A type A uncertainty can be determined using statistical methods. Table 5 presents the uncertainty calculation for one probe in the table on the Table 5A and for multiple probes in the table on the Table 5B. The difference between these two calculations is that in the case of a single probe, the sigma value of the calibration of the probe is used as an uncertainty factor, and a measurement with multiple probes uses the PFTM of the CMM calibration certificate as an uncertainty factor.

Table 5A

One stylus/probe		4.91 µm	
THP	Environment	Probe sigma	Part
1.6	1.49	0.5	1
A-type	A-type	B-type	B-type

Table 5B

Multiple stylus/probe		9.16 µm	
THP	Environment	Probe sigma	Part
1.6	1.49	3.9	1
A-type	A-type	B-type	B-type

Table 5. Calculation of the CMM measurement uncertainty.

In comparison measurement, a similar reference is used, which represents the comparison part. The method of measurement is the same in both, so the measurement result obtained from a known normal reference directly reveals the machine's ability to measure correctly. Moreover, repeating measurements provides a good idea of process dispersion. This is based on the actual errors and repetitiveness of the machine and takes into account the errors of probe calibration, machine temperatures, machine stability, and part effect.

The simplest comparison measurement can be done by scanning with a measuring ring. The scanning measurement of two different types of sensors using the gauge ring is presented in Figures 22 and 23. The sensors used in comparison measurement are the passive sensor based on the laser principle and the active sensor based on force coins. Both measurements have almost the same accuracy class CMM. In the ISO 10360-2:2009 calibration certificate, the measurement uncertainty of CMM is indicated as 0.5L/500 and 0.5L/1000. The form plots are filtered using cut-off values UPR 50 and UPR 60. These measurements are made in the XY plane. This position is easy because the gravity is parallel to the probe. It would be good to also indicate the same measurement at the YZ and XZ planes. The filtered result of the laser operates the passive sensor is 1.0 µm. This result is greater than the result of the standard 10360-2:2009. The MPE value of the passive sensor is 0.55 µm. The filtered result of the active sensor based on force coins is 0.3 µm, which is less than the standard 10360-2:2009 MPE result declared for the CMM. Moreover, the MPE value is 0.6 µm..

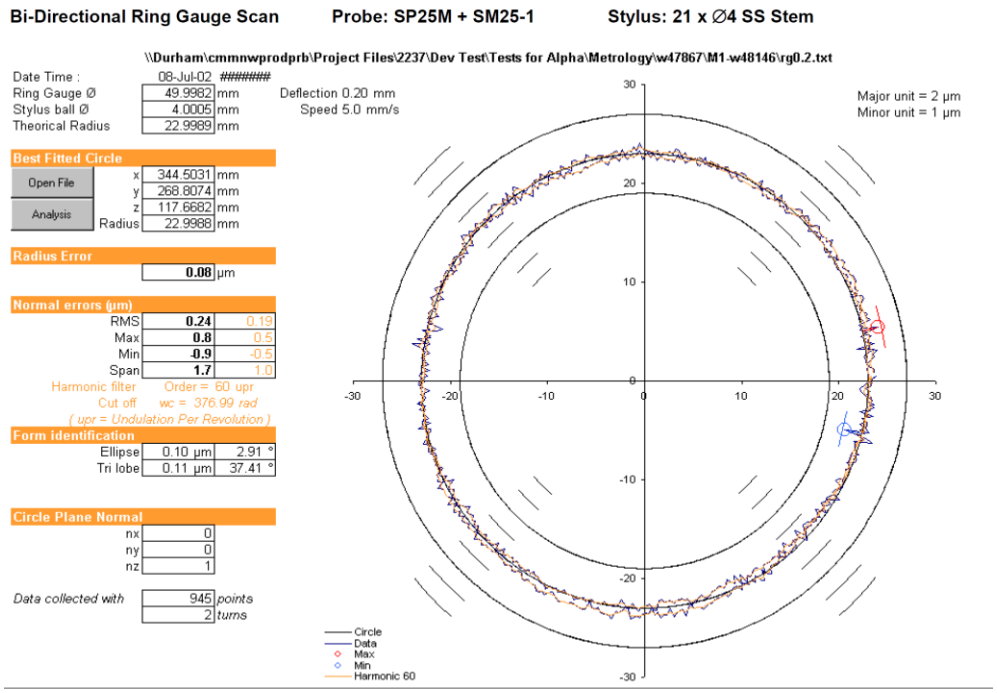

Figure 21. Performance of the laser operating passive sensor (Renishaw, n.d.-c., p. 8).

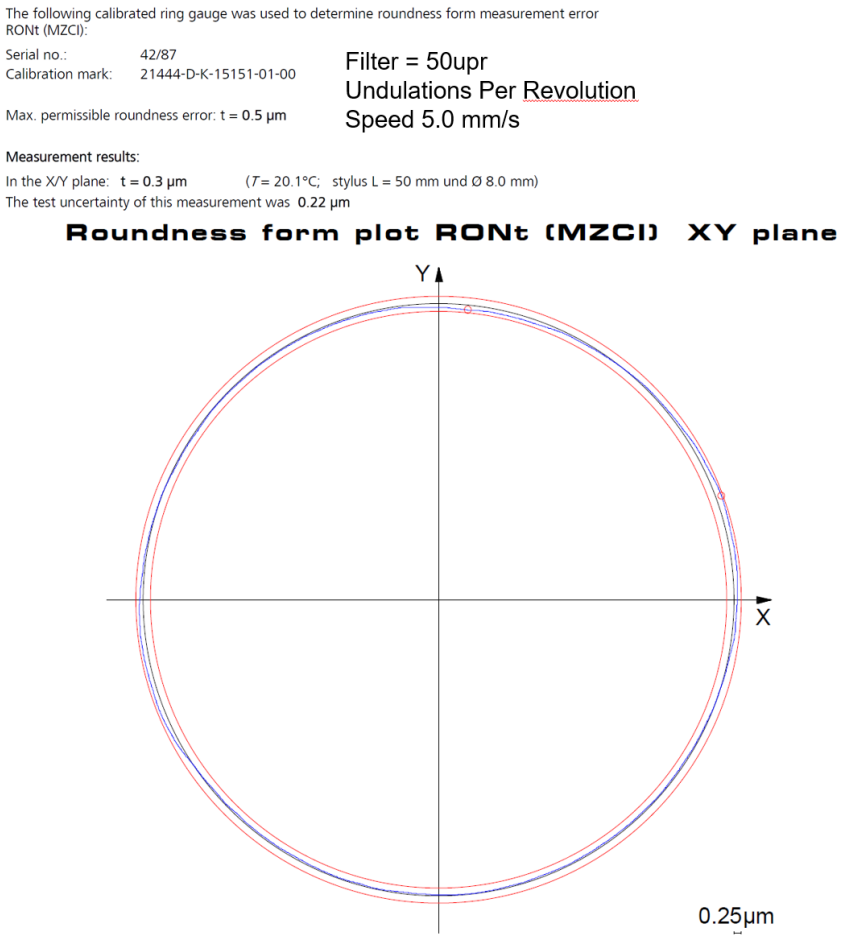

Figure 22. Performance of the active sensor based on the force coin principle.

5 Filtering of Measurement Results

Before processing the filtering subject, it is a good idea to look at filtering and its causes. Figure 24 presents the waves and their magnitudes. With a CMM, approximately 50 first waves (1–50) are measured. These first 50 waves represent the form of the part. The magnitude of the form defect of elements—such as plane, cylinder, line, or circle—is expressed by geometric tolerances such as straightness, flatness, roundness, or cylindricity. The emergence of a form error in a part is due to, for example, a straightness error in the machine tool guide, the spindle bearing runout, or the part clamping forces. These form errors are copied to the workpiece through the cutting tool of the machine.

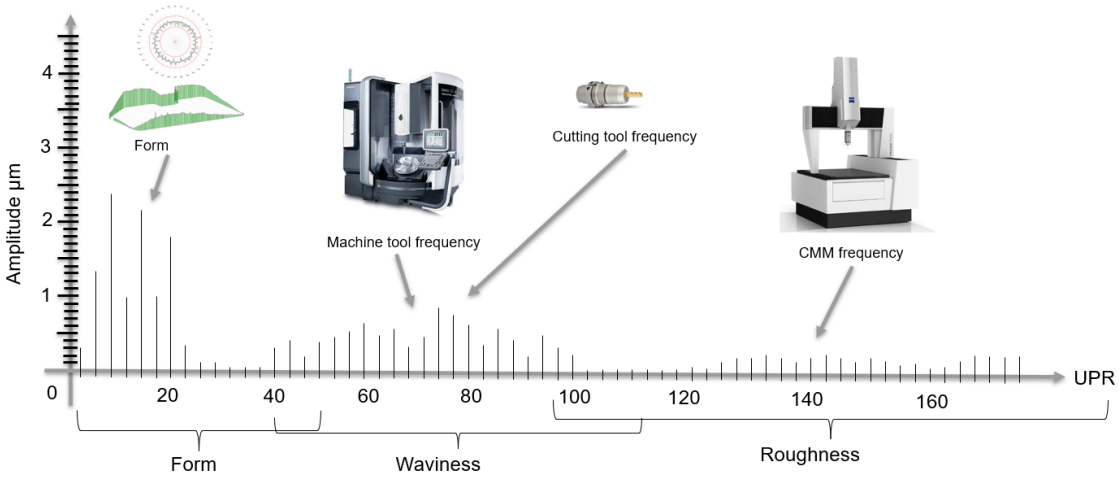

Figure 23. Waves and waves magnitudes.

The range between approximately 40 and 110 waves can be determined as waviness. Waviness must be measured with a form-measuring machine or surface roughness measurement device. The surface roughness measurement device must be a so-called “skidless” model. Devices that skid are not capable of measuring waviness. Waviness arises on the surface of the part, for example, from the vibration of a machine tool or a cutting tool.

Surface roughness begins from approximately 100 waves onward. There is no clear limit value for the end of the form or the onset of waviness. The same applies to the end of waviness and the beginning of surface roughness. Determination of the cut-off value is a very difficult question that is more philosophical in nature than metrological. Surface roughness waves form measurement data—for example, from CMM’s own

oscillation or friction between the probe and the workpiece. Friction causes oscillation, as the probe travels along the surface of the workpiece during a scanning measurement.

Once it is understood that there are three different quantities to be measured on the surfaces of the elements, the plots can be filtered to reveal the sheer form and eliminate waviness and surface roughness from the plot (see Figure 25). Traditional CMMs can only measure the form.

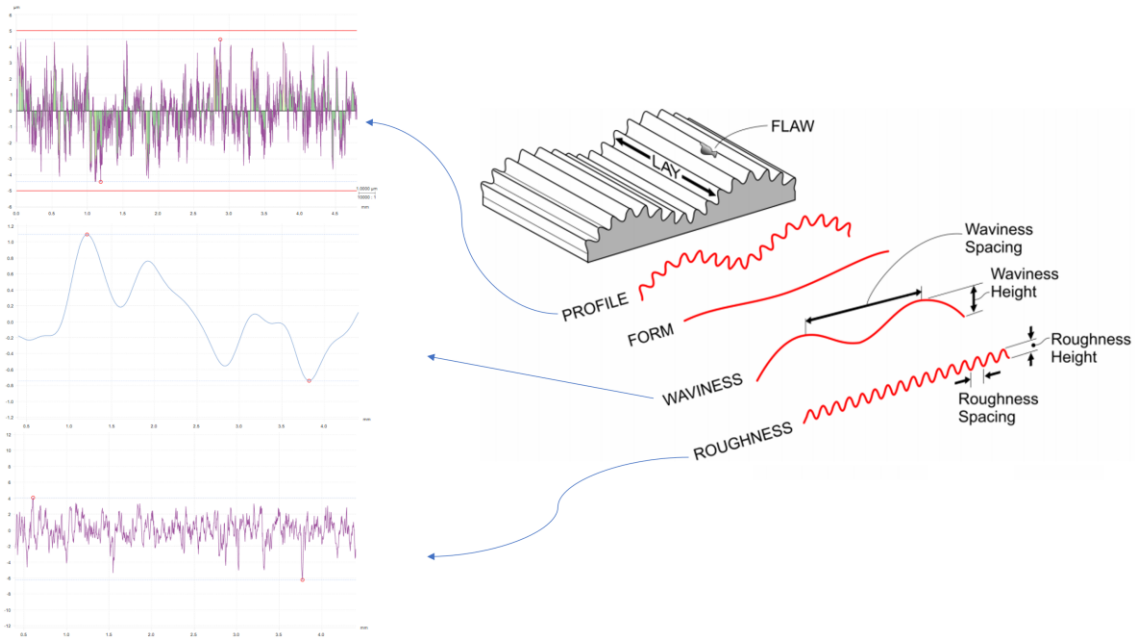

Figure 24. Form, waviness and roughness. (Original figure Adapa 2023; Modified by the author.)

Form, waviness, and roughness filters are discussed in the standard ISO 1101:2017 and in the standard series ISO 16610. When measuring the form, a low-pass filter is used. A band-pass filter is used for waviness and high-pass filter for surface roughness—for example, a long-pass filter eliminates short waves from measurement results.

The methods employed for measuring form and surface roughness are essentially the same. In measurement, it is common to use multiple measuring points to represent the entire surface. The user filters the measurement points to obtain only the information they want. For example, when examining surface roughness, the user retains a shorter wavelength for data analysis, but rejects long-wavelength data, because that information is not required. When measuring the form, the user filters from the short-

wavelength measurement data. In this case, in the measurement, the format is represented by long-wavelength data.

5.1 Harmonic waves

The distribution of a surface into its elements (spectrum) is called Fourier analysis. Modern measurement programs calculate them using a special, very fast algorithm, called the “Fast Fourier Transformation” (FFT25). Fourier analysis was invented by French mathematician and physicist Jean Baptiste Fourier (1768–1830).

To better understand Fourier analysis, it is important to note the following assumption. Surface structure is an overlay of sinusoidal vibrations of varying frequency and amplitude. These vibrations are described as harmonious. This implies that each surface is broken down into sinusoidal vibrations. The frequency of these vibrations increases for mathematical filtering, beginning with the first harmonic vibration. Harmonic vibrations have only one vibration over the entire measuring length, which can be, for example, up to 1000 harmonic vibrations. With each harmonic vibration, it is necessary to see how well the vibration fits the surface profile and how high the amplitude is. All harmonic vibrations are presented in the graph at their height (Roithmeier, 2006 p. 58; Roithmeier, 2009 pp. 60–61; Zeiss Academy, 2018, p. 58).

The Fourier plot is a histogram that depicts how strong different periodic deviations (harmonic vibrations) are in the measurement data. A Fourier plot is presented in Figure 26.

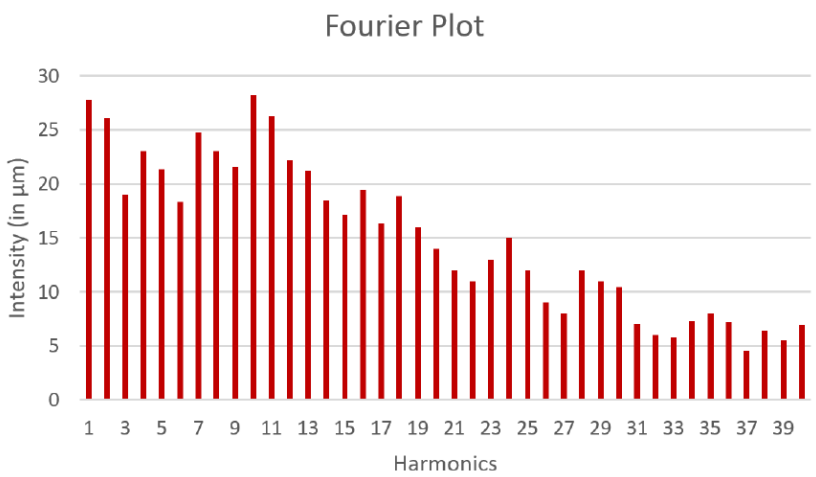

Figure 25. Fourier plot. (Zeiss Academy 2020, p. 86).

In reality, handling harmonic vibrations is not quite as simple as either 1 or 0. One implies that from the cut-off value of the measurement data, all values are filtered out. Zero implies that measurement data is not filtered. Then, from the measurement data, a Fourier plot is generated using the Fourier transform. This function is based on a continuous integral transformation that attenuates harmonic vibrations according to the curve. The filtering is not perfect because the Fourier transform preserves some harmonic vibration from the measurement data above and below the selected cut-off value. Thus, the remaining measurement data above and below the cut-off value is attenuated. A low-pass Gaussian filter of 15 UPR is presented in Figure 27 (Zeiss Academy Metrology, 2020, p. 88).

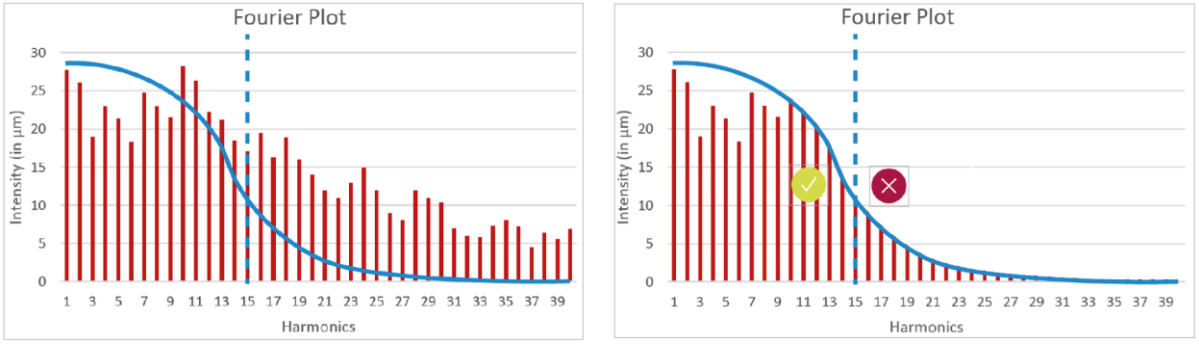

Figure 26. A low-pass Gaussan filter of 15 UPR. (Zeiss Academy 2020, p. 88).

5.2 Evaluation of the Gaussian filter

Carl Friedrich Gauß (1777–1855) was a German mathematician, astronomer, and physicist. Among other things, he developed the method of LSQ as part of the matching method and discovered a normal distribution in the form of a bell curve, which is called the Gaussian bell curve in his honor.

The Gaussian filtering calculus is a standard filtration method for measurements made using a coordinate measuring machine. This filtration method is standardized and widely used. It uses a moving average weighted by the Gaussian function. The mathematical algorithm for measuring shape is usually based on the 50% Gaussian algorithm (see Figure 28). All points measured from an element are weighted and

recalculated using the Gaussian bell curve. Gaussian filtering calculates the average for each measured point. Adjacent points are included in the calculation depending on the assumed width of the bell curve corresponding to the boundary wavelength. Filtration is stronger or weaker depending on the width of the bell curve (see Figure 29). Further, the emphasis is not linear, but follows the Gaussian bell curve (Roithmeier, 2015, pp. 47–50; SFS-EN ISO 16610-21, 2011, p. 2).

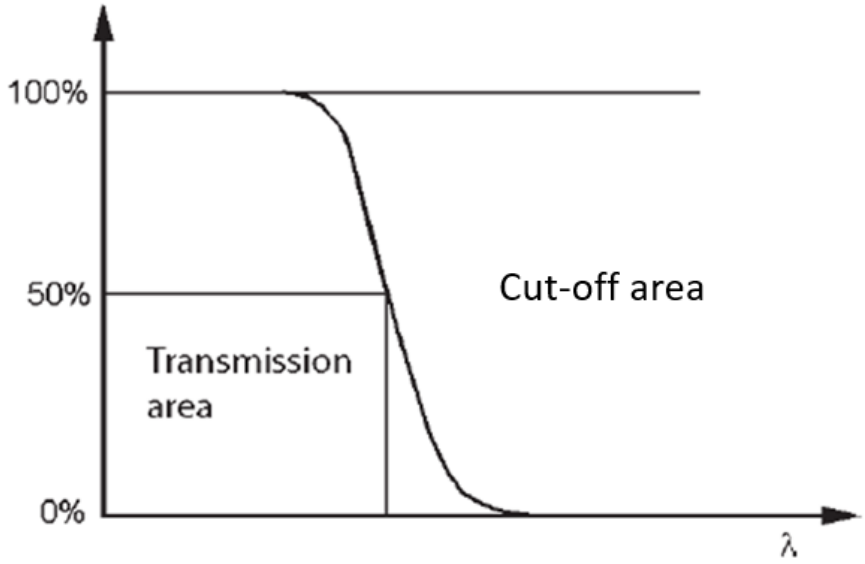

Figure 27. Gaussian 50 % algorithm. (Zeiss Academy 2018, p. 58)

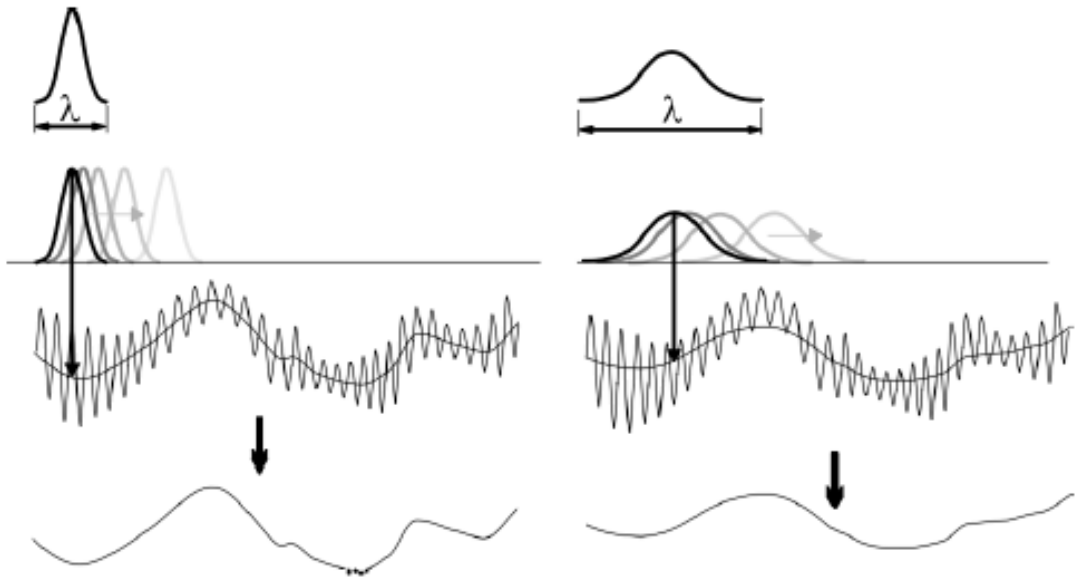

Figure 28. Width of the bell curve. (Zeiss Academy 2018, p. 57).

5.3 Undulations per revolution (UPR)

Historically, the default filter cut-off value for roundness measurement has been 50 undulations per revolution (UPR). While this filter cut-off value may be suitable for numerous use cases, it is not suitable for all. Fortunately, the new standards allow users to assign a filter cut-off directly to the drawing for any form tolerance. Choosing the correct filter cut-off value should be based on the element to be measured. The designing, manufacturing, and quality staff are all responsible for determining filter cut-off related to requirements, recording internal standards, and imposing filter limit values for internal and external vendors. Thus, the choice of filter has a significant impact on the analysis of measurement results.

The form filter of roundness is usually defined in terms of angle rather than length or distance. Determining the filter value is complicated by the fact that specifications are not given directly in degrees but in units. This unit is UPR. Many users choose 50 UPR as the standard value. This implies that the filter length is 1/50 of the circle, which is a 7.2-degree sector of the circle. A simple formula for the circumference of the cylinder is $\pi \times d$. A 4-mm diameter cylinder has a circumference of 12.57 mm and a filter value of 7.2-degrees yields an arc length with a surface of 0.25 mm. Further, a cylinder with a 20 mm diameter has a circumference of 62.83 mm, and a filter value of 7.2 degrees would correspond to an arc of 1.26 mm long (Schuetz, 2020).

When there are two waves in the hole, the plots showing the hole look like an oval. If the hole plots look triangular, there are three waves in the hole. A hole with four waves look like a square shape and so on. Due to manufacturing techniques, in reality, the hole is never perfectly round or oval. The shape of the hole contains many waves. Figure 30 and 31 depict the shape of the holes with one-lice different waves. Figure 32 presents the shape of the hole that contains several waves.

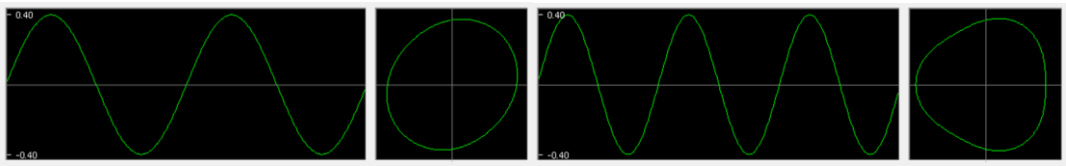

Figure 29. Left: A hole with two waves. Right: A hole with three waves.

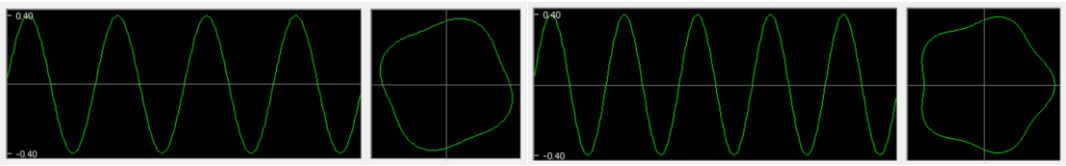

Figure 30. Left: A hole with four waves. Right: A hole with five waves.

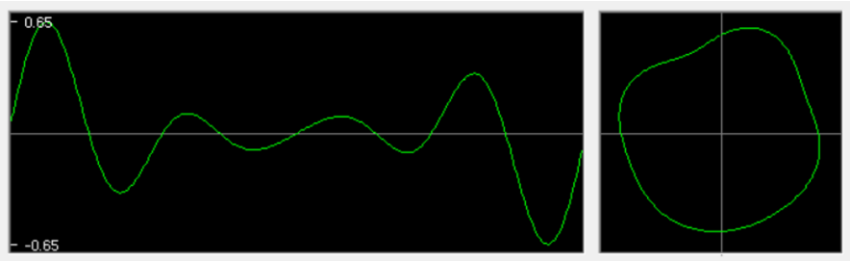

Figure 31. The real situation: there are many waves in the hole.

It is important to specify cut-off values for a filter. When filtering roundness, the cut-off value is indicated in undulation-per-revolution (UPR). For flatness and straightness, the cut-off value is given as the wavelength (Lc). The cut-off value determines the value from which forward waves are filtered out. In addition, it is important to specify the type of filter. There are three types of filters—low-pass filter, band-pass filter, and high-pass filter. In Figure 33, plots of the same measurement data are depicted from left to right with different filter cut-off parameters. The first from the left is a low-pass filter with the limit value UPR 50-. The middle one is a band-pass filter with a cut-off values of UPR 50- and UPR -150. The one on the extreme right is high-pass filter and its cut-off value is UPR -150. The cut-off value for long-wave pass filter UPR 50- provides a good representation of the hole form error. With a high-wave pass filter in the plot with a limit value of UPR -150, the form error is eliminated (ISO 1101, 2017, p. 291).

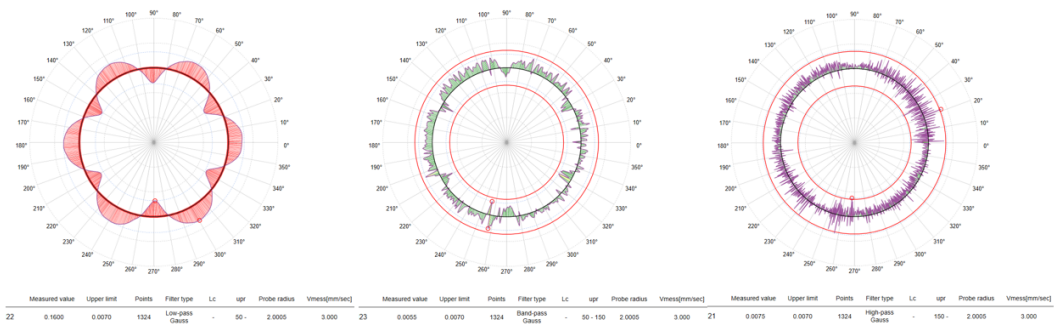

Figure 32. Low-pass filter UPR50-, band-pass filter UPR50- and UPR-150.

5.4 Wavelength (Lc)

Form filters can be confusing. For example, when measuring surface roughness, the filtering settings are in inches or millimeters. When a filter is set to 0.8 mm, this is generally understood to imply that surface deviations below 0.8 mm are considered surface roughness, while surface deviations greater than 0.8 mm are considered form defects. Many users choose 0.8 mm as the typical standard cut-off value. This implies that the filter is viewed in 0.8 mm length periods (see Figure 34).

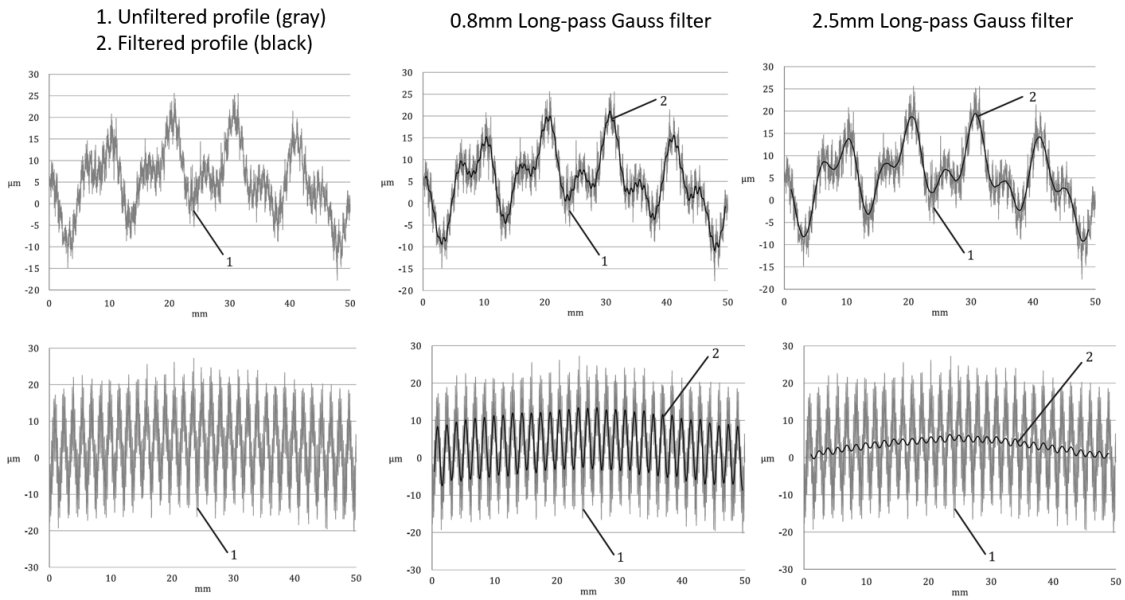

Figure 33. Surface profile low-pass filter (ISO 1101, 2017, pp. 283–288).

A mathematical algorithm—for example, 50% Gaussian filtering—is either a cut-off *Wc* or Lc. The UPR cut-off is used for circular and cylindrical elements. The wavelength cut-off value (Lc) is used for line and plane elements. The Lc cut-off value can be converted to the UPR cut-off value using the following formulas, where d is the diameter of the element (Roithmeier, 2015, p. 48):

$$Lc = \frac{\mathrm{d}\pi}{Wc} \qquad (2)$$

$$Wc = \frac{d\pi}{Lc} \tag{3}$$

Form filtrations used to measure straightness or flatness are defined as the length of the measurement period. Normally, for filtering mathematics, the Gaussian and Spline filters are used. The Gaussian and Spline filters work in basically the same manner. The profile is divided into short and long waves. When measuring the form, short wavelengths are ignored. The cut-off value indicates the value from which the measurement data is split in half (ISO 1101, 2017, pp. 134–136).

As already mentioned above, the Gaussian and Spline filters are very similar methods. Figure 35 presents the filtering of raw data using Gaussian and Spline calculation methods. The main drawback of Gaussian filtering is the inaccuracy of open profiles. Closed profiles, such as a circle, can be easily analyzed using a Gaussian filter. During line or plane filtering, the result is distorted at the beginning and end of the profile. Spline filtering computes the values of measurement points using third-order polynomial matching. With polynomial fitting, the beginning and end of the profile do not have the same distortion, which is the problem with the Gaussian filtering (Roithmeier, 2015 pp. 47–50).

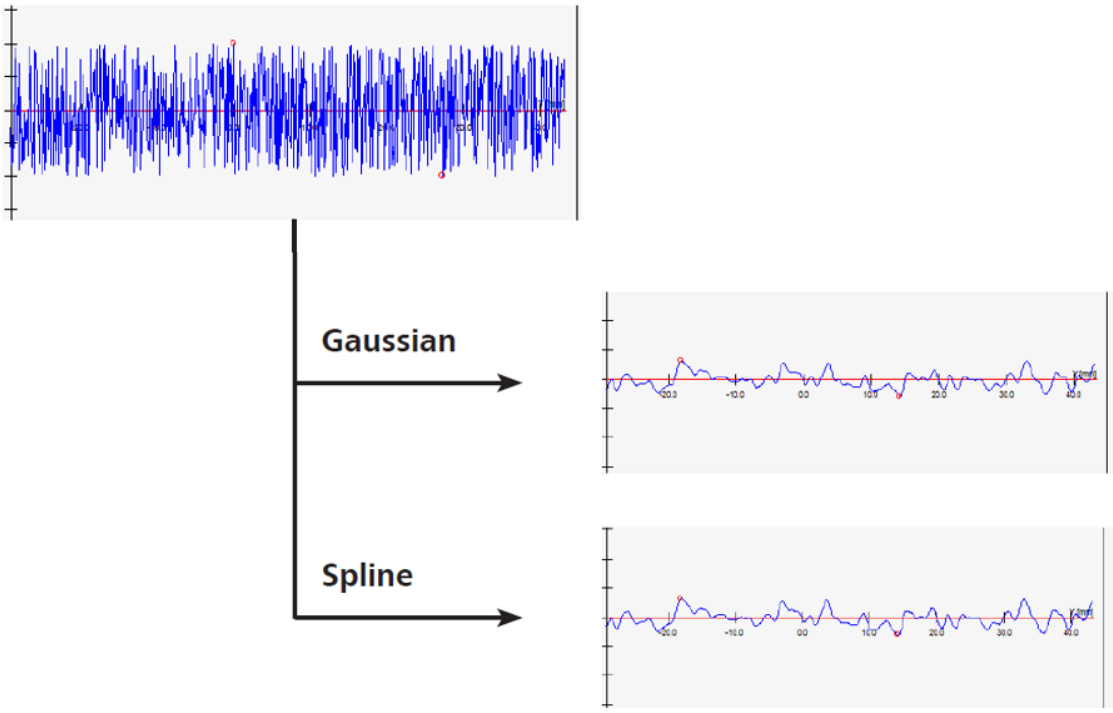

Figure 34. The Gaussian and Spline filters (Zeiss Academy, 2021, p. 10).

The size of the workpiece surface affects the selection of the filtration limit value. This implies that the length of the wave changes along with the surface area of the part. A shorter deformation is suitable for a 50 mm × 50 mm plate than a 1000 mm × 1000 mm plate. Thus, the filter cut-off must be modified according to the level size.

5.5 ISO 16610 standard series

The ISO 16610 standard series is a comprehensive set. All filter methods are barely ever available in the CMM manufacturer's software. Another problem is the lack of familiarity with filtering. In Finland, only a few CMM users conduct measurements with scanning. The problem is that CMM operators do not know how to use scanning effectively or the measuring machine is not capable of scanning. When an element is measured in individual points, then the points are negligible. The low score is due to the slowness of the method. Further, the low number of measuring points results in the measurement points not being sufficiently close to allow us to use filtering.

Roughly, it can be said that Spline and Gauss filtrations are used in tactile measurement and morphological filtering is used in camera measurement.

ISO 16610 standard series includes the following standards:

- Part 1: Overview and basic concepts
- Part 20: Linear profile filters—Basic concepts
- Part 21: Linear profile filters—Gaussian filters
- Part 22: Linear profile filters—Spline filters
- Part 28: Profile filters—End effects
- Part 29: Linear profile filters—Spline wavelets
- Part 30: Robust profile filters—Basic concepts
- Part 31: Robust profile filters—Gaussian regression filters
- Part 32: Robust profile filters—Spline filters
- Part 40: Morphological profile filters—Basic concepts
- Part 41: Morphological profile filters—Disk and horizontal line-segment filters
- Part 49: Morphological profile filters—Scale space techniques
- Part 60: Linear areal filters—Basic concepts

- Part 61: Linear areal filters—Gaussian filters

- Part 71: Robust areal filters—Gaussian regression filters

- Part 85: Morphological areal filters—Segmentation

- Part 26: Linear profile filters—Filtration on nominally orthogonal grid planar data sets

- Part 27: Linear profile filters—Filtration on nominally orthogonal grid cylindrical data sets

- Part 45: Morphological profile filters—Segmentation

- Part 62: Linear areal filters—Spline filters

- Part 69: Linear areal filters—Spline wavelets

- Part 70: Robust areal filters—Basic concepts

- Part 72: Robust areal filters—Spline filters

- Part 80: Morphological areal filters—Basic concepts

- Part 81: Morphological areal filters—Sphere and horizontal planar segment filters

- Part 89: Morphological areal filters—Scale space techniques

5.6 Mechanical filter

Whenever measured by tactile measurement, the sphere diameter of the probe acts on the workpiece surface as a mechanical filter. When increasing the diameter of the probe sphere, it should be accepted that the probe is no longer capable of measuring short waves. In this case, no small shapes are obtained in the measurement results. These short waves are caused, for example, by the vibration of the machine tool during the machining of the workpiece. Thus, the probe radius functions as a mechanical high-pass filter (see Figure 36).

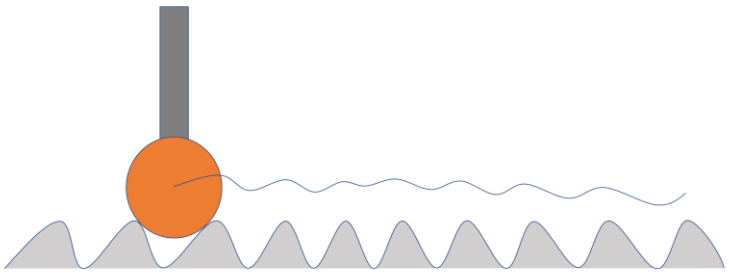

Figure 35. Mechanical high-pass filter.

The probe diameter is selected for measurement so that it is possible to measure the expected wavelength on the surface of the part. Figure 37 presents the ratio of the length of the wave to the diameter of the probe.

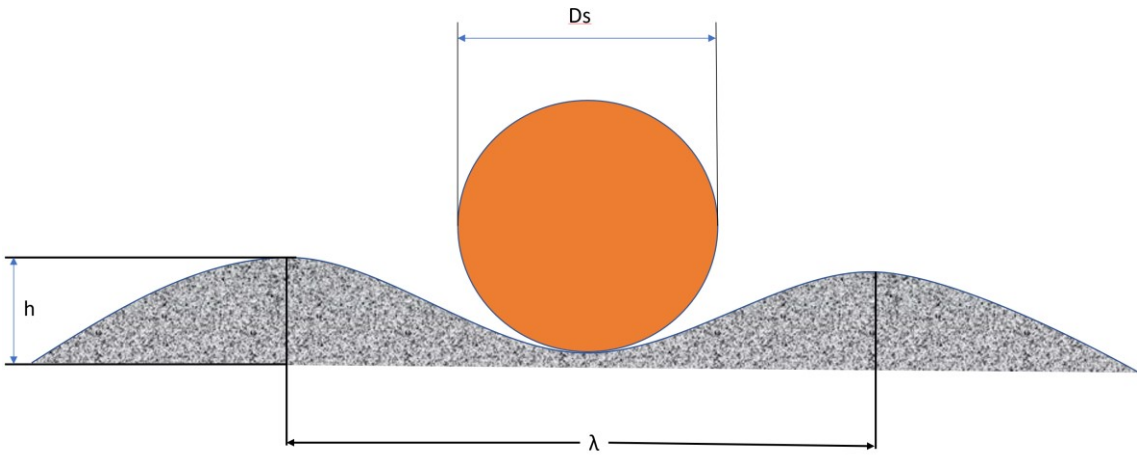

Figure 36. Largest admissible stylus diameter without influencing the amplitude height.

5.7 Outlier filter

It is important to know that in addition to mechanical and mathematical form filters, there is the so-called outlier filter. Outlier filtering removes random “error points” from measurement data. Thus far, automatic average-based filtering methods have been implemented in software to eliminate error points. Another more laborious method is to manually remove the error point from the measurement data. In this case, the operator removes points from the measurement data. Thus, the outlier filter is like a double-edged sword, as even bad workpieces become good workpieces through sufficient filtering.

5.7.1 Manual outlier filter

In handmade filtering, the operator removes the outlier point from the measurement data. An argument for removing a point can be that the value of a point differs markedly from the population average. Figure 38 presents the outlier point in the measurement of the diameter of the circle.

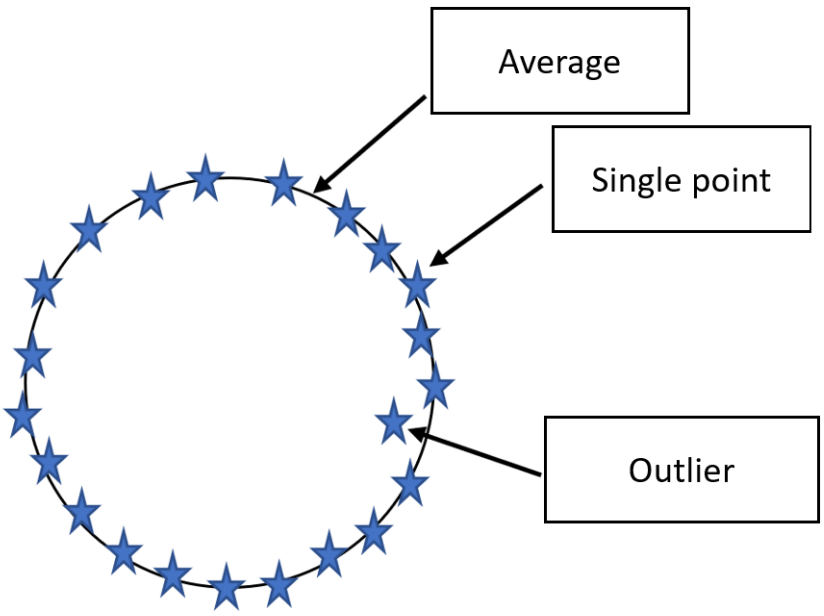

Point number	Point Value
1	20.001
2	20.001
3	20.003
4	20.001
5	20.004
6	20.001
7	19.999
8	19.999
9	19.997
10	20.000
11	20.001
12	20.003
13	19.985
14	20.001
15	19.998
16	20.001
17	19.999
18	20.002
19	20.003
20	20.000
21	19.999
22	20.002

Figure 37. Outlier point.

5.7.2 Automatic outlier filter

In an industrial environment, for example, a robotic cell often wants to utilize4 automatic outlier filtering. A point that differs from the average of a set of points can then be considered a “garbage point.” This point is filtered according to the cut-off value given to the software. For example, the limit value for outlier filtering can be given as a 3σ limit.

Using 3σ, 99.7% of the points remain for the element calculation and 0.3%—that is, points that exceed 3σ—are filtered out. The automatic filtering function is presented in Figure 39. First, an average is calculated for a set of points. Next, a Gaussian bell is matched for the set of points. Finally, there is a sigma limit value for both sides of the mean. The limit value to the mean of the distance is given by the shape of the Gaussian bell. In the bottom three images, from left to the right, are the limits 3σ, 2σ, and 1σ. The points that fall between the lines are used to calculate the measured element and the points left outside the lines are filtered out.

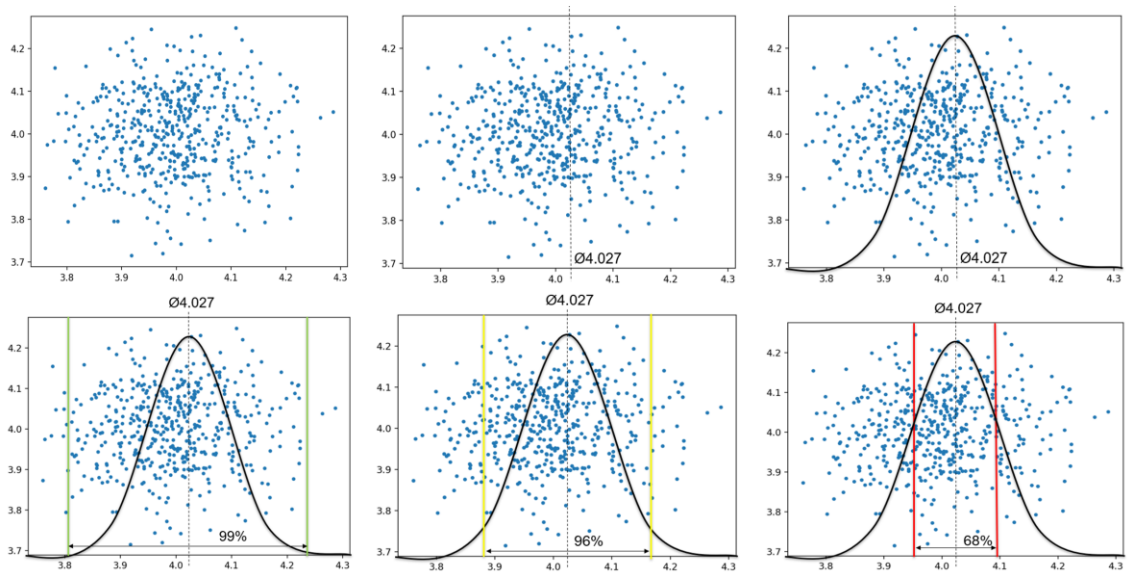

Figure 38. Automatic outlier filter.

Figure 40 contains the raw data of the scanning measurement. The roundness value is 0.0224 mm when the measuring points are 809 pcs. Using the raw data in a roundness plot reveals that the measurement data has three outliers, with peaks toward the center of the circle.

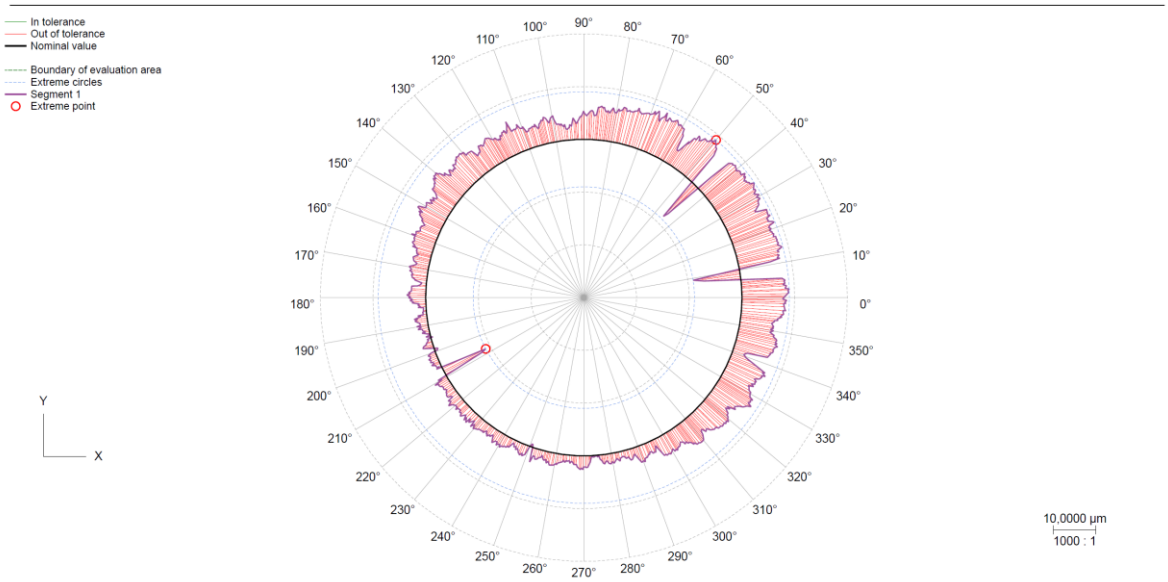

	Name	Measured value	Upper limit	Pisteet	Suodintyyppi	Lc	upr	Kärjen säde	Vmitt[mm/s]	Laskentamenetelmä
○	Ympyrämäisyys1	0,0224	0,0000	809	Ei suodatusta	-	-	1,0043	5,000	Pienin elementti

Figure 39. Raw data.

Figure 41 presents the same measurement data, but the outlier points have been automatically filtered out of the data. The data has been filtered with the 3σ. The points deviating from the average result are cut off. The roundness value changes significantly from the previous result; the roundness is 0.0078 mm and there are 779 points remaining.

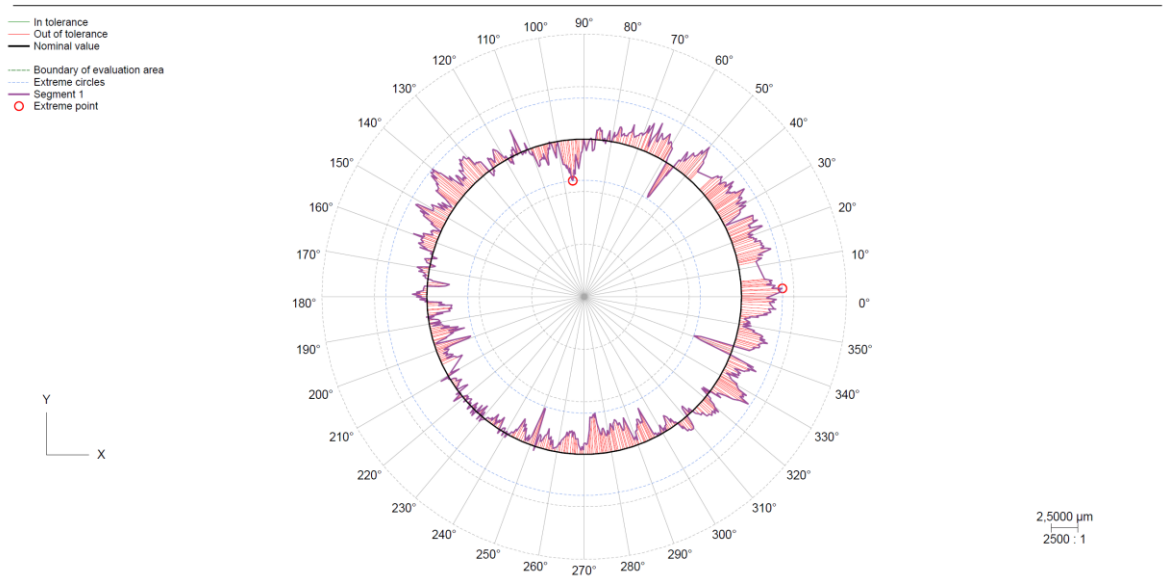

	Name	Measured value	Upper limit	Pisteet	Suodintyyppi	Lc	upr	Kärjen säde	Vmitt[mm/s]	Laskentamenetelmä
○	Ympyrämäisyys1	0,0078	0,0000	779	Ei suodatusta	-	-	1,0043	5,000	Pienin elementti

Figure 40. The roundness outlier filter.

Figure 42 has the same measurement data, but outlier points and the Gauss filter have been filtered out. The Gauss filter cut-off is 50 UPR. In this case, the roundness value changes again. The roundness is 0.0063 mm and there are still 779 points. Now the plot no longer has a sharp short wave and is much more readable. From the plot, you it is evident that the hole is “oval.” This implies that there are two waves in the hole. To ascertain the magnitude of the two waves, the Fourier plot in Figure 43 must be examined.

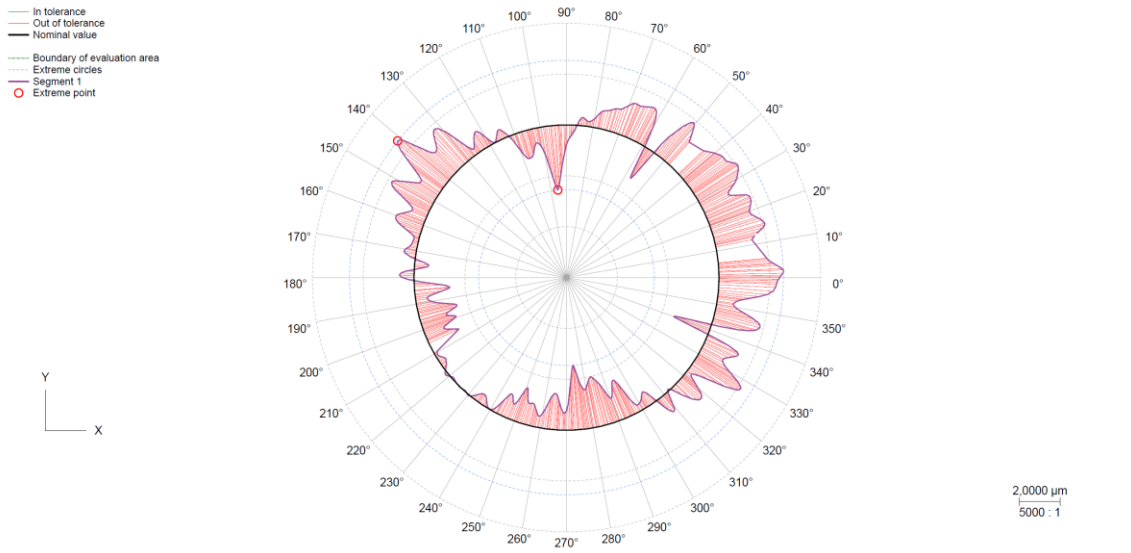

	Name	Measured value	Upper limit	Pisteet	Suodintyyppi	Lc	upr	Kärjen säde	Vmitt[mm/s]	Laskentamenetelmä
	Ympyrämäisyys1	0,0063	0,0000	779	Karheuden... Gauss	-	50 -	1,0043	5,000	Pienin elementti

Figure 41. The roundness outlier and Gauss 50 UPR filter.

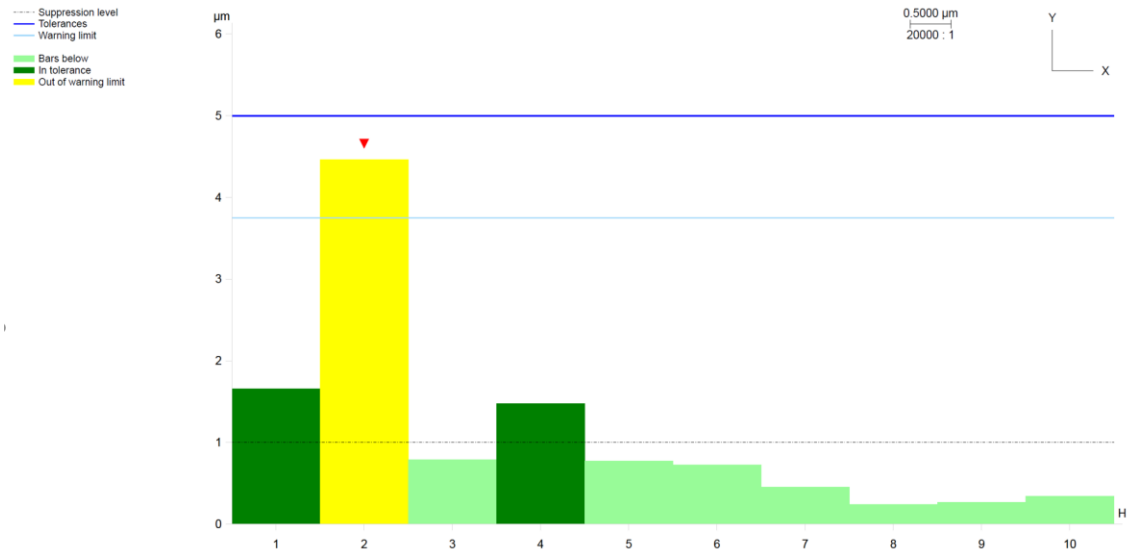

	Name	Measured value	Upper limit	Points	Filter type	Lc	upr	Probe radius	Vmess[mm/sec]	Evaluation method
	Waviness Ø12 -x-y	4.4609	5.0000	388	Low-pass Gauss	-	50 -	1.5016	5.000	Minimum Feature

Figure 42. Fourier plot.

6 Measurement Parameters

In this section, I present measurements made with active and passive sensors. A test part and different size gauge rings have been used for the measurements. Using the test part, I show how the number of measuring points affects the result of a diameter or form. The results presented in the plots of the measurements made on the test part are the averages of five measurements. I monitored the stability of five repeat measurements using a range value. The diameter and form error of the hole were measured by scanning at 4, 5, 6, 7, 8, 9, 10, 20, 40, 80, 160, 320, and 640 measuring points.

The calculation of the form error of the test part and measuring rings was performed by employing the Chebyshev method. The number of measuring points depends on the form error of the element to be measured. Roughly, it may seem that four points are sufficient to measure the form of a measuring ring, but this can be true only in the CAD model. The Chebyshev method is presented in the drawings according to ISO 1011:2017 with the letter C. The diameter calculation is the maximum inscribed feature. Figure 44 presents the calculation methods. ISO 1011:2017 specifies that the maximum inscribed feature is GX in the drawings. There were five gauge rings in the test measurements.

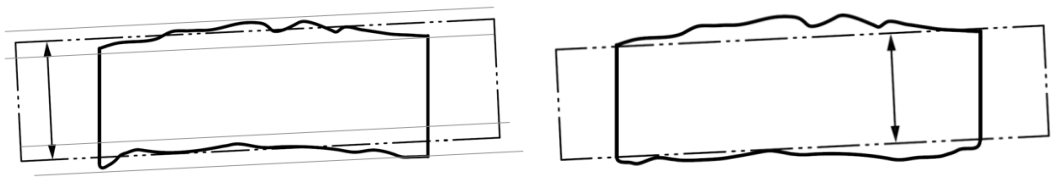

Figure 43. Left: The Chebyshev (C) method. Right: The maximum inscribed feature (GX) method (ISO 14405-1, 2016, p. 69-70).

6.1 The test part

The following measurements are made on the test part. The test part is a so-called NAS that is used to check the condition of machine tools. For example, the part is worked on a milling machine and then measured with a CMM. The NAS part reveals

errors in position, perpendicularity, roundness, and straightness of the machine axles. It is also possible to check the accuracy of the machine's ability to milling the circle. Figure 45 depicts a drawing of the NAS used in the test.

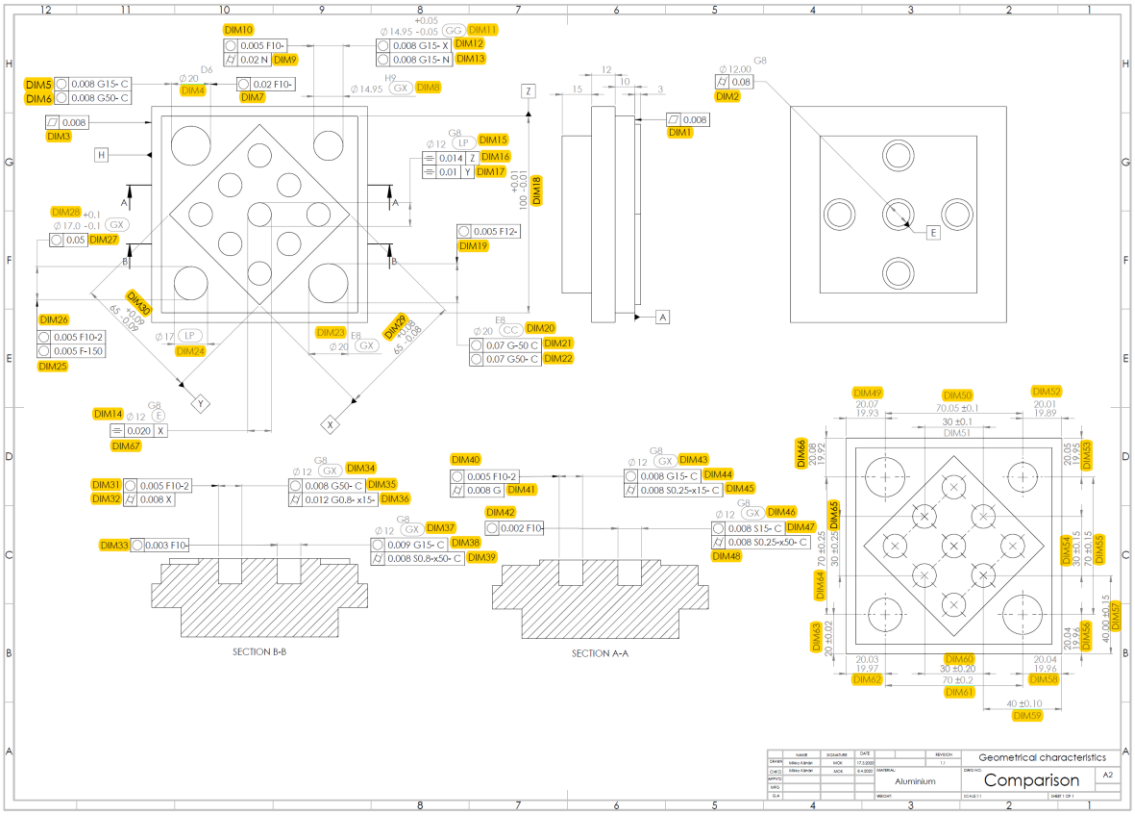

Figure 44. Drawing of the test part.

6.1.1 Roundness—hole with a small form error

In Figure 16, the shape error of the hole is presented on the vertical axis and the number of measuring points are presented on the horizontal axis. When the hole has small form error, the number of points of measurement does not affect the result of the form error. The smallest form error of the hole presented in Figure 46 can be calculated by six measuring points and the largest by twenty measuring points. The form error range is only approximately 3 µm. The range is lower than the total measurement uncertainty of the CMM.

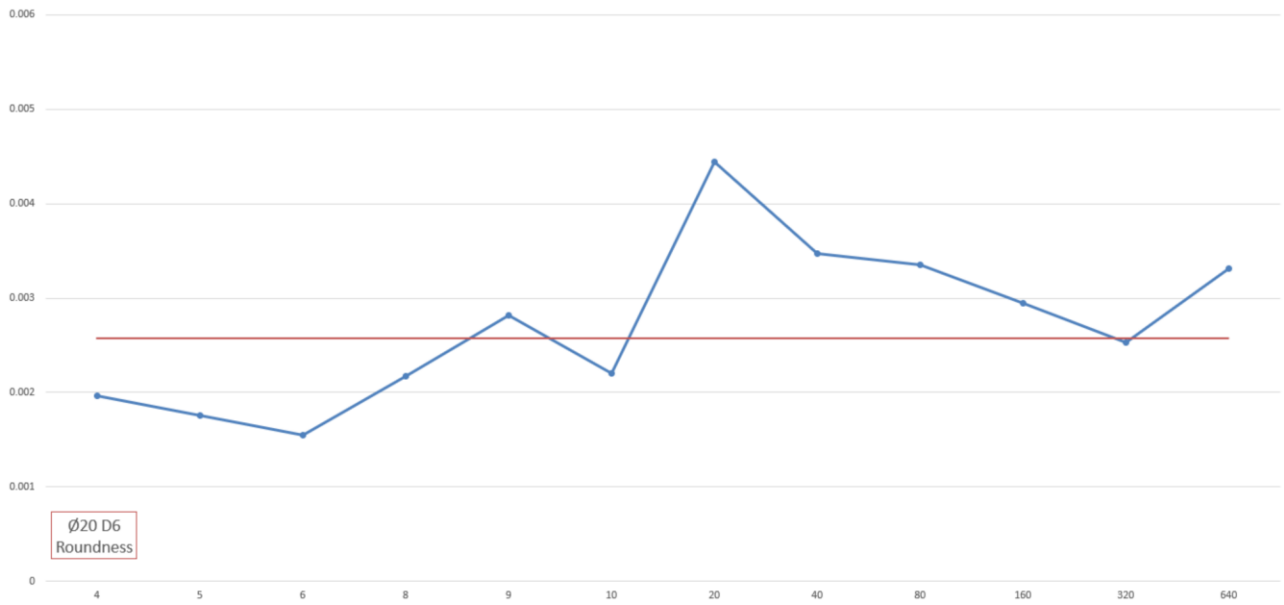

Figure 45. Variation in the roundness result at different measurement point quantities.

6.1.2 Roundness—hole with a big form error

In Figure 47, the form error of the hole is presented on the vertical axis, and the number of measuring points is presented on the horizontal axis. In the case in which the hole has a large form error, the effect of the number of measurement points is large in relation to the result of the form error. The smallest form error of the hole presented in Figure 47 can be calculated by five measuring points and the largest by eighty measuring points. The range of the form error is approximately 0.145 mm. It can be determined from the plot that the number of measuring points is sufficient to measure a form error after 160 measuring points. The result no longer changes and this point can be considered as a limit value for this measurement, after which the result of the form error barely changes even if more measurement points are added to the measurement.

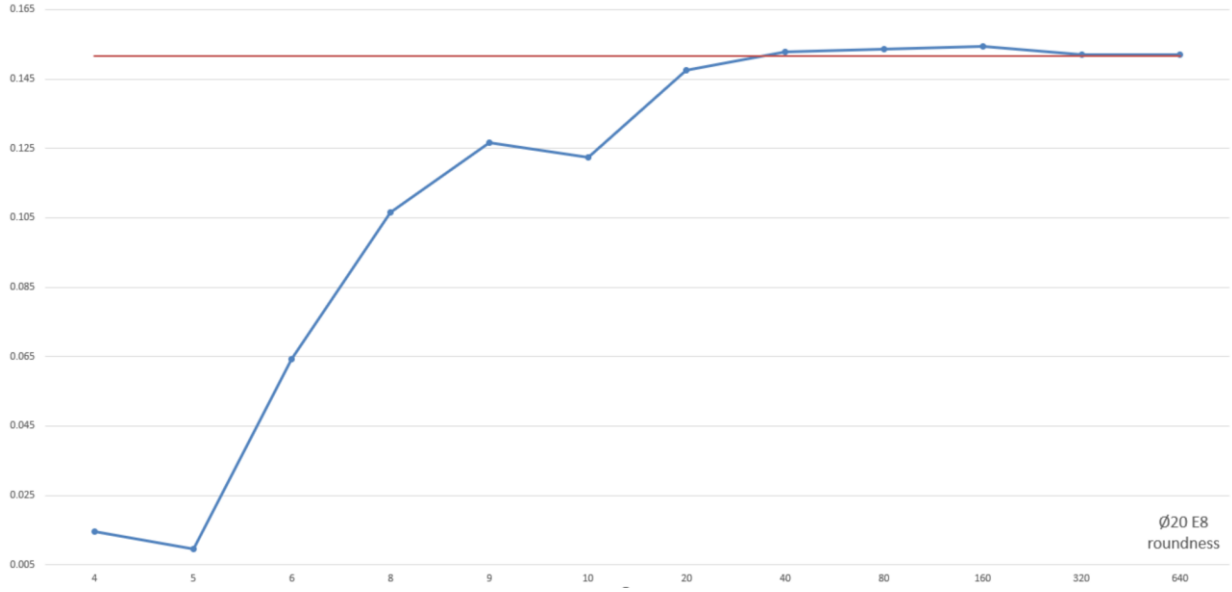

Figure 46. Variation in the roundness result at different measurement point quantities.

6.1.3 Diameter—hole with a small form error

A hole diameter is presented on the vertical axis in Figure 48. The horizontal axis, in turn, depicts the number of measuring points. When the form error is small, the size of the diameter does not vary when the number of measuring points varies. The diameter range is less than 2 µm. Thus, the range is lower than the total measurement uncertainty of the CMM.

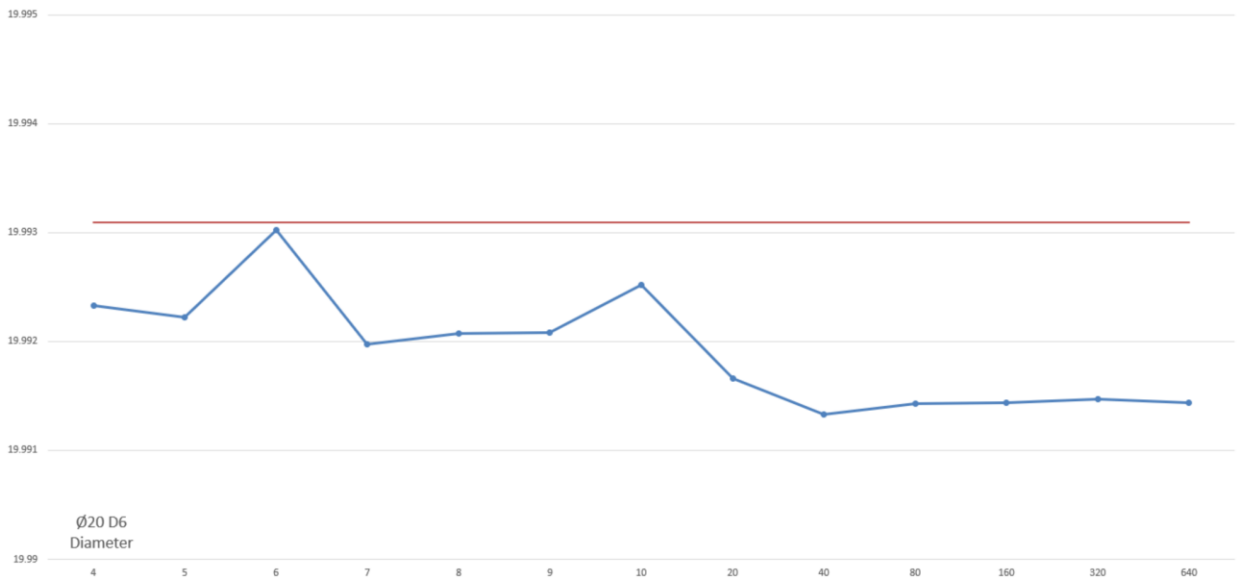

Figure 47. Variation in the diameter result at different measurement point quantities.

6.1.4 Diameter—hole with a big form error

Figure 49 presents the diameter of the hole on the vertical axis and the number of measuring points on the horizontal axis. In the case of a major defect in the form of the element, the effect of the number of points of measurement is significant in relation to the diameter result. The minimum diameter of the hole presented in Figure 49 can be calculated by six measuring points and the maximum by seven measuring points. The diameter range is approximately 0.1 mm. The plot can be used to determine a sufficient number of measuring points for measuring diameter. This limit value is 40 measuring points. After this, the result of the diameter will not change much, even if more measuring points are added to the measurement.

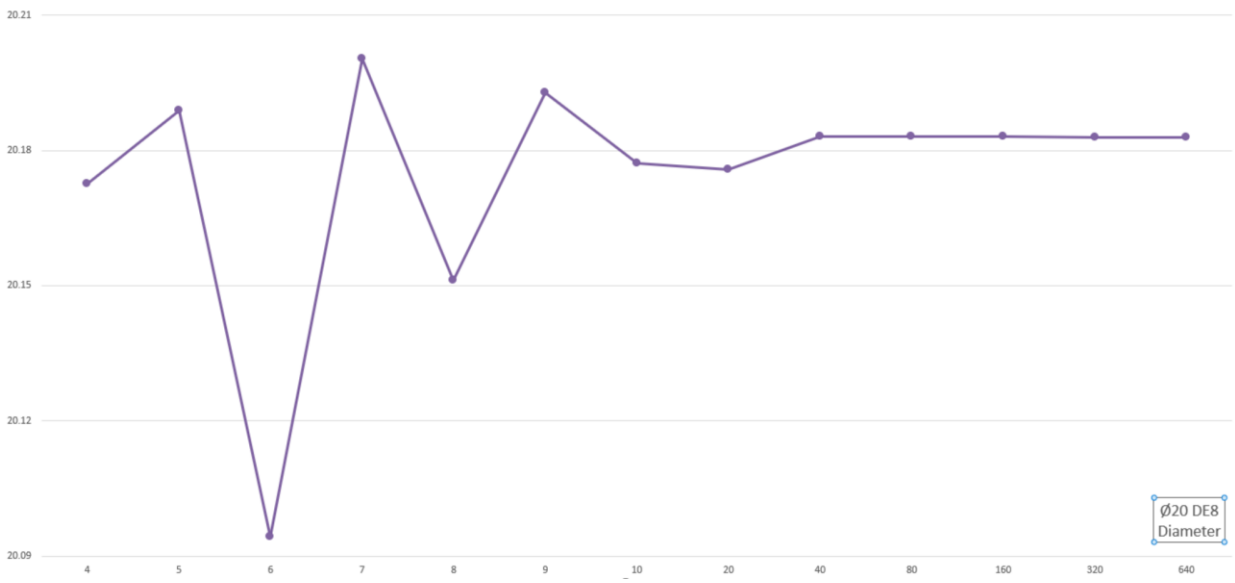

Figure 48. Variation in the diameter result with different measurement point quantities.

6.1.5 Repeatability—hole with a small form error

Figure 50 presents the frequency of five measurements at different measurement points. The range between five measurements remains within the uncertainty of the total measurement at all measurement points.

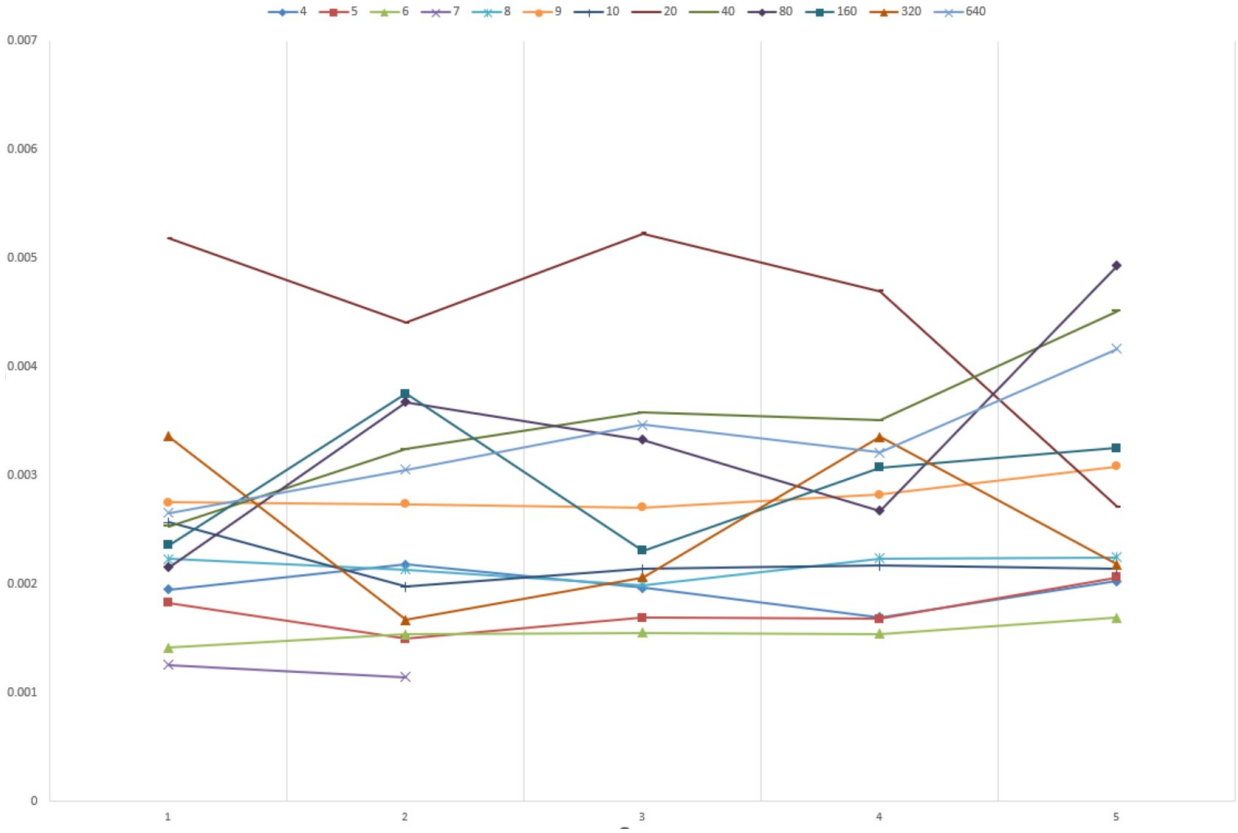

Figure 49. Five measurement repetitions with different measuring point quantities.

6.1.6 Repeatability—hole with a big form error

Figure 51 presents the frequency of five measurements at different measurement points. The range among the five measurements remains within the uncertainty of the total measurement at all measurement points.

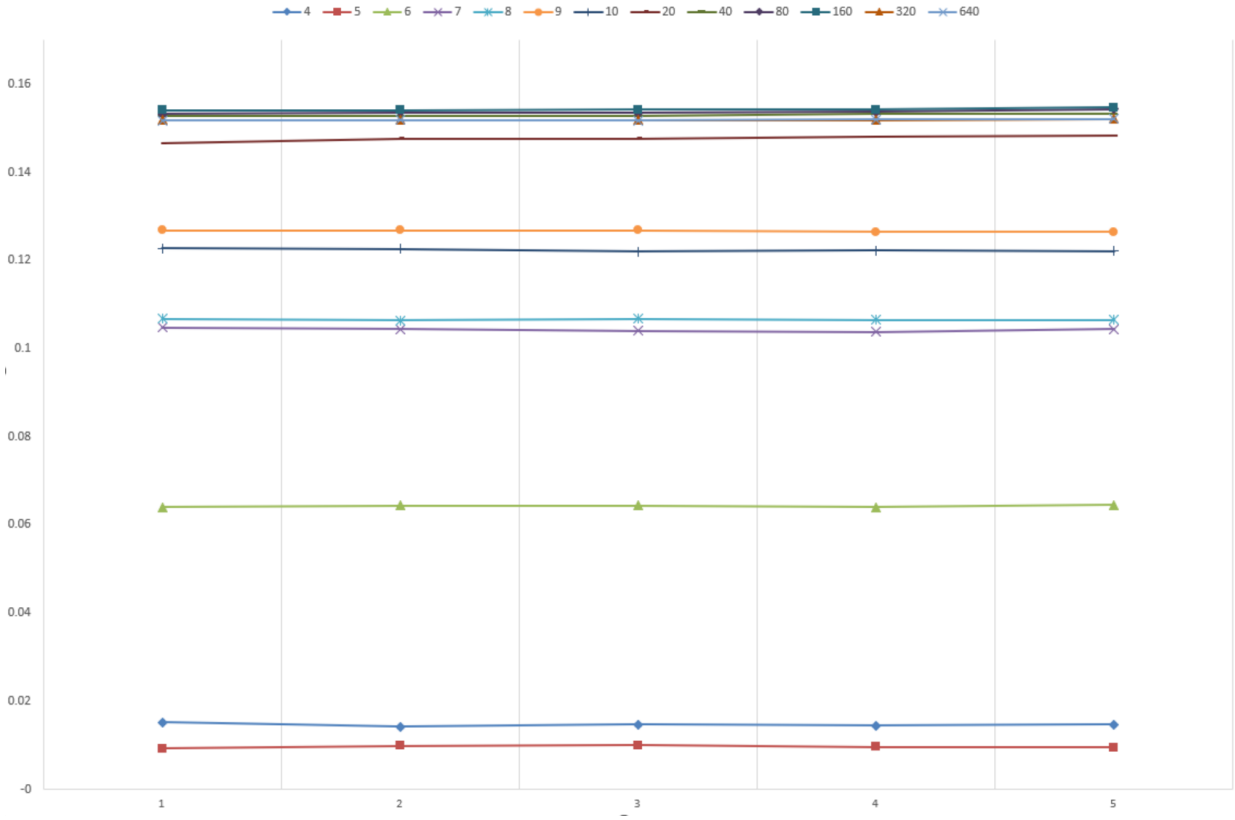

Figure 50. Five measurement repetitions with different measuring point quantities.

6.2 Flatness

I used outlier filtering to measure the reference plane. I made this decision because there was an unusual vibration at the other end of the plane. I examined the surface and there was no impurity or surface damage. I measured the plane of surface roughness from all sides and there was no difference in the surface roughness. I assumed this vibration was due to the fact that the material was not homogeneous. It is likely that there was a different coefficient of friction on different sides of the plane. Figure 52 presents a plane plot without outlier filtering and Figure 53 presents a plane plot with outlier filtering.

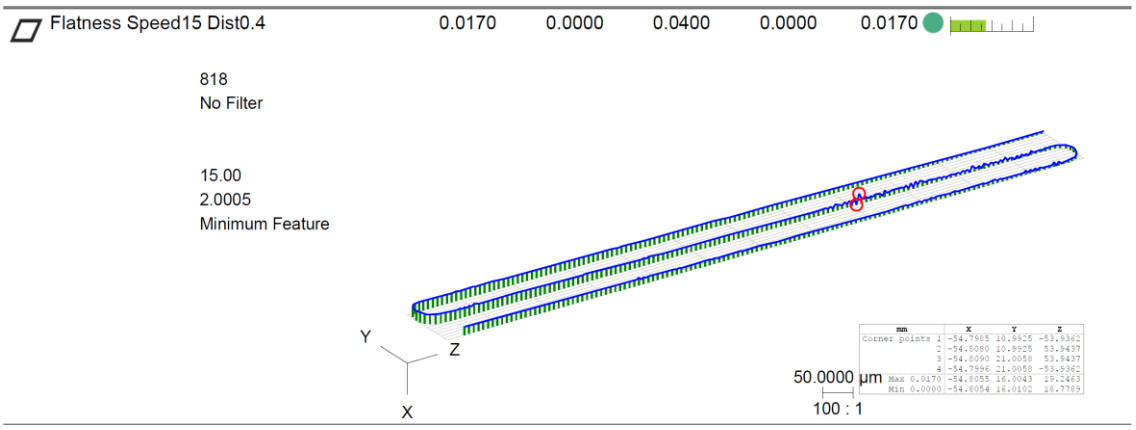

Figure 51. Flatness without an outlier filter.

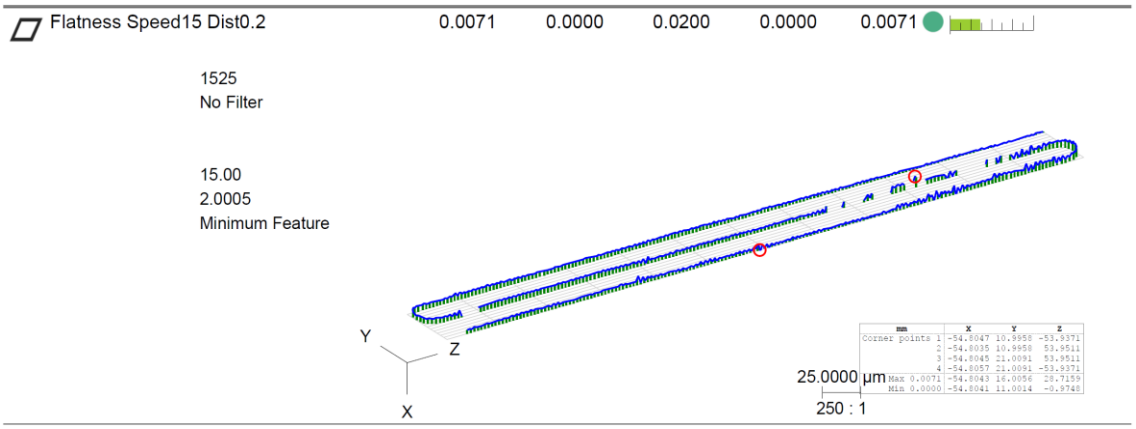

Figure 52. Flatness with an outlier filter.

A reference plane measurement at different step lengths is presented in Figure 54. The step lengths are 0.2 mm, 0.4 mm, 0.8 mm, 1.6 mm, 3.2 mm, 6.4 mm, 12.8 mm, 25.6 mm, and 51.2 mm. The step length is the distance the probe covers from the surface of the element between two measuring points. All step lengths have the same scanning speed of 15 mm/s. At steps 0.2 mm, 0.4 mm, 0.8 mm, 1.6 mm, and 3.2 mm, the mean result is approximately 0.006 mm. The mean result of the steps 6.4 mm, 12.8 mm, and 25.6 mm is the same—that is, approximately 0.03 mm. The result of the step length 51.2 mm is less than that of the step length 0.02 mm and differs from the previous step lengths. Due to the presence of fewer points, it may be difficult to find the maximum and minimum points of the form error on the plane.

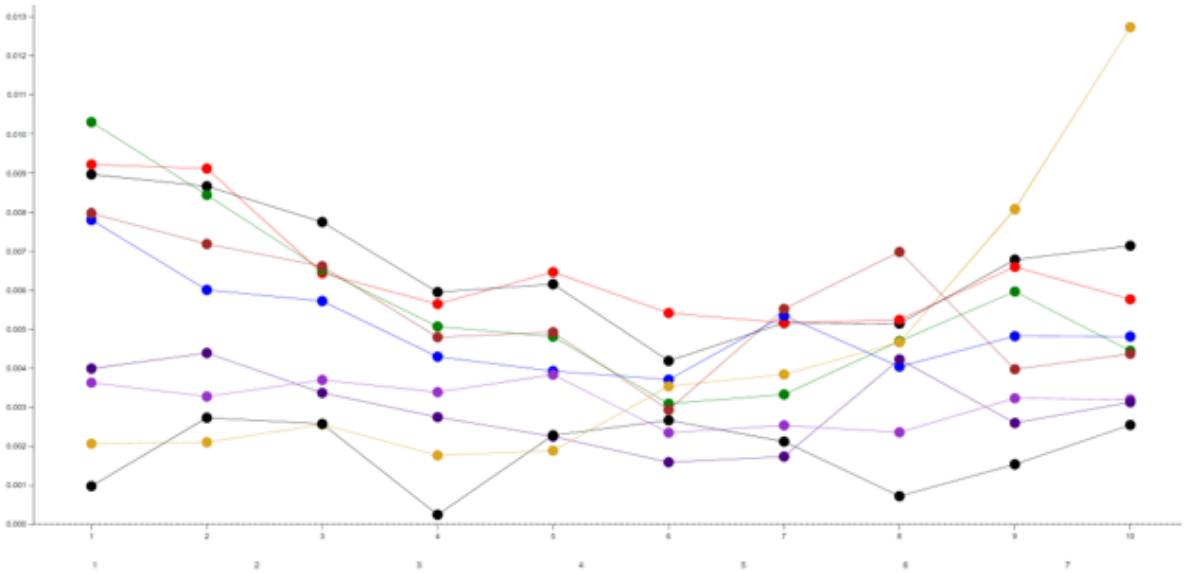

Flatness Speed15 Dist0.2		Flatness Speed15 Dist1.6		Flatness Speed15 Dist12.8	
Average value:	0.00653	*Average value:*	0.00581	*Average value:*	0.0034
Minimum:	0.0042	*Minimum:*	0.0031	*Minimum:*	0.00178
Maximum:	0.00896	*Maximum:*	0.0103	*Maximum:*	0.00808
Range:	0.00477	*Range:*	0.0072	*Range:*	0.0063

Flatness Speed15 Dist0.4		Flatness Speed15 Dist3.2		Flatness Speed15 Dist25.6	
Average value:	0.00659	*Average value:*	0.00566	*Average value:*	0.003
Minimum:	0.00517	*Minimum:*	0.00294	*Minimum:*	0.0016
Maximum:	0.00922	*Maximum:*	0.00798	*Maximum:*	0.0044
Range:	0.00404	*Range:*	0.00504	*Range:*	0.0028

Flatness Speed15 Dist0.8		Flatness Speed15 Dist6.4		Flatness Speed15 Dist51.2	
Average value:	0.00508	*Average value:*	0.00315	*Average value:*	0.00177
Minimum:	0.00372	*Minimum:*	0.00236	*Minimum:*	0.00025
Maximum:	0.00781	*Maximum:*	0.00384	*Maximum:*	0.00274
Range:	0.00409	*Range:*	0.00149	*Range:*	0.00249

Figure 53. Variation in the flatness result at different measurement point quantities.

For a plane with a single wave, a change in scan speed has little effect on the flatness result—the number of measuring points remains the same. By reducing the number of points, the result of the form error is reduced because the measuring points may not hit the maximum and minimum points of the plane form error. Figure 55 depicts the measurement of the level of the form error by 2812 points and 11 points. The flatness at 2812 measuring points is 0.4719 mm and that at 11 measuring points is 0.2287 mm.

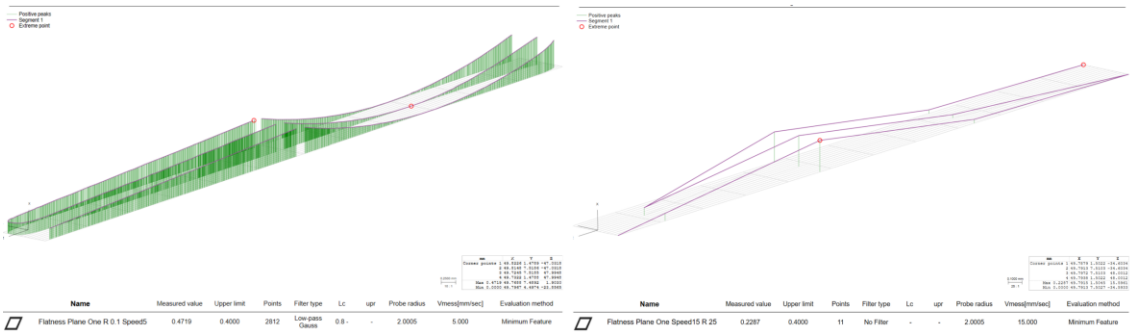

Figure 54. Variation in flatness results at different measurement point quantities.

In Figure 56, plane measurements are presented at three different scanning speeds. For all three measurements, the mean result of the flatness is the same taking when considering measurement uncertainty. The change between measurements is 3 µm. Figure 57 presents the same plane with different step lengths. The step lengths are 0.2 mm, 0.4 mm, 0.8 mm, 1.6 mm, 3.2 mm, 6.4 mm, 12.8 mm, 25.6 mm, and 51.2 mm. All step lengths have a scanning speed of 15 mm/s. Red line is upper tolerance. For three denser measuring point networks—0.2 mm, 0.4 mm, and 0.8 mm, the flatness results are the same at approximately 0.466 mm. The minimum flatness result of 0.233 mm is obtained at a step length of 25.6 mm.

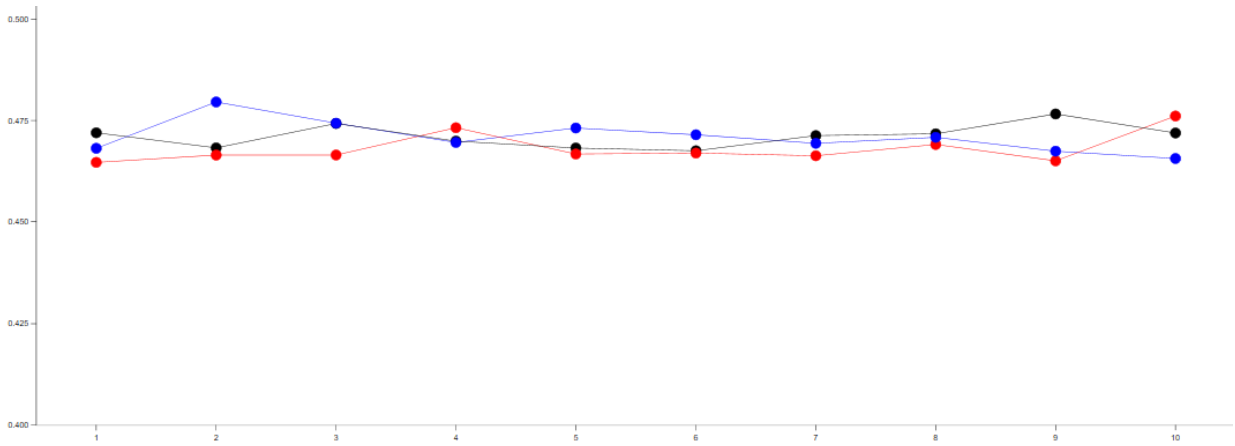

Average value:	0.47117	*Average value:*	0.46811	*Average value:*	0.47096
Minimum:	0.46754	*Minimum:*	0.46468	*Minimum:*	0.46563
Maximum:	0.47662	*Maximum:*	0.4761	*Maximum:*	0.47957
Range:	0.00908	*Range:*	0.01142	*Range:*	0.01395

Figure 55. Effect of scanning speed on form error.

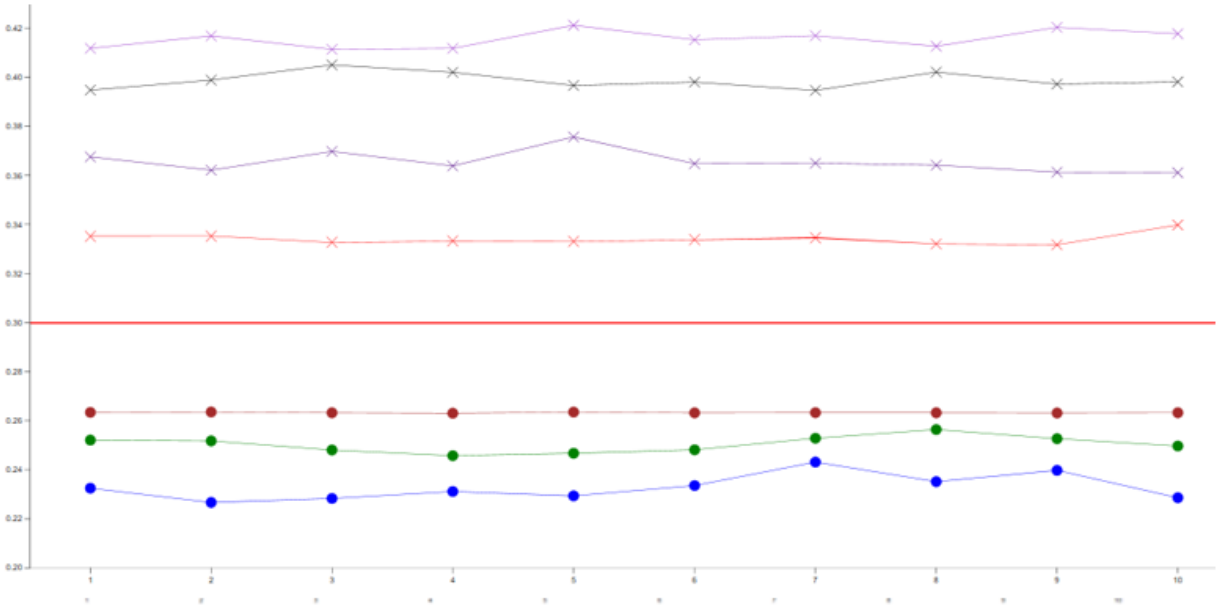

Flatness Plane One Speed15 R 0.2	Flatness Plane One Speed15 R 3.2	Flatness Plane One Speed15 R 16	Flatness Plane One Speed15 R 46
Average value: 0.46965	*Average value:* 0.48344	*Average value:* 0.39879	*Average value:* 0.26339
Minimum: 0.46446	*Minimum:* 0.47719	*Minimum:* 0.39467	*Minimum:* 0.26314
Maximum: 0.47415	*Maximum:* 0.48708	*Maximum:* 0.40508	*Maximum:* 0.26366
Range: 0.00969	*Range:* 0.00989	*Range:* 0.01041	*Range:* 0.00051
Flatness Plane One Speed15 R 0.4	Flatness Plane One Speed15 R 6.4	Flatness Plane One Speed15 R 19.2	
Average value: 0.46643	*Average value:* 0.41565	*Average value:* 0.33423	
Minimum: 0.463	*Minimum:* 0.41143	*Minimum:* 0.33189	
Maximum: 0.47411	*Maximum:* 0.42126	*Maximum:* 0.33976	
Range: 0.01112	*Range:* 0.00983	*Range:* 0.00787	
Flatness Plane One Speed15 R 0.8	Flatness Plane One Speed15 R 9.6	Flatness Plane One Speed15 R 25	
Average value: 0.46649	*Average value:* 0.46832	*Average value:* 0.23288	
Minimum: 0.46324	*Minimum:* 0.46263	*Minimum:* 0.22674	
Maximum: 0.47123	*Maximum:* 0.47156	*Maximum:* 0.2432	
Range: 0.008	*Range:* 0.00893	*Range:* 0.01646	
Flatness Plane One Speed15 R 1.6	Flatness Plane One Speed15 R 12.8	Flatness Plane One Speed15 R 45	
Average value: 0.45336	*Average value:* 0.36553	*Average value:* 0.2505	
Minimum: 0.44874	*Minimum:* 0.36109	*Minimum:* 0.24583	
Maximum: 0.45896	*Maximum:* 0.37568	*Maximum:* 0.25649	
Range: 0.01022	*Range:* 0.01459	*Range:* 0.01066	

Figure 56. Variation in flatness results at different measurement point quantities.

For a plane with dense wave-like deformation, the change in scanning speed has little effect on the form error result when the number of measuring points remains the same. By reducing the number of points, the result of the form error is reduced because the measuring points may not reach the maximum and minimum points of the plane form error. The measurement of the plane form error by 2897 points and 11 points is presented in Figure 58. The flatness at 2897 measuring points is 0.0609 mm and at 11 measuring points is 0.0260 mm.

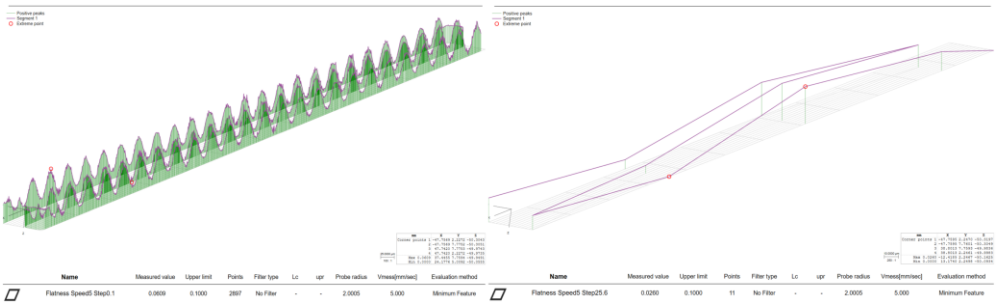

Figure 57. Variation in the flatness result at different measurement point quantities.

In Figure 59, the plane measurements are presented at five different scanning speeds . For all five measurements, the mean result of the flatness is the same, taking into account the measurement uncertainty. Moreover, the change between measurements is 3 µm. The same plane at different step lengths is presented in Figure 60. The step lengths are 0.2 mm, 0.4 mm, 0.8 mm, 1.6 mm, 3.2 mm, 6.4 mm, 12.8 mm, and 25.6 mm. All step lengths have the same scanning speed of 15 mm/s. For two denser measuring point networks—0.2 mm and 0.4 mm—the flatness results are the same at approximately 0.0585 mm. The minimum flatness result of 0.0284 mm is obtained with a step length of 25.6 mm.

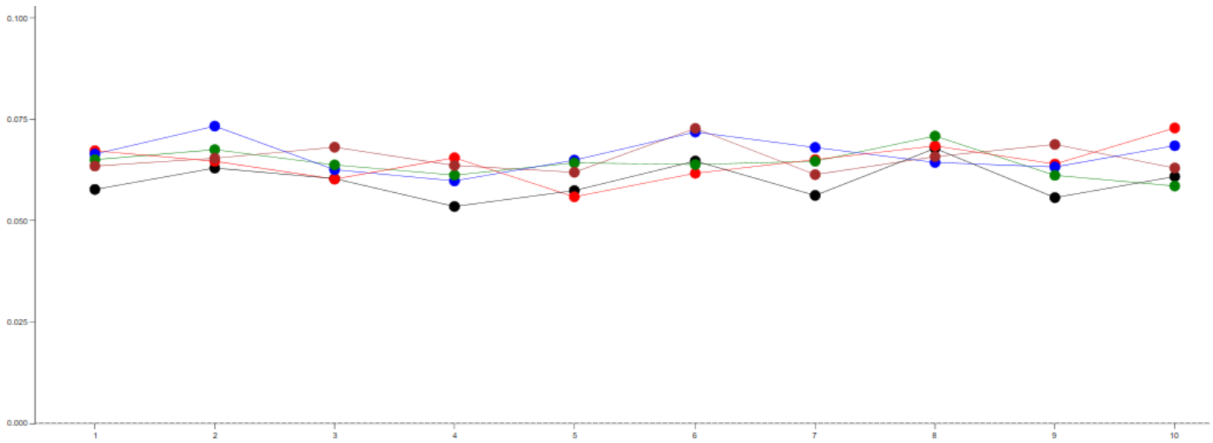

Flatness Speed5 Step0.1		Flatness Speed10 Step0.1		Flatness Speed15 Step0.1	
Average value:	0.0597	*Average value:*	0.06453	*Average value:*	0.06628
Minimum:	0.05347	*Minimum:*	0.05586	*Minimum:*	0.05977
Maximum:	0.0678	*Maximum:*	0.07283	*Maximum:*	0.0733
Range:	0.01433	*Range:*	0.01698	*Range:*	0.01352

Flatness Speed20 Step0.1		Flatness Speed25 Step0.1	
Average value:	0.06406	*Average value:*	0.0654
Minimum:	0.05853	*Minimum:*	0.06134
Maximum:	0.07085	*Maximum:*	0.07273
Range:	0.01232	*Range:*	0.0114

Figure 58. Effect of scanning speed on form error.

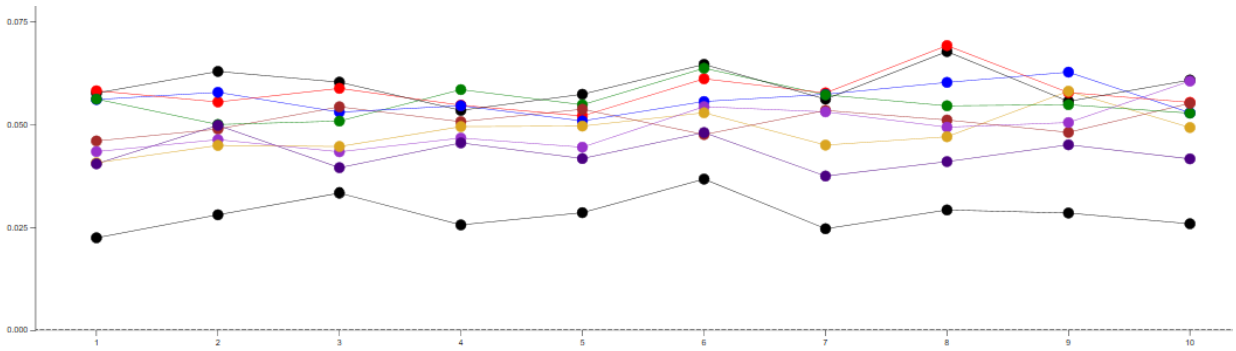

Average value:	0.0597	*Average value:*	0.05807	*Average value:*	0.05614
Minimum:	0.05347	*Minimum:*	0.05209	*Minimum:*	0.05088
Maximum:	0.0678	*Maximum:*	0.06926	*Maximum:*	0.06278
Range:	0.01433	*Range:*	0.01716	*Range:*	0.01189
Average value:	0.05536	*Average value:*	0.05092	*Average value:*	0.04923
Minimum:	0.05002	*Minimum:*	0.04601	*Minimum:*	0.04337
Maximum:	0.06372	*Maximum:*	0.05518	*Maximum:*	0.0606
Range:	0.0137	*Range:*	0.00917	*Range:*	0.01722
Average value:	0.04818	*Average value:*	0.04303	*Average value:*	0.0284
Minimum:	0.04068	*Minimum:*	0.03747	*Minimum:*	0.02257
Maximum:	0.05813	*Maximum:*	0.04982	*Maximum:*	0.03672
Range:	0.01745	*Range:*	0.01236	*Range:*	0.01416

Figure 59. Variation in the flatness result with different measurement point quantities.

For the measurement of flatness, the rate of scanning is not very important for the measurement result when the number of measuring points is sufficient.

6.3 Gauge ring test

The scanning speed is affected by the size of the element to be measured, the operating principle of the sensor, as well as the length and strength of the measuring probe. The gauge rings used in this study had three measuring rings of different sizes. The gauge ring diameters are 175 mm, 70 mm, and 20 mm. The measurements on the gauge rings were repeated 10 or 25 times. The number of points used to measure the measuring rings was determined by a step length of 0.05 mm. The measuring point was recorded on the surface of the element 0.05 mm after the distance movement. The scanning speeds used for the measurements are 5 mm/s, 10 mm/s, 20 mm/s, 30 mm/s, and 50 mm/s.

The measurements on the gauge rings are made with the probes and the sensors depicted in Figure 61. The probe on the passive sensor is 5 mm in diameter and 50 mm in length. The probe is presented on the left in Figure 61. The passive sensor is

depicted in Figure 61 on the upper right corner. Three probes of different lengths have been used on the active sensor. In Figure 61, the second probe on the left is a reference probe because it is short and firm. The probe has a diameter of 8 mm and a length of 50 mm. The third probe on the left is 3 mm in diameter and 90 mm in length. The first probe from the right is 6 mm in diameter and 250 mm in length. With these three styli, the influence of the length of the probe on the measurement has been proven

.

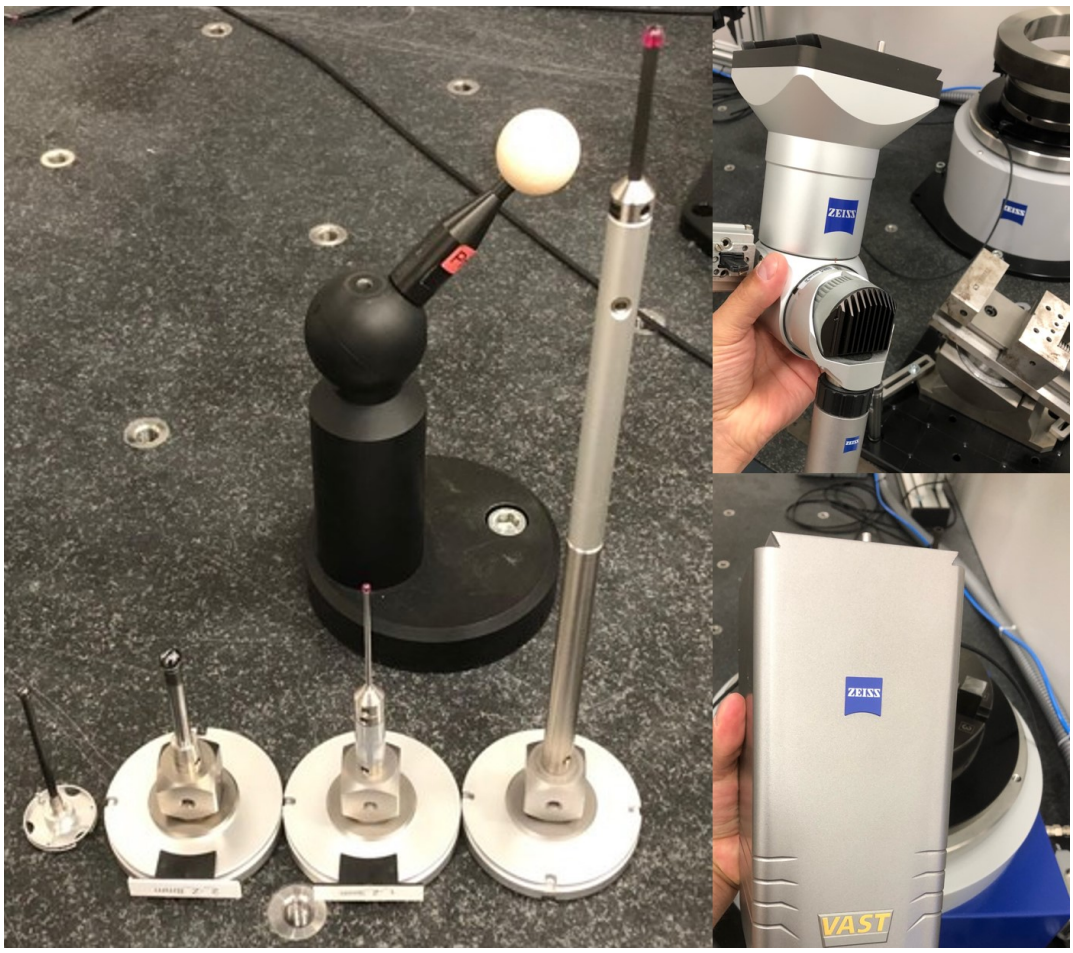

Figure 60. Stylus and sensors for gauge ring measurements.

6.3.1 Scanning speed passive sensor

The measurement of the diameter of the 20 mm gauge ring is presented in Figure 62 at five different scanning speeds. A passive sensor has been used for all measurements of this chapter. The diameter of the probe is 5 mm and its length is 50 mm. For

measurement, the scanning speeds are 5 mm/s, 10 mm/s, 20 mm/s, 30 mm/s, and 50 mm/s. The diameters are calculated using the GX calculation method. From Figure 62, it is evident that the results for scanning speeds of 30 mm/s and 50 mm/s differ from the three slower scanning speeds. The average diameter result at three slower scanning speeds is 20.000 mm. Moreover, at 50 mm/s, the average diameter is 19.998 mm.

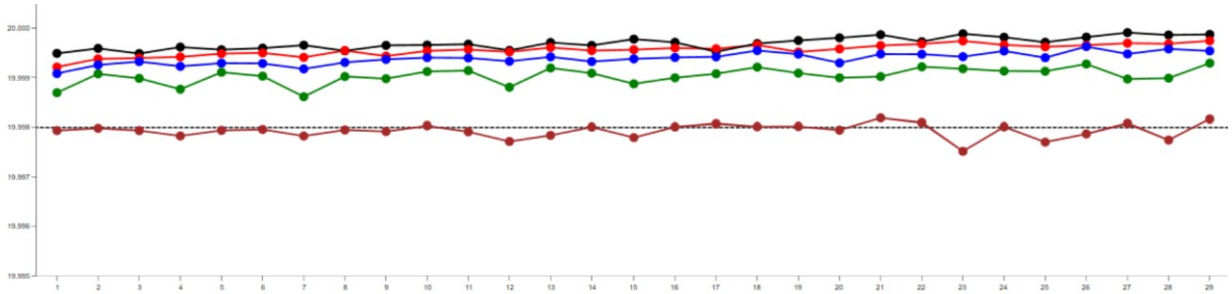

All		Diameter_Circle Ø19.998 GX speed10		Diameter_Circle Ø19.998 GX speed30	
Average value:	19.99912	*Average value:*	19.99955	*Average value:*	19.99903
Minimum:	19.99752	*Minimum:*	19.99921	*Minimum:*	19.99861
Maximum:	19.9999	*Maximum:*	19.99974	*Maximum:*	19.99929
Range:	0.00239	*Range:*	0.00053	*Range:*	0.00068
Diameter_Circle Ø19.998 GX speed5		Diameter_Circle Ø19.998 GX speed20		Diameter_Circle Ø19.998 GX speed50	
Average value:	19.99969	*Average value:*	19.99938	*Average value:*	19.99793
Minimum:	19.99948	*Minimum:*	19.99908	*Minimum:*	19.99752
Maximum:	19.9999	*Maximum:*	19.99962	*Maximum:*	19.99818
Range:	0.00042	*Range:*	0.00055	*Range:*	0.00066

Figure 61. 20mm gauge ring diameter and roundness with different scanning speeds.

The measurement of the form error of the 20 mm gauge ring at five different scanning speeds is presented in Figure 63. In all measurements in this chapter, the Chebyshev method is used for calculating the form error. The plot indicates that the result of the form error at 30 mm/s and 50 mm/s scanning speeds changes from that at the three other scanning speeds. The average form error at three slower scanning speeds is 0.0005 mm. Moreover, the average deform error at 30 mm/s is 0.0009 mm and at 50 mm/s is 0.0017 mm.

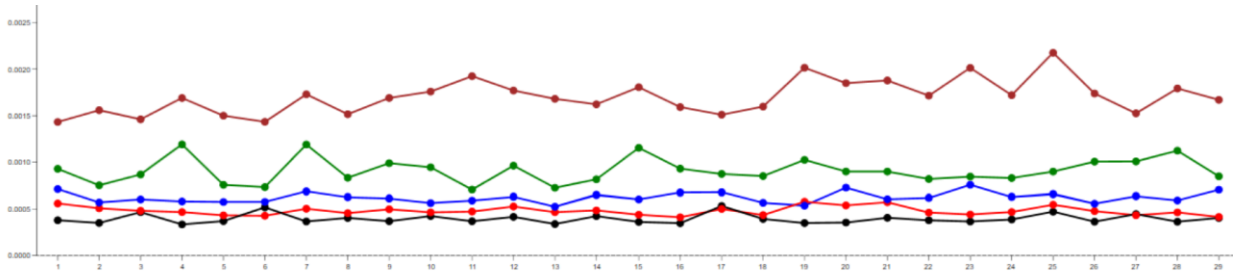

All		Roundness_Circle Ø19.998 GX speed10		Roundness_Circle Ø19.998 GX speed30	
Average value:	0.00082	*Average value:*	0.00048	*Average value:*	0.00091
Minimum:	0.00034	*Minimum:*	0.00041	*Minimum:*	0.0007
Maximum:	0.00218	*Maximum:*	0.00058	*Maximum:*	0.00119
Range:	0.00184	*Range:*	0.00017	*Range:*	0.00049

Roundness_Circle Ø19.998 GX speed5,...		Roundness_Circle Ø19.998 GX speed20		Roundness_Circle Ø19.998 GX speed50	
Average value:	0.0004	*Average value:*	0.00062	*Average value:*	0.0017
Minimum:	0.00034	*Minimum:*	0.00053	*Minimum:*	0.00143
Maximum:	0.00053	*Maximum:*	0.00076	*Maximum:*	0.00218
Range:	0.0002	*Range:*	0.00023	*Range:*	0.00074

Figure 62. 20mm gauge ring diameter and roundness with different scanning speeds.

The measurement of the diameter of the 70 mm gauge ring at five different scanning speeds is presented in Figure 64. The plot reveals that at a scanning speed of 50 mm/s, the result of the diameter changes to four other scanning speeds. The average diameter is 69.999 mm for four slower scanning speeds. Moreover, at a scanning speed of 50 mm/s, the average diameter is 69.997 mm.

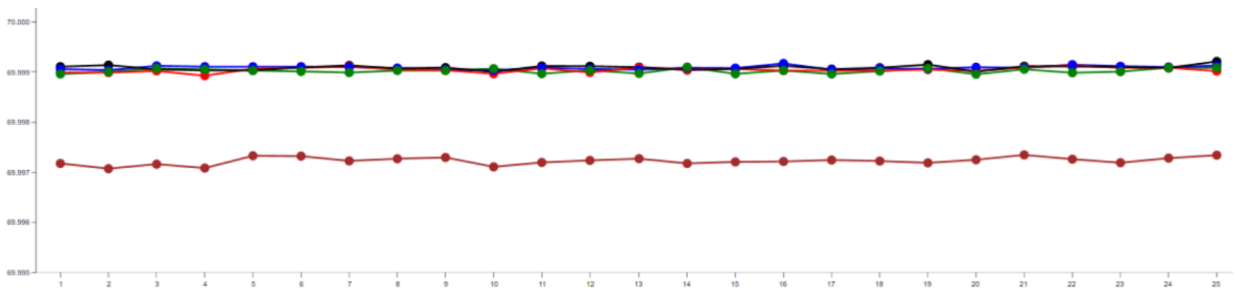

All		Diameter_Circle Ø69.998 GX speed10		Diameter_Circle Ø69.998 GX speed30	
Average value:	69.99869	*Average value:*	69.99904	*Average value:*	69.99902
Minimum:	69.99708	*Minimum:*	69.99892	*Minimum:*	69.99895
Maximum:	69.99921	*Maximum:*	69.99914	*Maximum:*	69.9991
Range:	0.00213	*Range:*	0.00021	*Range:*	0.00014

Diameter_Circle Ø69.998 GX speed5		Diameter_Circle Ø69.998 GX speed20		Diameter_Circle Ø69.998 GX speed50	
Average value:	69.99909	*Average value:*	69.99909	*Average value:*	69.99723
Minimum:	69.999	*Minimum:*	69.99903	*Minimum:*	69.99708
Maximum:	69.99921	*Maximum:*	69.99917	*Maximum:*	69.99735
Range:	0.0002	*Range:*	0.00014	*Range:*	0.00028

Figure 63. 70mm gauge ring diameter and roundness with different scanning speeds.

The measurement of the form error of the 70 mm gauge ring at five different scanning speeds is presented in Figure 65. The scanning speed of 50 mm/s differs considerably from the other four scanning speeds. The average result of the form error supports the interpretation of the plot. At the four slower scanning speeds, the result of the formal error is approximately 0.00015 mm; at 50 mm/s, the mean is 0.00045 mm..

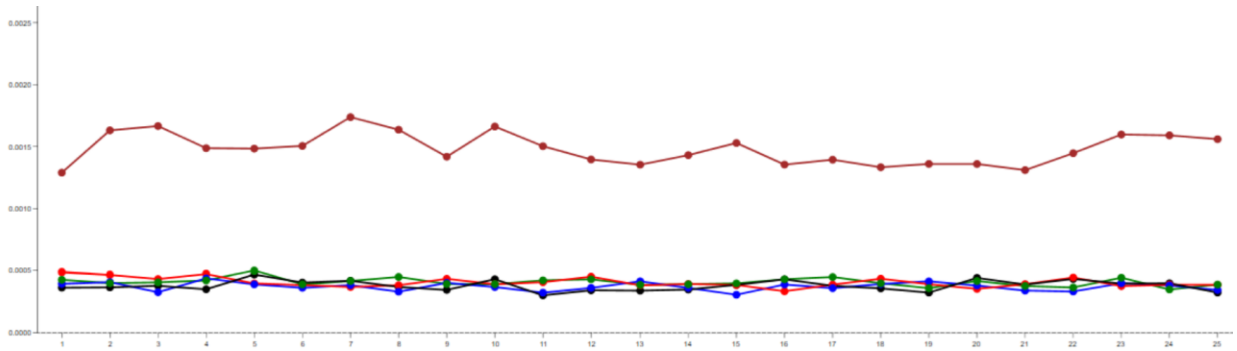

All	
Average value:	0.00061
Minimum:	0.0003
Maximum:	0.00174
Range:	0.00143

Roundness_Circle Ø69.998 GX speed10	
Average value:	0.00041
Minimum:	0.00034
Maximum:	0.00049
Range:	0.00015

Roundness_Circle Ø69.998 GX speed30	
Average value:	0.00041
Minimum:	0.00035
Maximum:	0.0005
Range:	0.00015

Roundness_Circle Ø69.998 GX speed5	
Average value:	0.00038
Minimum:	0.0003
Maximum:	0.00047
Range:	0.00017

Roundness_Circle Ø69.998 GX speed20	
Average value:	0.00037
Minimum:	0.00031
Maximum:	0.00044
Range:	0.00013

Roundness_Circle Ø69.998 GX speed50	
Average value:	0.00148
Minimum:	0.00129
Maximum:	0.00174
Range:	0.00045

Figure 64. 70mm gauge ring diameter and roundness with different scanning speeds.

The measurement of the diameter of a gauge ring of 175 mm at five different scanning speeds is presented in Figure 66. The plot indicates that the change in diameter is rather small at different scanning speeds. It can be concluded from the graph that the importance of scanning speed decreases when measuring a larger hole..

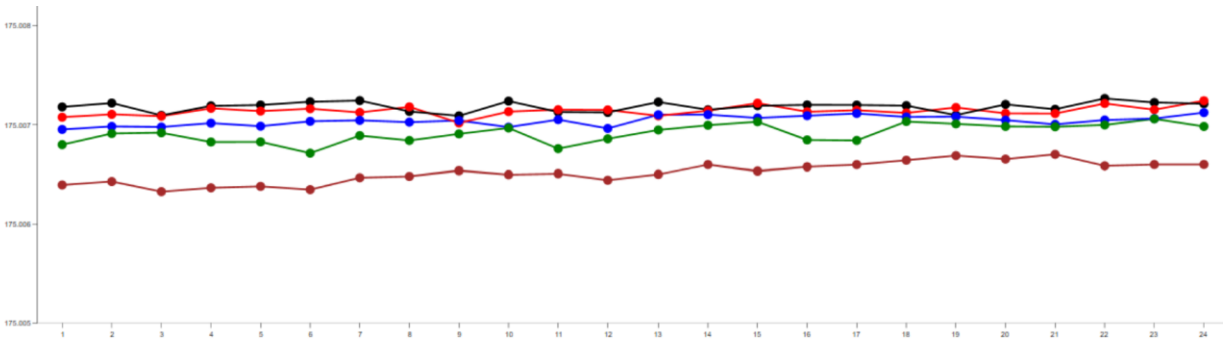

All		Diameter_Circle Ø175.005 GX speed10		Diameter_Circle Ø175.005 GX speed30	
Average value:	175.00696	*Average value:*	175.00714	*Average value:*	175.00691
Minimum:	175.00633	*Minimum:*	175.00702	*Minimum:*	175.00671
Maximum:	175.00727	*Maximum:*	175.00724	*Maximum:*	175.00706
Range:	0.00094	*Range:*	0.00022	*Range:*	0.00035

Diameter_Circle Ø175.005 GX speed5		Diameter_Circle Ø175.005 GX speed20		Diameter_Circle Ø175.005 GX speed50	
Average value:	175.00718	*Average value:*	175.00704	*Average value:*	175.00652
Minimum:	175.00709	*Minimum:*	175.00695	*Minimum:*	175.00633
Maximum:	175.00727	*Maximum:*	175.00712	*Maximum:*	175.0067
Range:	0.00018	*Range:*	0.00017	*Range:*	0.00037

Figure 65. 175mm gauge ring diameter and roundness with different scanning speeds.

In Figure 67, a measurement of the form error of a 175 mm measuring tyre is presented at five different scanning speeds. The plot indicates that at 50 mm/s, the result of the form error changes with respect to the other four scanning speeds. At the four slowest scanning speeds, the result of the form error is approximately 0.0002 mm; at 50 mm/s, the mean scanning speed is 0.0005 mm.

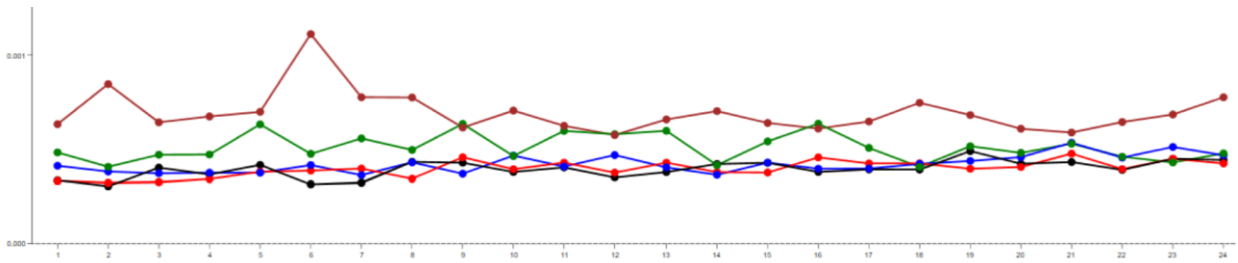

All		Roundness_Circle Ø175.005 GX speed10		Roundness_Circle Ø175.005 GX speed30	
Average value:	0.00048	*Average value:*	0.0004	*Average value:*	0.00051
Minimum:	0.00031	*Minimum:*	0.00032	*Minimum:*	0.00041
Maximum:	0.00111	*Maximum:*	0.00048	*Maximum:*	0.00064
Range:	0.00081	*Range:*	0.00015	*Range:*	0.00023

Roundness_Circle Ø175.005 GX speed5		Roundness_Circle Ø175.005 GX speed20		Roundness_Circle Ø175.005 GX speed50	
Average value:	0.0004	*Average value:*	0.00042	*Average value:*	0.0007
Minimum:	0.00031	*Minimum:*	0.00036	*Minimum:*	0.00058
Maximum:	0.00049	*Maximum:*	0.00053	*Maximum:*	0.00111
Range:	0.00019	*Range:*	0.00017	*Range:*	0.00054

Figure 66. 175mm gauge ring diameter and roundness with different scanning speeds.

6.3.2 Scanning speed active sensor

The measurement of the diameter of the 20 mm gauge ring at five different scanning speeds is presented in Figure 68. An active sensor has been used for all measurements in this chapter. The probe has a diameter of 8 mm and length of 50 mm. For measurements, scanning speeds are 5 mm/s, 10 mm/s, 20 mm/s, 30 mm/s, and 50 mm/s. The diameters are calculated using the GX calculation method. From Figure 68, it is evident that the results for scanning speeds of 30 mm/s and 50 mm/s differ from the three slower scanning speeds. The average diameter result at three slower scanning speeds is 19.9995 mm; moreover, the average diameter is 19.997 mm at a scanning speed of 50 mm/s.

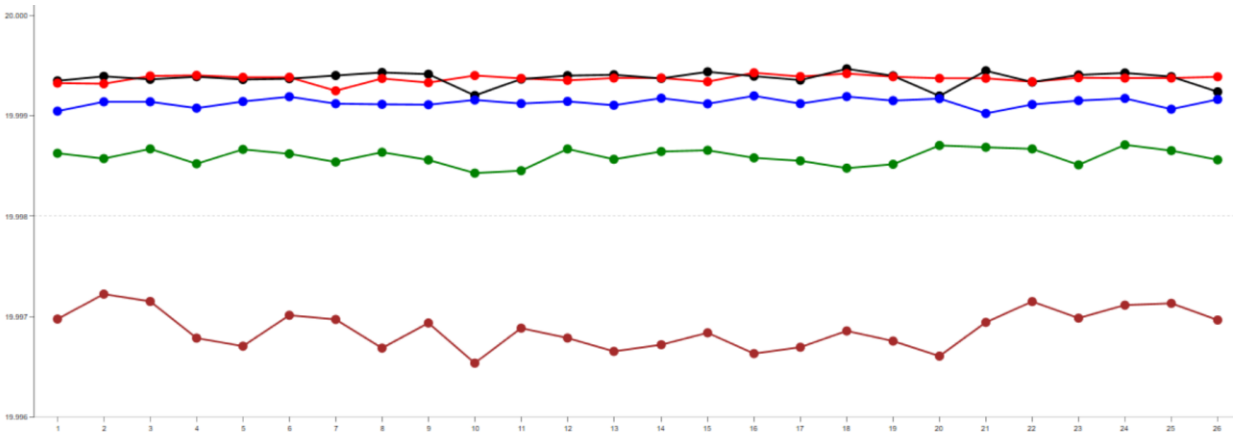

All		Diameter_Circle Ø19.998 GX speed10		Diameter_Circle Ø19.998 GX speed30	
Average value:	19.99867	*Average value:*	19.99937	*Average value:*	19.9986
Minimum:	19.99654	*Minimum:*	19.99925	*Minimum:*	19.99843
Maximum:	19.99947	*Maximum:*	19.99943	*Maximum:*	19.99871
Range:	0.00293	*Range:*	0.00018	*Range:*	0.00028
Diameter_Circle Ø19.998 GX speed5		Diameter_Circle Ø19.998 GX speed20		Diameter_Circle Ø19.998 GX speed50	
Average value:	19.99938	*Average value:*	19.99913	*Average value:*	19.99688
Minimum:	19.9992	*Minimum:*	19.99903	*Minimum:*	19.99654
Maximum:	19.99947	*Maximum:*	19.9992	*Maximum:*	19.99723
Range:	0.00027	*Range:*	0.00018	*Range:*	0.00069

Figure 67. 20mm gauge ring diameter and roundness with different scanning speeds.

The measurement of the form error of the gauge ring at five different scanning speeds is presented in Figure 69. In all measurements in this chapter, the method for calculating the form error is Chebyshev. At scanning speeds of 30 mm/s and 50 mm/s, the result of the form error changes to three other scanning speeds. The average form error at three slower scanning speeds is 0.0002 mm and that of the scanning speed 30

mm/s is 0.0016 mm; moreover, at a scanning speed of 50 mm/s, the average is approximately 0.0004 mm.

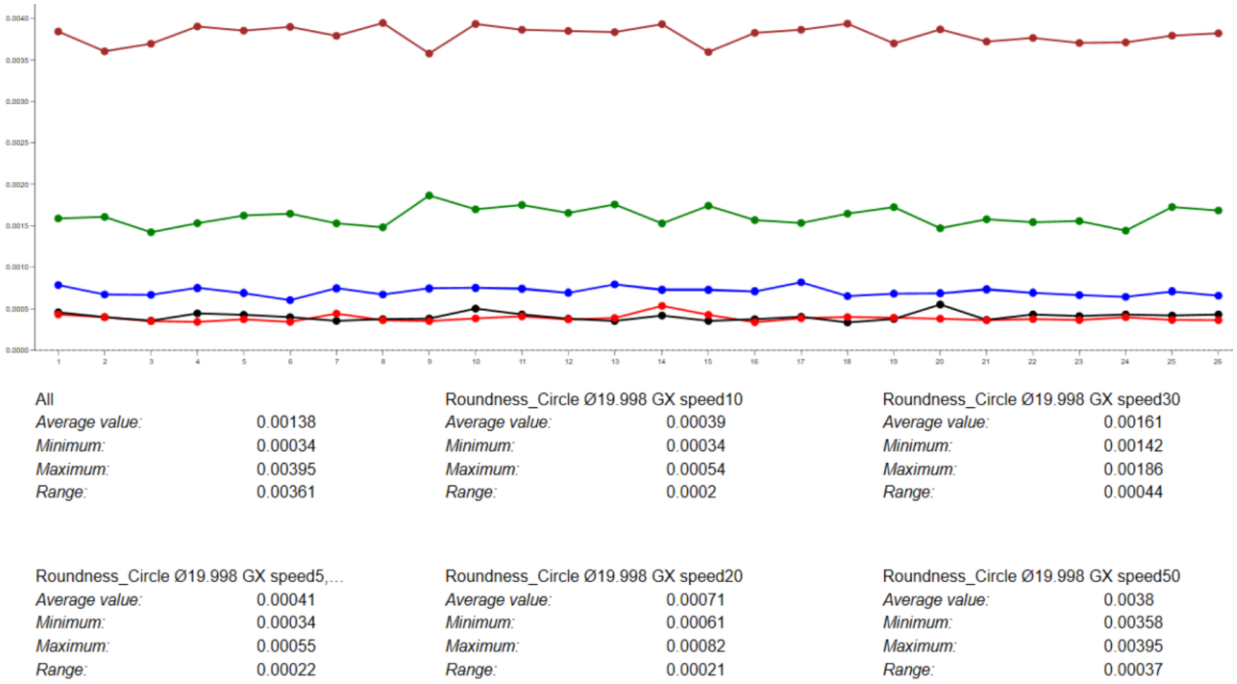

Figure 68. 20mm gauge ring diameter and roundness with different scanning speeds.

The measurement of the diameter of the 70 mm gauge ring at five different scanning speeds is presented in Figure 70. The change in scanning speed does not significantly affect the diameter result.

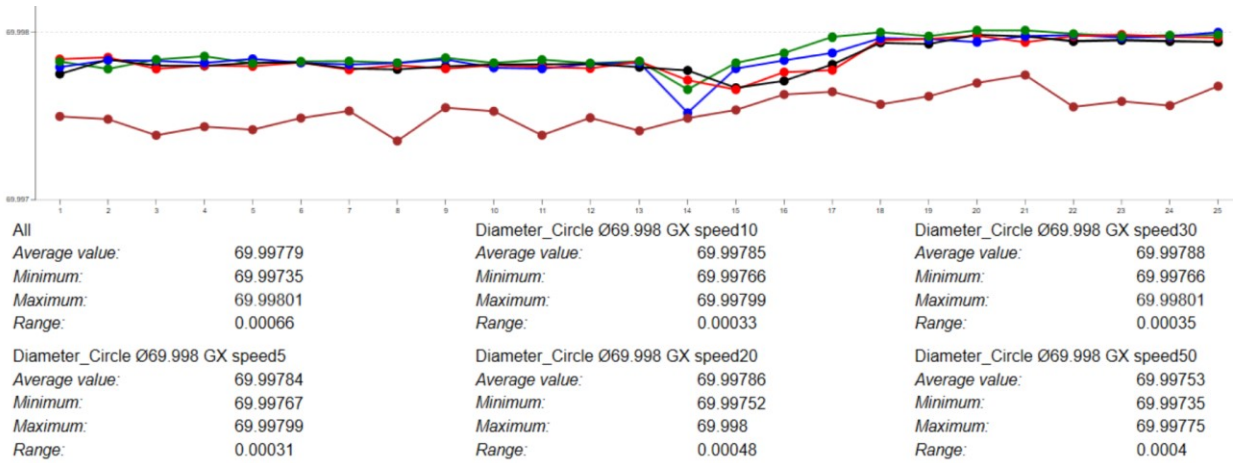

Figure 69. 70mm gauge ring diameter and roundness with different scanning speeds.

In Figure 71, a measurement of the shape error of the 70 mm gauge ring is presented at five different scanning speeds. At a scanning speed of 50 mm/s, the result of the form error is clearly different from that of the other four scanning speeds. At the four slowest scanning speeds, the result of the form error is approximately 0.0004 mm. The mean scanning speed of 50 mm/s is 0.0009 mm.

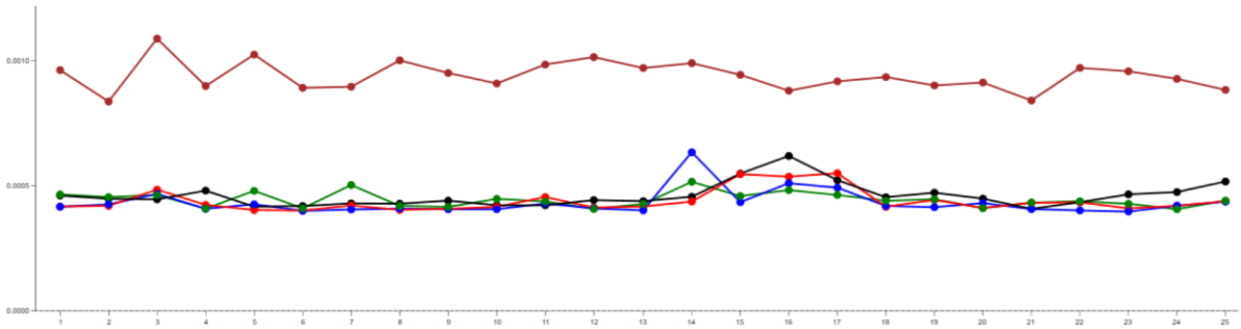

All		Roundness_Circle Ø69.998 GX speed10		Roundness_Circle Ø69.998 GX speed30	
Average value:	0.00054	*Average value:*	0.00044	*Average value:*	0.00044
Minimum:	0.0004	*Minimum:*	0.0004	*Minimum:*	0.00041
Maximum:	0.00109	*Maximum:*	0.00055	*Maximum:*	0.00051
Range:	0.00069	*Range:*	0.00015	*Range:*	0.00011

Roundness_Circle Ø69.998 GX speed5		Roundness_Circle Ø69.998 GX speed20		Roundness_Circle Ø69.998 GX speed50	
Average value:	0.00046	*Average value:*	0.00043	*Average value:*	0.00094
Minimum:	0.00041	*Minimum:*	0.0004	*Minimum:*	0.00084
Maximum:	0.00062	*Maximum:*	0.00063	*Maximum:*	0.00109
Range:	0.00021	*Range:*	0.00024	*Range:*	0.00025

Figure 70. 70mm gauge ring diameter and roundness with different scanning speeds.

The measurement of the diameter of a gauge ring of 175 mm at five different scanning speeds is depicted in Figure 72. The scan rate does not affect the diameter of the hole.

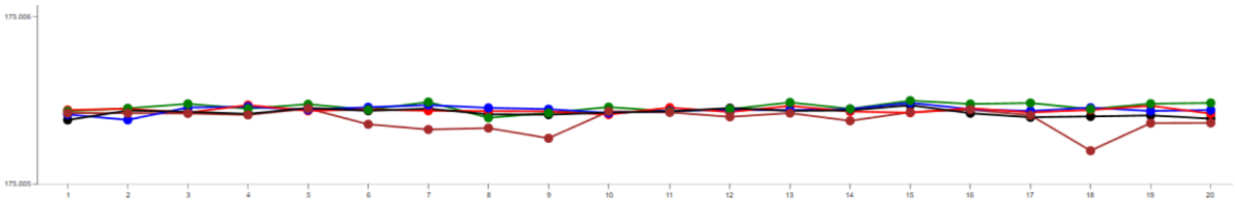

All		Diameter_Circle Ø175.005 GX speed10		Diameter_Circle Ø175.005 GX speed30	
Average value:	175.00543	*Average value:*	175.00544	*Average value:*	175.00546
Minimum:	175.0052	*Minimum:*	175.00542	*Minimum:*	175.0054
Maximum:	175.0055	*Maximum:*	175.00547	*Maximum:*	175.0055
Range:	0.0003	*Range:*	0.00006	*Range:*	0.0001

Diameter_Circle Ø175.005 GX speed5		Diameter_Circle Ø175.005 GX speed20		Diameter_Circle Ø175.005 GX speed50	
Average value:	175.00543	*Average value:*	175.00545	*Average value:*	175.00539
Minimum:	175.00539	*Minimum:*	175.00539	*Minimum:*	175.0052
Maximum:	175.00547	*Maximum:*	175.00549	*Maximum:*	175.00545
Range:	0.00009	*Range:*	0.0001	*Range:*	0.00025

Figure 71. 175mm gauge ring diameter and roundness with different scanning speeds.

In Figure 73, a measurement of the design error of 175 mm of the measuring tyre is depicted at five different scanning speeds. Scanning speeds of 30 mm/s and 50 mm/s repeatability should be dispersed. Moreover, the average form error result of the scanning speeds differs from the three slower scanning speeds. At three slower scanning speeds, the deform error is approximately 0.0004 mm and at 50 mm/s the mean is 0.0007 mm.

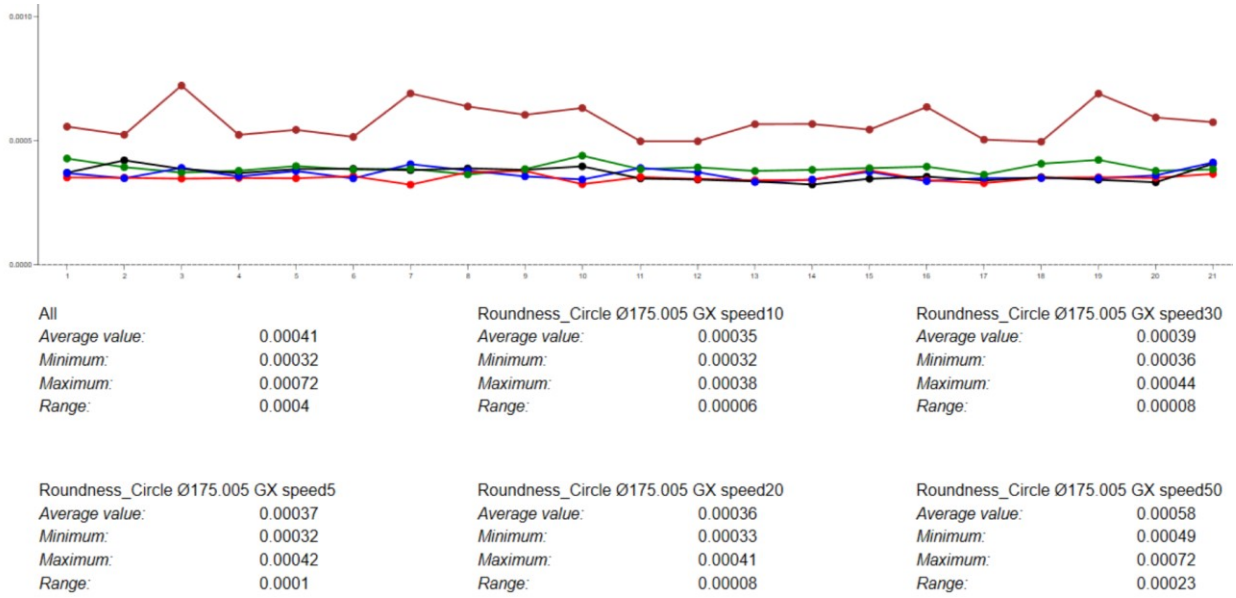

Figure 72. 175mm gauge ring diameter and roundness with different scanning speeds.

6.4 Effect of stylus length

A passive and an active sensor have been used for the measurements of the chapter. The passive sensor has one probe. The active sensor has three probes. Scan speeds are 5 mm/s, 10 mm/s, 20 mm/s, 30 mm/s, and 50 mm/s. The diameters are determined using the GX calculation method. In Figure 74, the diameters of the gauge rings are presented in ascending order of 20 mm, 70 mm, and 175 mm at five different scanning speeds. The diameter result reveals a clear correlation between the scanning speed and the length of the probe. With longer probe and faster scanning speed, the value of the diameter result moves further from the reference result. With long probes, the frequency range increases at high scanning speeds. As the diameter of the gauge ring increases, the impact of the length of the probe on the diameter result decreases.

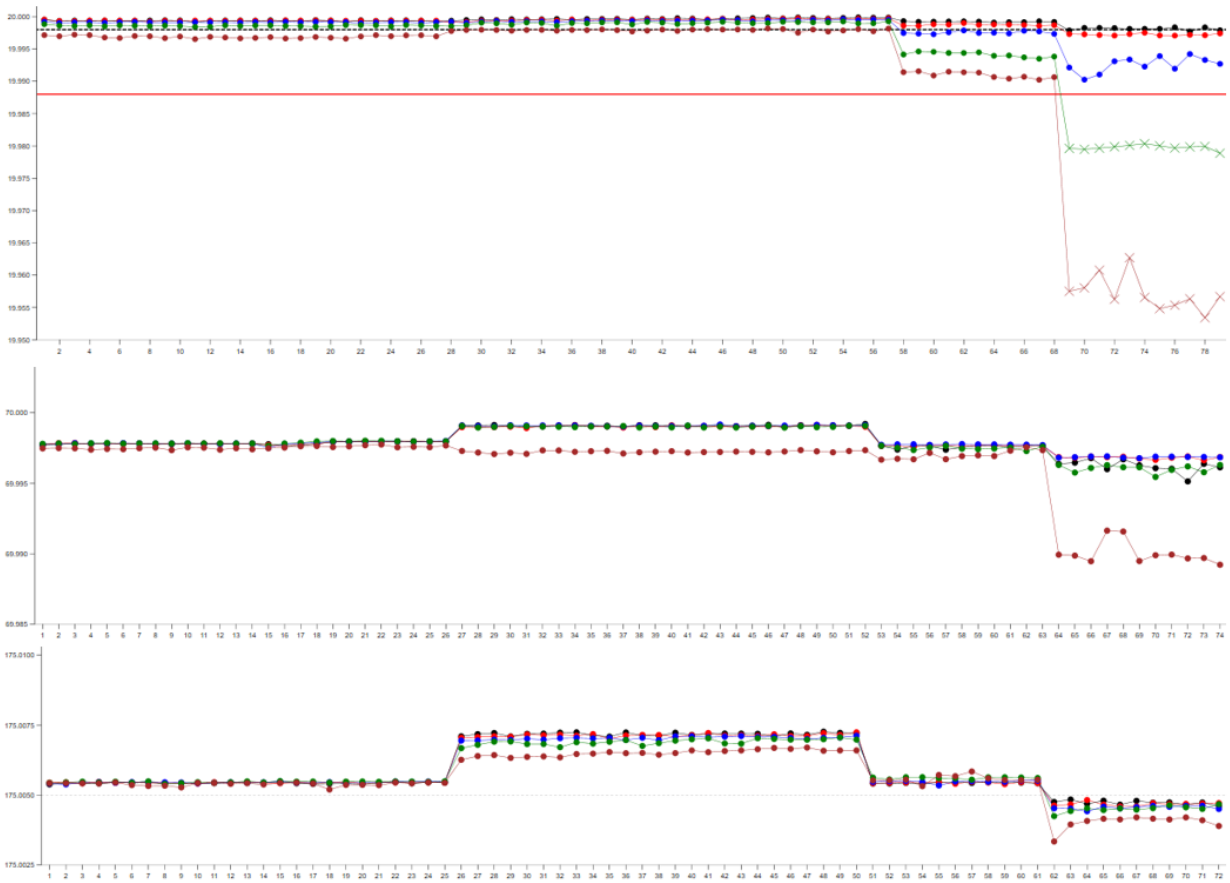

Figure 73. Diameter with different lengths stylus.

In Figure 75, a measurement of the form error of 20 mm, 70 mm, and 175 mm at five different scanning speeds is depicted from top down. In all measurements of this chapter, the method for calculating the form error is Chebyshev. The result of the form error reveals a clear correlation between the scanning speed and the length of the probe. With longer probes and faster scanning speed, the value of the form error moves further from the reference result. Moreover, the frequency range of the measurement increases with a long probe and high scanning speeds. As the diameter of the gauge ring increases, the effect of the length of the probe on the result of the form error decreases. The abovementioned phenomenon is repeated by all diameters of the gauge ring interpreter.

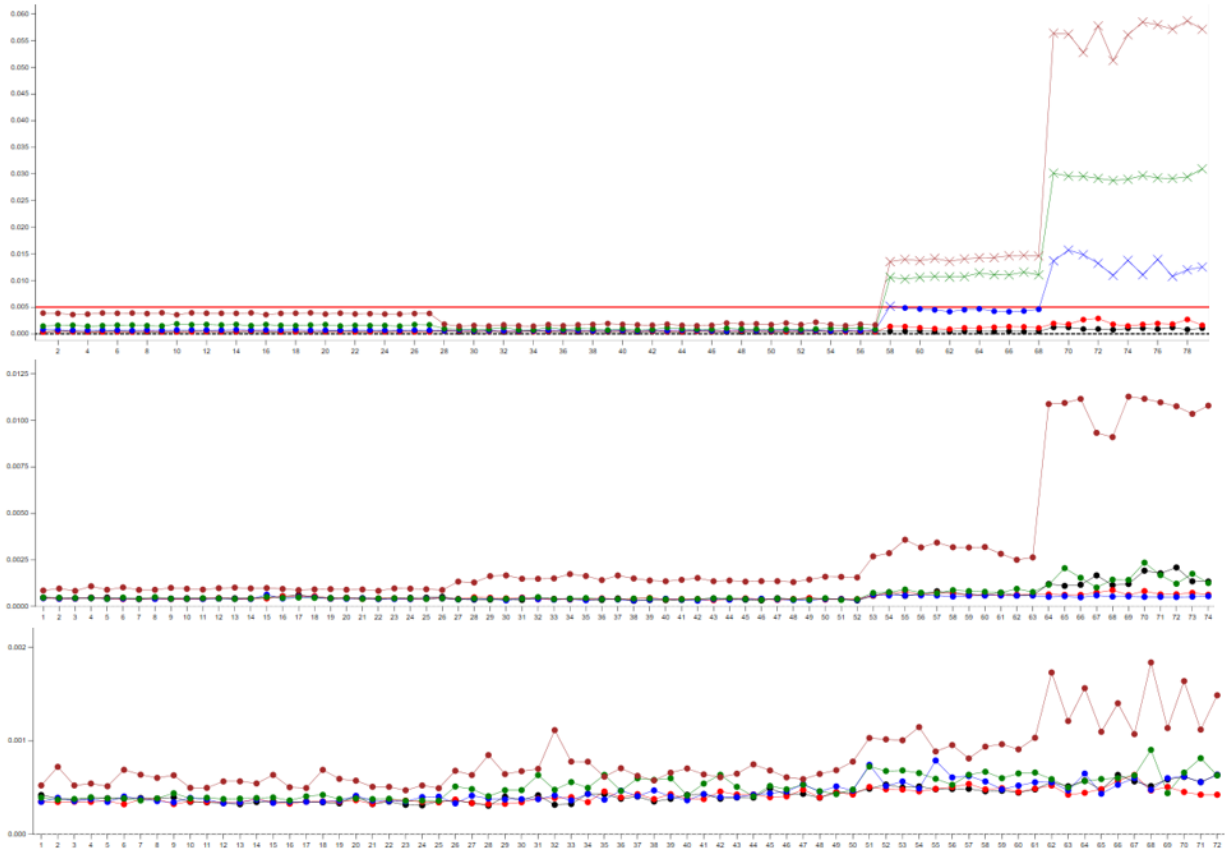

Figure 74. Diameter with different lengths stylus.

7 Recommended Values of Measurement Parameters

Tikka (2007) has examined the number of measurement points for point to point CMMs in his book Koordinaattimittaus. Tikka defined the number of measurement points as dependent on the size of the element. Since the point-to-point CMMs are slower to measure than scanning CMMs. The number of points in a point-to-point measurement is also affected the economy of measurement. Tikka's main idea was that the element is measured with a sufficient range of measuring points, so that the measuring time of the element would still be economical (Tikka, 2007 pp. 257–259).

By scanning, CMM obtains 5000 points at the same time as 40 points achieved using point-by-point measurement.

Geometria-elementti	Matemaattinen minimipisteluku	Mittaustekninen minimipisteluku	Käytännön tavoite Edustava pisteluku	Elementin koosta riippuva käytännön pistemäärä *)
Suora	2	3	20	5 - 20
Taso	3	4	81	9 - 81
Ympyrä	3	4	36	9 - 81
Pallo	4	6	40	12 - 144
Lieriö	5	8	54	9 - 144
Kartio	6	12	72	36 - 164

Table 6. Number of measurement points (Tikka, 2007 p. 275).

The trigger sensor has two recommended values. The upper value is based on the measurement economy and the lower on the length of the measurement period. The length of the measurement period is proportional to the size of the element. The distance between points is the same regardless of the size of the element. When measuring large diameters or large planes with active and passive measuring sensors, the scanning speed can be increased. However, simultaneously, it is also necessary to increase the length of the step. This is due to the fact that the control of the CMM is unable to register measuring points with short step length at high scanning speeds.

7.1 Free form element

It is challenging to provide general guidance on measurement parameters for a free-form element, such as a turbine wing, as the shape itself determines the rate of scanning and the number of measuring points. A general rule for all free forms could be given: The smaller the shape and the more often the shape is repeated in the element to be measured, the slower the scanning speed must be. The number of measuring points increases as the frequency of the form to be measured increases.

7.2 Circle

The recommended probe diameter is 3 mm and the length 35mm–75 mm

Sensor	Diameter	Circle position Scanning speed	Cylinder position Scanning speed	Form Scanning speed	Angle	Point number
Trigger	0–8mm	-	-	-	360˚	9–27
Trigger	0–8mm	-	-	-	360˚	27–47
Passive	0–8mm	5mm/s	3mm/s	2mm/s	400˚	Step width 0.05mm
Active	0–8mm	10mm/s	5mm/s	3mm/s	400˚	Step width 0.05mm
Trigger	8–25mm	-	-	-	360	27–53
Trigger	8–25mm	-	-	-	360	53–93
Passive	8–25mm	5mm/s	5mm/s	3mm/s	380˚	Step width 0.05mm
Active	8–25mm	15mm/s	10mm/s	5mm/s	380˚	Step width 0.05mm
Trigger	26–80mm	-	-	-	360	53–81
Trigger	26–80mm	-	-	-	360	81–141
Passive	26–80mm	10mm/s	5mm/s	3mm/s	380˚	Step width 0.05mm
Active	26–80mm	30mm/s	10mm/s	5mm/s	380˚	Step width 0.05mm
Trigger	81–250mm	-	-	-	360˚	81–108
Trigger	81–250mm	-	-	-	360˚	108–189
Passive	81–250mm	20mm/s	10mm/s	5mm/s	380˚	Step width 0.08mm
Active	81–250mm	40mm/s	15mm/s	10mm/s	380˚	Step width 0.08mm
Trigger	250mm→	-	-	-	360˚	108–135
Trigger	250mm→	-	-	-	360˚	135→
Passive	250mm→	20mm/s	15mm/s	5mm/s	380˚	Step width 0.1mm

Active	81–250mm	40mm/s	25mm/s	10mm/s	380°	Step width 0.1mm

7.3 Plane

The recommended probe diameter is 3 mm and the length 35 mm–-75 mm

Sensor	Plane size L × W	Scanning speed	Point number
Trigger	0–25mm	-	9–27
Trigger	0–25mm	-	27–47
Passive	0–25mm	3mm/s	Step width 0.1mm
Active	0–25mm	5mm/s	Step width 0.1mm
Trigger	26–80mm	-	27–63
Trigger	26–80mm	-	63–111
Passive	26–80mm	5mm/s	Step width 0.1mm
Active	26–80mm	10mm/s	Step width 0.1mm
Trigger	81–250mm	-	63–99
Trigger	81–250mm	-	99–173
Passive	81–250mm	10mm/s	Step width 0.3mm
Active	81–250mm	20mm/s	Step width 0.3mm
Trigger	250mm→	-	99–136
Trigger	250mm→	-	136→
Passive	250mm→	15mm/s	Step width 1mm
Active	250mm→	30mm/s	Step width 1mm

7.4 Line

The recommended probe diameter is 3 mm and the length 35 mm–-75 mm

Sensor	Line length L	Scanning speed	Point number
Trigger	0–25mm	-	7–21
Trigger	0–25mm	-	21–37
Passive	0–25mm	3mm/s	Step width 0.1mm
Active	0–25mm	5mm/s	Step width 0.1mm
Trigger	26–80mm	-	21–49
Trigger	26–80mm	-	49–85
Passive	26–80mm	5mm/s	Step width 0.1mm
Active	26–80mm	10mm/s	Step width 0.1mm
Trigger	81–250mm	-	49–77
Trigger	81–250mm	-	77–135
Passive	81–250mm	10mm/s	Step width 0.3mm
Active	81–250mm	20mm/s	Step width 0.3mm
Trigger	250mm→	-	77–105

Trigger	250mm→	-	105→
Passive	250mm→	20mm/s	Step width 1mm
Active	250mm→	40mm/s	Step width 1mm

7.5 Cylinder

With a cylinder diameter/length ratio of 2×D, 3×D or more and requirement is ISO standard, the cylinder shall be measured at a minimum of 3 on a circular route. In the ASME standard drawings the cylinder is measured on two circular routes. The measurement parameters of the circle can be found in Chapter 7.2.

7.6 Cone

In order to increase the reliability of the conical angle, the cone should be measured on a minimum of 3 three circular routes. The measurement parameters of the circle can be found in Chapter 7.2.

8 Thinking about what was discovered

The aim of the thesis was to create a uniform measurement parameter for tactile coordinate measurement, which would achieve consistent measurement results regardless of the CMM brand, operator, software, or sensor.

There are several uncertainty factors that affected the measurement results and thus also the conclusions. The biggest uncertainty factor in determining measurement parameters is the operator. The decisions made by the measurer directly affect the measurement results. This uncertainty factor must be made as small as possible or excluded from the measurement results. Other uncertainty factors in test measurements were measuring devices, measuring tips, environments, and measurement objects.

Further, uncertainties were minimized using various tests. These tests also determined the magnitude of other uncertainties. To ensure the reliability of the test measurements, the CMMs were calibrated and had a metrological traceability chain to the meter. CMM temperature sensors were used in the measurements, with which the measurement results were compensated for the temperature of 20˚C degrees required by the corresponding standard ISO 1:2022. During the measurements, the temperature stability of the test part was monitored by measuring the temperature at the beginning, middle, and end of the measurement program. Appendix 1 presents the results of temperature measurement from three CMMs.

The suitability of the measurement parameters selected for the measurement program of the test part is proven by tests performed on gauge rings. The tests reveal that an excessively high scanning speed distorts the measurement results of the form and diameter. The tests performed on the test part reveal the influence of small numbers of measurement points on the shape and diameter measurement results. The measuring ring study also indicates that there is a strong correlation between the length of the measuring tip and the scanning speed.

To prove the repeatability and reproducibility of the tests, I measured the test part with four different CMMs and five different measuring heads. In addition, I measured the test part five times with each measuring head. Appendix 2 presents the reproducibility and repeatability of the measurements as measurement results with different coordinate measuring machines. The so-called normalized error E_n was used in the evaluation of the ratio of the measurement results to the measurement uncertainty. The E_n number is obtained when the difference measure (*Result – ReferenceResult*) is divided by the measurement uncertainty. If the calculated measurement uncertainty (U) and the reference measurement uncertainty (U_{REF}) (both with k = 2) are almost equal, the difference measure is divided by the squared sum of the uncertainties. This can be obtained using the following formula:

$$E_n = \frac{\text{Result} - \text{Referenceresult}}{\sqrt{{U_{RFE}}^2 + U^2}} \qquad (4)$$

In the broader comparison measurements of reference laboratories related to official supervision, the E_n number is used. Certain limit values have been defined for the acceptability of the results. An acceptable number for the E_n number is less than or equal to 1, and a bad E_n number is a value that exceeds 1. (Hiltunen, et al., 2011 p. 72).

The most accurate CMM of the tests was used as a reference machine in the E_n formula. The uncertainty according to the ISO 10360-2:2009 standard specified by the CMM manufacturer was *0.5 + L/500*. The estimated measurement uncertainties were slightly large, because the E_n numbers of the CMM comparison measurement are much below the limit value of 1. In contrast, if the E_n numbers were all above one, then the estimated uncertainties would be too small. In this case, a smaller uncertainty could have been used in the calculations. Appendix 3 presents the reproducibility and repeatability of the measurements as a numerical value of E_n with different measuring heads.

8.1 Conclusions

This research reveals that the number of measurement points is not of great importance when measuring parts without shape defects. Often, in comparative CMM measurements, a part or reference nominals without form defects are used. References can be a plug gauge, ring gauge, or calibration sphere. The so-called least squares (LSQ) calculation is often used to calculate the element of these comparison measurements. LSQ is a mathematical optimization method that aims to find the best fit of measurement points. In the LSQ method, the estimators of the regression coefficients are determined by minimizing the sum of the squares of the error terms. With the CMM comparison measurement, it is possible to determine the total measurement uncertainty of the CMM.

The scanning speed has an effect on the diameters and form errors, even if the element does not have form errors. Simultaneously, it is beneficial to remember that the scanning speed also affects the position of the element. These factors affect all geometric tolerances.

Due to the manufacturing techniques, the parts always have a form error. It is important for there to be sufficient measurement points in order to find the minimum and maximum points of the form error in the element being measured. When measuring a part with shape defects, the number of measurement points is of great importance to the measurement result. When measuring large diameters or planes, the scanning speed does not have a very large effect on the measurement result. The importance of the measurement speed increases as the smaller element is measured. According to this research, large shapes can be measured faster than small shapes.

My research reveals that there is a strong correlation between probe length and scan speed. In the study, efforts have been made to determine the measurement parameters only for short and sturdy stylus. With this method, the uncertainty of the stylus was rather small. The recommended measurement parameters given in chapter 7 apply to a long supporting stylus that is 35 mm–75 mm long. The position of the stylus is -Z.

The study recommends CMM users to define their own measurement parameters for a stylus that differ from the abovementioned specification. This can be easily determined

by measuring the reference normal, for example, on a ring gauge with the stylus in question. The ring gauge should be a maximum of 25% larger or smaller than the element to be measured with the stylus.

The research reveals that making a comprehensive measurement parameter table is a challenging task, if not an impossible one. There are several factors that influence the measurement result, such as the number of measurement points, the rigidity of the part, cleanliness, material, temperature, shape defects of the elements and surface roughness. In addition, the condition, temperature, cleanliness, and calibration of the measuring device all affect the measurement result. The length, sturdiness, and scanning speed of the stylus must also be taken into account. The influence of the environment comes from, for example, temperature, humidity, cleanliness, and floor vibrations. The measurer's urgency, motivation, experience, alertness, and methods are also reflected in the measurement results.

The most difficult task of defining the measurement parameters in this thesis was the definition of the measurement parameters of free-form elements—for example, a turbine blade, because the shape of the turbine blade depends on the size of the turbine.

It can be said that the main results of the research is that when identifying reliable measurement parameters for measuring lines and circles, it is relatively easy to determine the measurement parameters of plane, cylinder, and cone. The plane, cylinder, and cone are constructs of individual lines or circles. According to this study, the measurement points are scaled in relation to the size of the element. The distance between the measuring points remains the same, which enables reasonable filtering of the measuring points. Since this thesis is only concerned with measurement and one measurement position, a comprehensive table of measurement parameters is not presented.

Determining the filter values for the form of the measurement element is located in "no man’s land." In my view, designers should take more responsibility for determining these values. I base my view on the fact that they also specify other tolerances. However, the problem is that designers often do not have a sufficient understanding of the subject and training for it is poorly available. Therefore, I believe that companies or universities should invest in the research of determining filter values. This research

should be conducted on a tripartite basis, which would include designing, manufacturing, and measurement.

As a follow-up study, it would be beneficial to prove the impact of the measurement position on the measurement results. For my research, I selected a favorable position for gravity measurements. Moreover, I used a stylus pointing straight down for the measurements of the measuring ring. The stylus points directly toward the earth's gravity. In the test part, I used a stylus that is in a horizontal position, but the probe I used were sturdy and short. Figure 39 depicts the positions of the stylus used in the measurements of the test part and the ring gauge. Another aspect for future research is to make a separate measurement parameter table for video measurements.

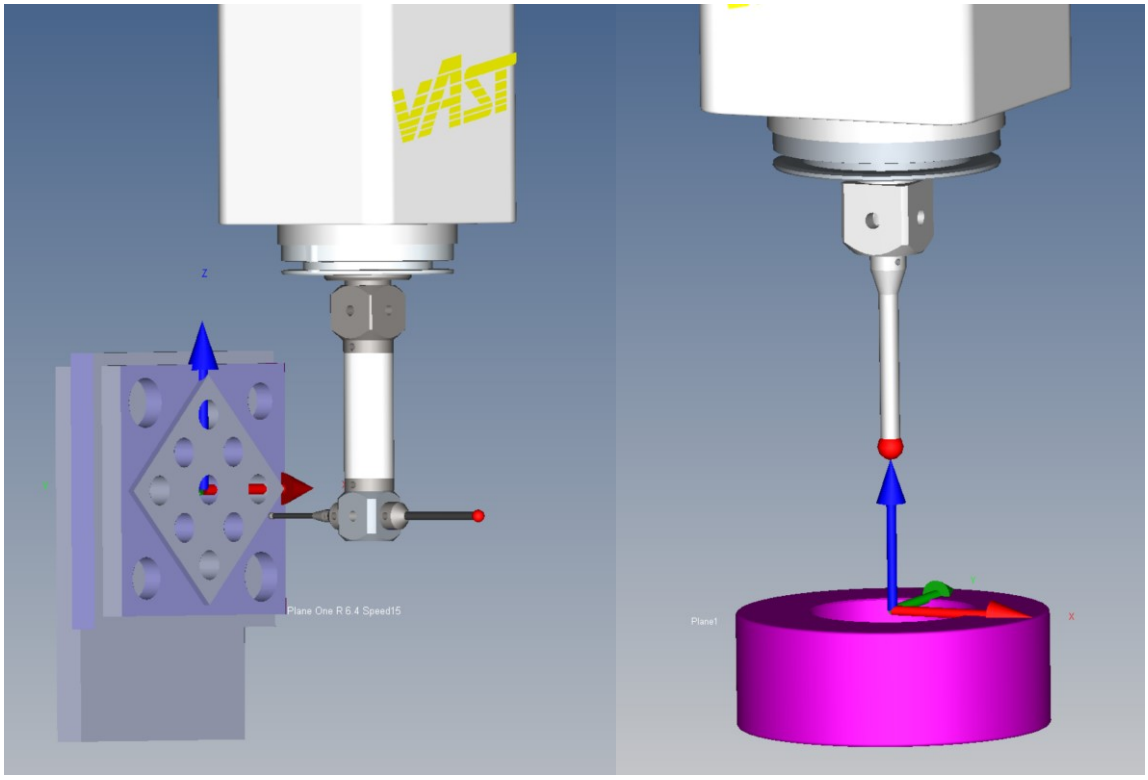

Figure 75. Probing direction.

References

Adapa. (n.d.). *The definition of surface roughness.* Retrieved April 9, 2023, from https://adapamoulds.com/the-definition-of-surface-roughness/

AUKOM. (2017a) [AUKOM stage 1 training cource material]. https://www.aukom.info/en/aukom-training-courses/training-content.html

AUKOM. (2017b) [AUKOM stage 2 training cource material]. https://www.aukom.info/en/aukom-training-courses/training-content.html

EA-4/02 M:2022. *Evaluation of the uncertainty of measurement in calibration*. (2022). European Accreditation.

SFS-EN ISO 1:2022. *Geometrical product specifications (GPS). Standard reference temperature for the specification of geometrical and dimensional properties.* (2022). International Organization for Standardization.

ISO 5459:2011. *Geometrical product specifications (GPS). Geometrical tolerancing. Datums and datum systems.* (2011). International Organization for Standardization.

ISO 16792:2021. *Technical product documentation - Digital product definition data practices.* (2021). International Organization for Standardization.

ISO 10360-2:2009. *Geometrical product specifications (GPS). Acceptance and reverification tests for coordinate measuring machines (CMM). Part 2: CMMs used for measuring linear dimensions.* (2009). International Organization for Standardization.

ISO 10360-4 2000. *Geometrical Product Specifications (GPS) — Acceptance and reverification tests for coordinate measuring machines (CMM) — Part 4: CMMs used in scanning measuring mode — Technical Corrigendum 1.* (2000). International Organization for Standardization.

ISO 12181: 2011. *Geometrical product specifications (GPS) — Roundness — Part 1: Vocabulary and parameters of roundness.* (2011). International Organization for Standardization.

ISO 15530-3 2011. *Geometrical product specifications (GPS). Coordinate measuring machines (CMM): Technique for determining the uncertainty of measurement. Part 3: Use of calibrated workpieces or measurement standards.* (2011) International Organization for Standardization.

ISO 14253-2:2011. *Geometrical product specifications (GPS). Inspection by measurement of workpieces and measuring equipment. Part 2: Guidance for the estimation of uncertainty in GPS measurement, in calibration of measuring equipment and in product verification. Technical Corrigendum 1.* (2011).

International Organization for Standardization.

ISO 10360-5 2021. *Geometrical product specifications (GPS) - Acceptance and reverification tests for coordinate measuring systems (CMS) - Part 5: Coordinate measuring machines (CMMs) using single and multiple stylus contacting probing systems using discrete point and/or scanning measuring mode.* (2021). International Organization for Standardization.

ISO 1101 2017. *Geometrical product specifications (GPS). Geometrical tolerancing. Tolerances of form, orientation, location, and runout.* (2017). International Organization for Standardization.

ISO 14405-1:2016. *Geometrical product specifications (GPS). Dimensional tolerancing. Part 1: Linear sizes. (2011). International Organization for Standardization.* (2016). International Organization for Standardization.

JCGM 100:2008. GUM 1995 with minor corrections. *Evaluation of measurement data – Guide to the expression of uncertainty in measurement.* (2008). Joint Committee for Guides in Metrology.

Hitunen, E., Linko, L,. Hemminki, S., Hägg, M., Järvenpää, E., Saarinen, P., Simonen, S., Kährä, P. (2011) *Laadukkaan mittaamisen perusteet.* MIKES.

Rapinoja, J-P., Pulkkinen, A., Nieminen, J., Laaksonen, T., Simons, J., Uski, P., Salmi, H., & Vainionpää, M. (2016). *Malliperustaisen tuotemäärittelyn (MBD) mahdollisuudet*. METSTA; Teknologiateollisuus; SMACC. https://teknologiainfo.net/sites/teknologiainfo.net/files/download/MBD_Raportti_2016.pdf

Rapinoja, J-P., Henell, A., Kellokoski, M., Hinkkanen, M., Pulkkinen, A., Nieminen, J., Laaksonen, T., Simons, J., Uski, P. & Kähäri, M. (2022) *Opastusta mallipohjaisen tuotemäärittelyn (MBD) käyttöönottoon*. METSTA. https://metsta.fi/wp-content/uploads/2021/12/MBD-opas.pdf

Renishaw. (n.d.-a). *Touch-trigger probes*. Retrieved April 10, 2023, from https://www.renishaw.com/en/touch-trigger-probes--6652

Renishaw (n.d.-b). *technical paper SP25M* Retrieved April 10, 2023, from https://www.nm3diberica.com/download/102/275a2f9c11334daa89a9e6496839e487/sp25m.pdf

Renishaw (n.d.-c). *SP25M Scanning performance data* April 10, 2023, from https://www.renishaw.com/resourcecentre/download/presentation-sp25m- scanning-test-data--2995?userLanguage=en&

Roithmeier, R. (2009) *Productive Measurement Function and production-oriented coordinate metrology*. Aalen Carl Zeiss 3D academy

Roithmeier, R. (2006) *Measurement strategies in contact coordinate metrology*. Aalen Carl Zeiss 3D academy

Roithmeier, R. (2015) M*easurement Strategies in tactile coordinate metrology.* Aalen Zeiss metrology academy

Schuetz, G. (2020) Tips for Choosing Filter Settings When Measuring Round Shapes. Mahr Inc. Retrieved April 10, 2023, from https://www.mmsonline.com/articles/tips-for- choosing-filter-settings-when-measuring-round-shapes 9.11.2022.

Thalmann, R., Meli, F., & Küng, A. (2016). State of the art of tactile micro coordinate metrology. *Appl. Sci.*, *6*(5), [150]. Retrieved April 10, 2023, from https://doi.org/10.3390/app6050150

Tikka, H. (2007). *Koordinaattimittaus.* Juvenes Print.

Zeiss Metrology Academy. (2020). *Calypso expert training manual* [Internal training material].

Zeiss Metrology Academy. (2018). *CALYPSO Advanced Level 2 training manual* [Internal training material].

Zeiss Metrology Academy. (2021). *Calypso Form and Location errors training manual* [Internal training material].

Appendix 1

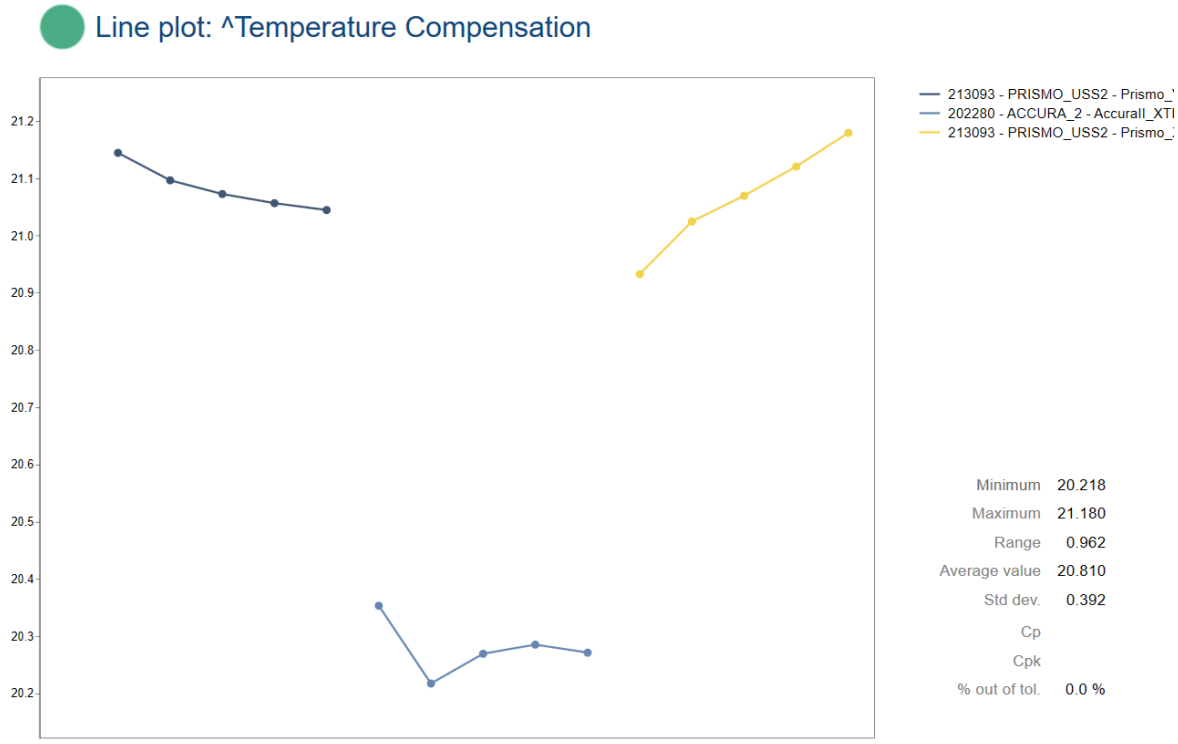

Figure 76. Temperature stability.

Appendix 2

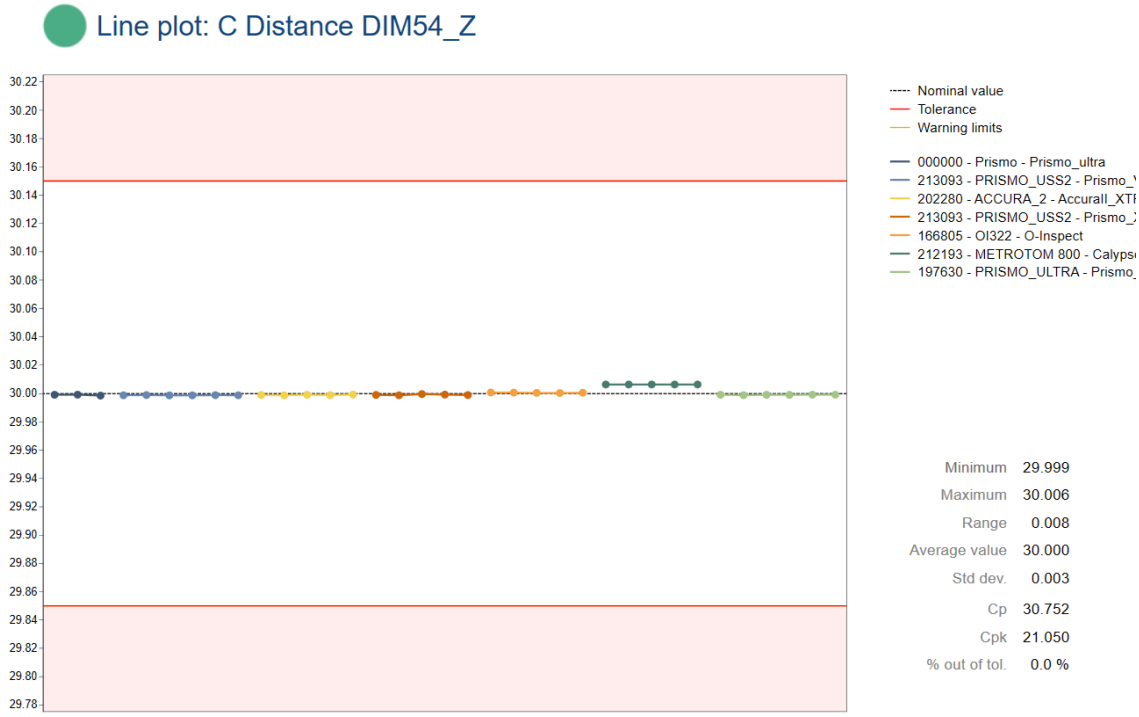

Figure 77. Reproducibility and repeatability.